

Inaugural dissertation

Submitted to the

Combined Faculty of Mathematics, Engineering and Natural Sciences
of the
Ruprecht - Karls - University
Heidelberg

for the degree of
Doctor of Natural Sciences

Presented by

Stephanie Tanja Zeuch (geb. Rothe), M.Sc.

born in Heidelberg, Germany

oral examination on 14th March 2023

Identification of Novel Substrates of the Insoluble Protein Deposit (IPOD) in the yeast *S. cerevisiae*

Referees:

PD Dr. Axel Mogk
Prof. Dr. Sebastian Schuck

I hereby declare that I have written the submitted dissertation myself and, in this process, have used no other sources or materials than those explicitly indicated. The work was carried out at the Department of Internal Medicine I and Clinical Chemistry, University Hospital Heidelberg, Heidelberg, in the research group of Dr. Jens Tyedmers.

Heidelberg, January 2023

Stephanie Zeuch

*To my mother Inge Sophie Rothe, geb. Apfel (1948 – 2022),
whose support and love will always be a constant source of inspiration.*

Abstract

Cells have evolved elaborate protein quality control systems (PQS), which include molecular chaperones and proteolytic machineries. However, when the occurrence of misfolded proteins exceeds the PQS's capacity, they accumulate and can form aggregates. More and more evidence suggests that the accumulation of misfolded protein species into specific spatially separated deposition sites is a cytoprotective response of the cell. The yeast *S. cerevisiae* has at least three different such protein quality control sites: the JUxtaNuclear Quality control (JUNQ)/IntraNuclear Quality control site (INQ) and the Cyto-Q harbours unstructured, amorphously misfolded proteins, while the perivacuolar Insoluble PrOtein Deposit (IPOD) has been initially described as a deposition site for amyloid aggregates. However, more recently it has been suggested that the IPOD may also harbour other types of substrates, such as oxidatively damaged proteins and inactive/damaged proteasomes or subunits thereof. Interestingly, many of these potential substrate classes can form high molecular weight aggregates or represent large protein complexes, respectively. Because the IPOD lies directly adjacent to the phagophore assembly site at the vacuole, it was hypothesized that the perivacuolar IPOD may represent a sorting center for aggregates and larger protein complexes destined for autophagic turnover.

This study focuses on the enrichment of IPODs visualized with the model substrate PrD-GFP under different conditions, including oxidative stress, to characterize other IPOD substrates through an unbiased mass spectrometry approach. This strategy identified several proteins that co-enriched with the IPOD, mainly after oxidative stress. Among these was Pyruvate decarboxylase 1 (Pdc1), a protein susceptible to carbonylation which has been previously hypothesized to be present at the IPOD after oxidative insult.

For a Pdc1-mCh fusion protein, it was observed that the number of cells which formed Pdc1-mCh foci was increased after different forms of oxidative stress such as H₂O₂ or menadione treatment. The majority of these stress-induced foci colocalized with PrD-GFP marked IPODs. Other proteins found enriched at the IPOD after oxidative stress include Enolase 2 (Eno2) and Glyceraldehyde-3-phosphate dehydrogenase isozyme 3 (Tdh3). Along these lines, by staining for carbonylated proteins it was found that the overall levels of carbonylated proteins co-enriching with IPODs were much higher after application of oxidative stress. This supports the

hypothesis that aggregates of oxidatively damaged proteins are another substrate group for the IPOD.

Furthermore, it has been shown that aberrant stress granules transiently associate with the aggresome on their way to autophagic degradation in mammalian cells. I hypothesized that the IPOD may play a similar role to the aggresome in yeast in this regard and indeed, in a dCuz1 background that hinders proteasomal degradation of stress granules and makes them more persistent, a proportion of aberrant arsenite-induced stress granules marked by Pab1-mCh colocalized with the IPOD after arsenite stress.

Zusammenfassung

Zellen haben ausgeklügelte Systeme zur Kontrolle der Proteinqualität (PQS) entwickelt, zu denen molekulare Chaperone und proteolytische Mechanismen gehören. Wenn jedoch das Auftreten von fehlgefalteten Proteinen die Kapazität des PQS übersteigt, häufen sie sich an und können Aggregate bilden. Es gibt immer mehr Hinweise darauf, dass die Anhäufung fehlgefalteter Proteinspezies an bestimmten, räumlich getrennten Ablagerungsstellen eine zytoprotektive Reaktion der Zelle darstellt. Die Hefe *S. cerevisiae* verfügt über mindestens drei verschiedene solcher Protein-Qualitätskontrollstellen: Die JUxtaNuclear Quality control (JUNQ)/IntraNuclear Quality control site (INQ) und die Cyto-Q beherbergen unstrukturierte, amorphe, fehlgefaltete Proteine, während das perivakuoläre Insoluble PrOtein Deposit (IPOD) zunächst als Ablagerungsstelle für Amyloid-Aggregate beschrieben wurde. In jüngerer Zeit wurde jedoch vermutet, dass das IPOD auch andere Arten von Substraten beherbergen kann, wie zum Beispiel oxidativ geschädigte Proteine und inaktive/beschädigte Proteasomen oder deren Untereinheiten. Interessanterweise können viele dieser potenziellen Substratklassen Aggregate mit hohem Molekulargewicht bilden bzw. große Proteinkomplexe darstellen. Da der IPOD direkt neben dem PAS (Phagophore Assembly Site) an der Vakuole liegt, wurde die Hypothese aufgestellt, dass der perivakuoläre IPOD ein Sortierzentrum für Aggregate und größere Proteinkomplexe darstellen könnte, die für den autophagischen Abbau bestimmt sind.

Diese Studie konzentriert sich auf die Anreicherung von IPODs, die mit PrD-GFP markiert wurden, unter verschiedenen Bedingungen, einschließlich oxidativem Stress, um andere IPOD-Substrate durch einen unvoreingenommenen massenspektrometrischen Ansatz zu charakterisieren. Mit dieser Strategie wurden mehrere Proteine identifiziert, die sich mit dem IPOD anreicherten, vor allem nach oxidativem Stress. Darunter befand sich auch Pyruvat-Decarboxylase 1 (Pdc1), ein für Carbonylierung anfälliges Protein, von dem zuvor angenommen wurde, dass es nach oxidativem Stress am IPOD vorhanden ist.

Bei einem Pdc1-mCh-Fusionsprotein wurde beobachtet, dass die Anzahl der Zellen, die Pdc1-mCh-Foci bildeten, nach verschiedenen Formen von oxidativem Stress wie H₂O₂- oder Menadion-Behandlung erhöht war. Die Mehrzahl dieser stressinduzierten Foci kolokalisierte mit mit PrD-GFP markierten IPODs. Zu den anderen Proteinen, die nach oxidativem Stress am

IPOD angereichert wurden, gehören Enolase 2 (Eno2) und Glyceraldehyd-3-phosphat-Dehydrogenase-Isoenzym 3 (Tdh3). Bei der Detektion carbonylierter Proteine wurde festgestellt, dass die Gesamtmenge an carbonylierten Proteinen, die mit IPODs angereichert waren, nach oxidativem Stress deutlich erhöht war. Dies stützt die Hypothese, dass Aggregate oxidativ geschädigter Proteine eine weitere Substratgruppe für den IPOD darstellen.

Darüber hinaus hat sich gezeigt, dass in Säugerzellen aberrante Stressgranula auf ihrem Weg zum autophagischen Abbau vorübergehend mit dem Aggresom assoziieren. Ich stellte die Hypothese auf, dass das IPOD in Hefe in dieser Hinsicht eine ähnliche Rolle wie das Aggresom spielen könnte. Tatsächlich kolokalisierte in einem dCuz1-Hintergrund, der den proteasomalen Abbau von Stressgranula behindert und diese persistenter macht, ein Teil der durch Pab1-mCh markierten aberranten Arsenit-induzierten Stressgranula mit dem IPOD nach Arsenitstress.

Contents

1. Introduction	1
1.1. Protein folding, misfolding and aggregation.....	1
1.2. Protein Quality Control Systems (PQS)	3
1.2.1. Temporal quality control	3
1.2.1.1. Chaperone-mediated protein folding	4
1.2.1.2. Chaperone-mediated disaggregation	4
1.2.1.3. Proteasome-mediated degradation of protein aggregates.....	6
1.2.1.4. Aggregate clearance via autophagy.....	8
1.2.2. Spatial quality control	10
1.2.2.1. JUxtaNuclear Quality control compartment (JUNQ) / IntraNuclear Quality control compartment (INQ).....	11
1.2.2.2. Cytoplasmic Quality Control Sites (CytoQ)	12
1.2.2.3. Intramitochondrial Quality Control (iMIQ)	12
1.2.2.4. Insoluble Protein Deposit (IPOD)	13
1.2.2.5. Stress Granules (SGs)	14
1.3. Yeast Prions.....	17
1.3.1. PrD-GFP as a model IPOD substrate	19
1.4. Oxidative Stress.....	20
1.4.1. Protein Carbonylation	20
2. Materials and Methods.....	25
2.1. Materials	25
2.1.1. Software and Equipment	25
2.1.1.1. Computer software	25
2.1.1.2. Equipment.....	25
2.1.1.3. Microscopes	25
2.1.2. Expendable items.....	27
2.1.2.1. Chemicals	27
2.1.2.2. Media and Buffers.....	30
2.1.2.3. Plasmids and Primers	30
2.1.2.4. Yeast strains	35
2.1.2.5. Antibodies	36
2.2. Methods.....	37
2.2.1. Molecular Biology Methods.....	37
2.2.1.1. Agarose gel electrophoresis.....	37

2.2.1.2. Restriction digestion of DNA.....	37
2.2.1.3 Purification of DNA fragments.....	37
2.2.1.4. Polymerase Chain Reaction (PCR).....	38
2.2.2. Bacterial methods.....	39
2.2.2.1. Transformation of competent E.coli.....	39
2.2.2.2. Plasmid isolation.....	39
2.2.3. Yeast Methods.....	40
2.2.3.1. Yeast transformation.....	40
2.2.3.2. Spotting Assay.....	40
2.2.3.3. Preparation of yeast cell lysates for western blot.....	41
2.2.3.4. Preparation of yeast cell lysates for IPOD enrichment using a bead mill (Cryolysis) ..	41
2.2.4. Biochemical methods.....	42
2.2.4.1. BCA Assay.....	42
2.2.4.2. SDS -polyacrylamide gel electrophoresis (SDS-PAGE).....	42
2.2.4.3. Coomassie-Silver staining.....	42
2.2.4.4. Western blot.....	42
2.2.4.5. Oxyblot for detection of protein carbonyls.....	43
2.2.4.6. Immunoprecipitation from yeast lysates.....	43
2.2.5. FACS-based approach for IPOD enrichment.....	44
2.2.6. Microscopy.....	44
2.2.6.1. Fixation of yeast cells for standard epifluorescence microscopy.....	44
2.2.6.2. Microscopy image acquisition, processing, and data interpretation.....	45
2.2.7. In-gel tryptic digestion and LC-MS/MS analysis.....	45
2.2.8. Individual modification site statistics in carbonyl proteomics.....	45
2.2.9 Statistical analysis.....	46
3. Aims.....	47
4. Results.....	48
4.1. Methods for the enrichment of IPODs.....	48
4.1.1. Fluorescence Activated Cell Sorting (FACS)-based enrichment of IPODs.....	48
4.1.2. Immunoprecipitation (IP)-based enrichment of IPODs.....	55
4.2. Proteomic analysis of IPOD composition under different conditions.....	58
4.2.1 IPOD composition after oxidative stress.....	58
4.2.2. IPOD composition after mitochondrial stress.....	61
4.2.3. Comparing IPOD composition of oxidatively and mitochondrially stressed cells.....	64
4.3. Oxidatively damaged proteins are enriched at the IPOD.....	64
4.3.1. Carbonylated proteins are enriched at the IPOD.....	64

4.3.2. Carbonyl Proteomics.....	65
4.3.3. Oxidative stress-induced foci formation.....	72
4.4. Aberrant stress granules transiently colocalize with the IPOD.....	77
4.5. Analysis of stress-induced localization changes of mitochondrial proteins	81
5. Discussion and Outlook.....	84
5.1. Discussion.....	84
5.1.1. Strategies for IPOD-enrichment.....	85
5.1.2. Carbonylation-prone proteins accumulate at the IPOD	86
4.1.2. Stress granules transiently colocalize with the IPOD.....	90
4.1.3. Possibility of other substrate classes	92
4.2. Outlook	94
6. References	96
7. Acknowledgements.....	114

1. Introduction

1.1. Protein folding, misfolding and aggregation

A defining characteristic of biological systems is that even the most complex and intricate of their component molecular structures can self-assemble correctly with precision and fidelity¹. Proteins perform a multitude of cellular functions and therefore their correct folding into their native conformation is crucial to ensure proper cellular function. Only correctly folded proteins have biological function, long-term stability and can interact selectively with their respective partners. A wide variety of highly specific structures result from protein folding and enable close positioning of functional groups, energy generation, trafficking molecules to specific cellular locations, and the regulation of cellular growth and differentiation. Protein molecules can adopt a variety of different conformational states in-between their synthesis at the ribosome and eventual proteolytic degradation and these states can interconvert on different timescales². However, many proteins, e.g. α -synuclein or tau, are largely unstructured in solution and thereby often described as intrinsically disordered, but can fold into more defined structures upon interaction with specific binding partners³.

The folding process does not occur over a series of mandatory steps but can rather be viewed as a stochastic search through multiple available conformations⁴⁻⁶. On average, the more native-like interactions between amino acid residues are more stable than non-native ones and therefore more persistent and the nascent polypeptide chain can find its lowest-energy structure through a trial-and-error process. Because the funnel-shaped so-called “energy landscape” is determined by the amino acid sequence, proteins have evolved in such a way that they can assemble rapidly and efficiently, with only a small number of possible conformational states needing to be sampled⁴⁻⁷.

Most nascent polypeptides attain their native conformation through the formation of one or more partially folded intermediate states. Classically, a natively folded protein is thought of as a highly constrained, compact structure. Many proteins can contain significant intrinsically disordered regions (IDRs) as well. The different conformational states a protein can adopt involve a highly complex series of equilibria, the thermodynamics and kinetics of which are determined by their primary amino acid sequence as well as interactions with molecular

chaperones and other components of the protein quality control machinery¹. Natively folded states are mostly those structures that are thermodynamically most stable under physiological conditions⁶.

If a protein is incorrectly or incompletely folded, it almost invariably exposes some hydrophobic structures, which are usually buried in the core of the protein in its native folding state. This makes them prone to inappropriate interactions with other proteins in the crowded cellular environment⁸. Under healthy conditions, a cell recognizes aberrantly folded or damaged proteins and can correct or eliminate them using elaborate protein quality control systems (PQS) including molecular chaperones and proteolytic machineries^{9,10}. When the amount of misfolded and damaged proteins exceeds the capacity of the PQS, they accumulate and can coalesce into aggregates, which can cluster into specialized deposition sites limiting aberrant and potentially toxic interactions with other proteins¹¹⁻¹⁶. Protein aggregation describes the association of proteins into larger assemblies associated with loss of secondary, tertiary or quaternary structure¹⁷, when the cell is unable to maintain cellular and protein homeostasis (proteostasis). Aggregation of proteins can also be a response to cellular stress, for example through environmental changes. These aggregates vary in size, from protein oligomers to visible cytosolic inclusion bodies¹⁸. Their structure can be more disordered and amorphous, but also highly-structured and compact (amyloids).

If proteome homeostasis cannot be upheld, this results in the accumulation protein aggregates. Over time, those aggregates are causal for diseases termed proteinopathies. Aggregation of a specific disease-related protein due to amino acid mutations and changes to the proteins' primary structure is a hallmark of many neurodegenerative diseases, including Amyotrophic Lateral Sclerosis (ALS), Alzheimer's, Parkinson's, and Huntington's Disease (AD, PD, and HD, respectively). The characteristics of the soluble forms of the disease-related proteins vary greatly, from compact globular proteins to more largely unstructured ones. However, their aggregated forms share many properties¹⁹. A specific type of aggregate are amyloid aggregates. These are highly ordered, insoluble fibrous aggregates rich in β -sheets that are oriented perpendicularly to the fibril axis¹⁹. The fibrillar structures tend to be rather long (often several micrometres), unbranched, often twisted structures and are a few nanometres in diameter^{20,21}. While the ability to form amyloid structures appears to be generic, the propensity of a given protein to undergo this process varies greatly and depends

on many factors. Among these are physicochemical properties of the protein, like charge, secondary structure-propensities and hydrophobicity²². The intrinsic aggregation propensity can be obvious, e.g. in expanded polyQ tracts that can form high molecular weight aggregates, for instance huntingtin in HD. Most proteins contain at least one aggregation prone region, which is normally hidden by structural features, e.g. burying in a hydrophobic core, and therefore protected from aggregation²³.

Although protein aggregate inclusions are common in many diseases, they can indeed also be seen in aged neuronal cells of healthy individuals^{24,25}. This strengthens the idea that they are a normal, cytoprotective response of the PQS machinery to misfolded proteins. However, the PQS capacity for processing misfolded and damaged proteins appears to decline with age, which may explain the increased incidence of certain amyloidoses with age²⁶⁻³². The aging process is associated with an increase in oxidative stress. With increased oxidative stress, oxidative post-translational modifications (PTMs) of proteins are induced, including glycation, glycooxidation, lipoxidation, and carbonylation (see section 1.3). An elevation of these modifications is also often seen in diseases like type II diabetes, chronic inflammation, or neurodegenerative diseases. It has been demonstrated that there is an association between carbonylation of the cellular proteome and age-related increases in protein aggregation³³.

1.2. Protein Quality Control Systems (PQS)

Protein quality control (PQC) is essential for the maintenance of a functional cellular proteome. Therefore, cells have evolved systems to efficiently maintain protein folding, both during de novo synthesis and under conditions of cellular stress that lead to the unfolding and aggregation of proteins³⁴. Misfolded or toxic proteins are either refolded or degraded by a system of temporal PQC or they can be sequestered into aggregates and inclusions by a system of spatial PQC^{10,35,36}. *Saccharomyces cerevisiae* has been used extensively to study PQC mechanisms, which are highly conserved from simple unicellular organisms like yeasts to highly complex organisms like for example mammals among different organisms.

1.2.1. Temporal quality control

Molecular chaperones are proteins that aid in the folding or assembly of other proteins without being a part of their final structure³⁷. They play a fundamental role in de novo protein folding, protein transport and degradation, protein complex assembly, and aggregate

dissociation and refolding of denatured proteins. Chaperones of the temporal PQC system act to ensure the proper folding of nascent proteins as well as the refolding of misfolded ones and promote the degradation of proteins which cannot be refolded effectively^{38–40}. Many are Heat shock proteins (HSPs), termed such because their synthesis is induced under conditions of cellular stress that affect proteostasis, like heat shock or oxidative stress. Chaperone proteins were originally classed according to their molecular weight, e.g. Hsp40s, Hsp60s, Hsp70s, Hsp90s, Hsp100s and small Hsps.

1.2.1.1. Chaperone-mediated protein folding

Chaperones involved in de novo protein folding and refolding are regulated in an ATP-dependent manner and recognize exposed hydrophobic amino acid residues, which are later buried in the core of the natively folded protein. These include the Hsp70s, Hsp90s and chaperonins. Chaperones recognize non-native states of many proteins by binding to hydrophobic stretches. They promote protein folding through a mechanism of kinetic partitioning. Under physiological conditions, an unfolded protein undergoes a rapid collapse into a partially folded, compact intermediate, guided by intramolecular interactions between amino acid residues, e.g. hydrogen bonds, disulfide bonds, electrostatic and hydrophobic interaction⁴¹. This amino acid chain collapse restricts the conformational states which need to be searched en route to the native state, however, folding intermediates often represent aggregation-prone, kinetically trapped states^{42,43}. Many chaperones switch between high- and low-affinity states for the unfolded or partially folded protein substrate in an ATP-dependent manner, resulting in cycles of protein binding and release. In this mechanism, release of hydrophobic parts allows folding, while binding of non-native protein blocks aggregation and can help reverse misfolded states^{43,44}.

1.2.1.2. Chaperone-mediated disaggregation

Cells combat the formation of toxic protein aggregates via a host of molecular chaperones, which prevent aggregation by their interaction with hydrophobic stretches of unfolded proteins or folding intermediates^{1,45}. However, when this process fails, cells can resort to two rescue mechanisms. They can either digest the protein by proteases or employ a disaggregation strategy. Disaggregation is achieved by disaggregases like ClpB (caseinolytic peptidase B) in prokaryotic cells or Hsp104 in eukaryotic cells. These disaggregases solubilize

aggregated proteins together with their corresponding Hsp70 system in an ATP-dependent manner. Their activity can be enhanced by small Hsp proteins (sHsps). sHsps are also referred to as holdases or aggregases. They bind misfolded proteins, concentrating them into aggregates, which prevents further interactions⁴⁶. Hsp40 co-chaperones are also involved early in the recognition of aggregates by binding unfolded protein regions and recruit Hsp70 to bind the aggregate. Because Hsp70s have protein folding capacities, they are also termed foldases. Their binding restricts access of proteases to the aggregate and allows substrate transfer to Hsp104. Hsp70-mediated substrate binding to Hsp104 activates its ATPase activity, which results in the threading of misfolded polypeptides through the central pore of the hexameric Hsp104⁴⁷⁻⁴⁹. Once Hsp104 encounters a tightly folded domain, it dissociates from the substrate, ensuring optimal refolding⁵⁰.

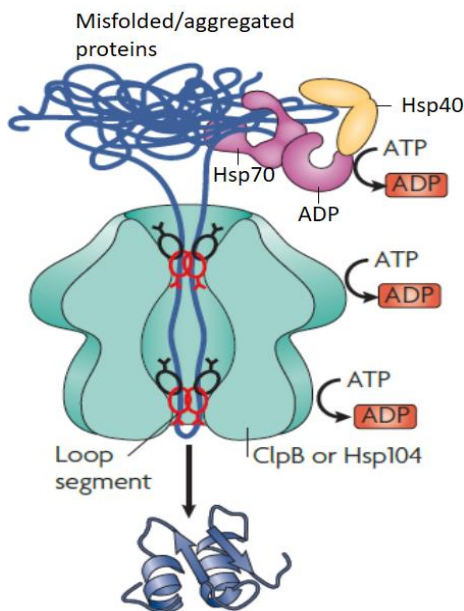


Figure 1. Protein disaggregation by the Hsp70-Hsp100 bi-chaperone system. Hsp70 along with its co-chaperones recognizes and binds to misfolded aggregated proteins before transferring them to the Hsp104 disaggregase. Substrate binding activates Hsp104 (ClpB)'s ATPase activity. ATP hydrolysis provides the energy required for the threading of single polypeptide chains one by one through the central pore of the Hsp104 hexamer. This process proceeds until a tightly folded domain is encountered, leading to substrate dissociation. The unfolded polypeptide chains can be refolded to their native state by the Hsp70 system. The figure was adapted and modified from⁵¹.

The specific set of chaperones recruited to an aggregate depends on the type of proteotoxic stress. For example, in yeast, heat-induced aggregates are recognized by cooperation of the sHsps Hsp26 and Hsp42, Hsp40, Hsp70 and Hsp104. Aggregates induced by H₂O₂ are also recognized by the sHsps, but the recruitment of the Hsp70/Hsp104 system requires the peroxiredoxin Tsa1⁵². Peroxiredoxins are peroxide scavengers, but upon oxidative stress (like increased levels of intracellular H₂O₂) they undergo a functional shift to act as chaperones⁵³.

This shift is mediated by sulfinylation of a peroxidatic cysteine of Tsa1 and reversed by the sulfiredoxin Srx1⁵⁴. In order to efficiently resolve heat-induced aggregates, the major cytosolic Hsp40, Ydj1, is essential⁴⁷. However, for H₂O₂-induced aggregates, it is dispensable⁵² – instead, their clearance depends on Srx1-mediated reduction of sulfinylated Tsa1 as well as the Hsp40 Sis1⁵². An explanation for this could be that Ydj1 is inactivated under oxidative stress due to oxidation of its cysteine-rich zinc finger domain, which Sis1 lacks⁵². The different chaperone requirements under heat stress compared to oxidative stress support the notion that the composition and structure of aggregates formed under different stress conditions also differs⁵².

1.2.1.3. Proteasome-mediated degradation of protein aggregates

The primary pathway for proteolytic degradation of short-lived, misfolded and damaged proteins is the ubiquitin-proteasome system (UPS), which has important functions in the regulation of cellular signalling and transcription, including in cell cycle progression, cell survival and apoptosis. The 26S proteasome is a multicatalytic, ATP-dependent protease that is made up of two subcomplexes: a barrel-shaped, two-fold symmetric core particle (CP, or 20S proteasome) and a regulatory particle (RP or 19S particle) that is attached to one or both ends of the CP. Facing the interior space of the CP are three β -type subunits (β 1, β 2, and β 5), which have caspase-like, trypsin-like, and chymotrypsin-like activities, respectively, that digest the substrate protein into peptides of 2–24 amino acids length, ensuring that no protein remains intact after entry into the CP and providing an essential source for amino acids. The RP is composed of base and lid subunits serving to recognize ubiquitinated substrate proteins and prepare them for degradation in the CP⁵⁵. The central part of the RP consists of six AAA-ATPases forming the hexameric Rpt ring (Rpt1-6). These have several important functions, including hooking the RP to the heptameric α -ring of the CP (via their C-terminal tails), opening the gated substrate channel of the CP, unfolding the substrates using ATP hydrolysis-generated energy, and translocating the substrate through the narrow pore into the 20S channel⁵⁶.

Proteasomal abundance, function, and composition are tightly controlled on multiple levels: transcription of genes encoding proteasomal subunits and assembly factors, post-translational modifications (PTMs) modulating proteolytic capacity, as well as degradation of proteasomes via a type of selective autophagy termed proteaphagy.

Substrates are usually poly-ubiquitinated before being targeted for proteasomal degradation. This depends on the concerted action of three enzyme classes: E1, E2 and E3. E3 enzymes confer substrate specificity and play an important role in the ubiquitin-mediated proteolytic cascade. While there are many different E3 ligases, Ubr1 and San1 are examples of two E3 ligases in yeast that promote ubiquitination of misfolded cytosolic proteins^{57,58}. It has been shown that impairment of the proteasome system in yeast results not only in inhibited clearance of misfolding-prone proteins, but in their accumulation in specialized quality control compartments like the JUNQ/INQ and cytoQ, while rescue of proteasomal functions results in the clearance of these PQS compartments⁵⁹. Therefore, the UPS plays an important role in determining the fate of misfolded proteins.

Studies in primary mouse neurons show that disruption of the proteasomal system can lead to neurodegeneration, defects in aggregate clearance, and the formation of inclusions⁶⁰⁻⁶². Proteasomal capacity can be compromised by different internal and external insults. These include chemical inhibition, oxidative stress, aberrant proteins or aging-related decreased expression and oxidative modification of proteasomal proteins⁶³⁻⁶⁵. The resulting accumulation of unfolded, misfolded, and damaged proteins impairs the functioning of cells and their organelles severely, which has been recognized as a crucial factor in aging and a wide variety of diseases, including neurodegenerative and cardiovascular diseases, type II diabetes, and cancer. There are a range of examples of disease-relevant misfolding-prone proteins (like α -synuclein, A β , or huntingtin), which can affect proteasome function⁶⁶⁻⁶⁸.

Aggregated proteins cannot be degraded effectively by the UPS and are directed to a specific autophagy pathway termed aggrephagy⁶⁹. Proteins with long Poly-Q repeat stretches such as those of the mutant Huntingtin protein can cause a blockage of proteasomes, rendering them non-functional⁷⁰. Furthermore, Poly-Q stretches can sequester proteasomes and trap them in aggregate inclusions, through which they become unavailable for the clearance of other soluble misfolded proteins, which plays a role in cellular toxicity and disease pathogenesis^{68,71}.

As proteasome function is of vital importance to cellular fitness, therefore there are several ways for the cells to react to reduced proteasomal activity and altered needs. These include not only adjustment of UPS activity itself, but also compensatory and regulatory actions of other PQS network components like autophagy (reviewed⁷²).

1.2.1.4. Aggregate clearance via autophagy

The UPS system is integral for the degradation of small, short-lived proteins, but when the spatial capacity of proteasomes is exceeded by larger, more heterogeneous cytoplasmic species such as protein aggregates, organelles, lipid droplets, or invading bacteria, autophagy (Greek for “self-eating”) is the preferred degradative route. Autophagy is a process by which cells degrade (or “eat”) part of their own cytoplasmic content upon nutrient deficient conditions such as starvation. There are three different types of autophagy pathways: macroautophagy, microautophagy, and chaperone-mediated autophagy (CMA; only in mammals), which have in common the capacity to deliver cytosolic substrates to the lysosome or vacuole for degradation, yet they differ in the way the cargo is directed to the lytic compartment.

Macroautophagy (also termed non-selective or bulk autophagy) is the best-characterized form of autophagy. Its hallmark is the non-selective engulfment of cellular material by a double-membrane structure called the phagophore, which closes to form the autophagosome^{73,74}. Phagophore biogenesis requires a set of proteins called the core autophagy machinery^{75,76}. Unlike in mammalian cells, autophagosomes in yeast originate at a single small membranous organelle termed pre-autophagosomal structure (PAS), which is located in close proximity to the vacuole⁷⁷⁻⁸⁰. Ultimately, autophagosome outer membrane fuses with the lysosomal or vacuolar membrane to release its contents into the acidic vacuolar lumen, facilitating its degradation by vacuolar peptidases. Although macroautophagy also takes place under basal conditions, it is strongly induced by starvation⁸¹. Under normal conditions, autophagy is regulated by metabolism and growth-related signals⁸².

In contrast to macroautophagy, microautophagy does not involve autophagosomes as transport intermediates, but an endosome or lysosome directly engulfs and takes up autophagic cargo. Studies in yeast have shown several different selective autophagic processes, including microautophagy of peroxisomes (“pexophagy”)^{83,84}, cytosol^{85,86}, mitochondria (“mitophagy”)⁸⁷, parts of the nucleus⁸⁸, lipid droplets⁸⁹, the endoplasmic reticulum (ER) (“ER-phagy”)⁹⁰, certain cytosolic enzymes⁹¹ and vacuole membrane proteins⁹². The associated mechanisms differ quite a lot, suggesting that the term microautophagy conflates multiple distinct types of selective autophagy as well as general microautophagy. During starvation, the vacuole invaginates and produces microautophagic bodies⁹³.

General fission-type microautophagy does not utilize the core autophagy machinery, but instead depends on the ESCRT machinery^{93,94}. The ESCRT machinery is well-understood in the formation of multivesicular bodies (MVB) in the endocytic pathway. MVB formation and microautophagy share many similarities. TOR kinase is inhibited by starvation, which leads to the dephosphorylation of Vps27, a component of the ESCRT-0 complex, the complex's recruitment to the vacuole and initiation of microautophagy^{95,96}, but does not affect ESCRT activity at MVBs and specifically induces microautophagy⁹⁷. Fusion-type microautophagy, on the other hand, requires the core autophagy machinery and SNARE proteins (distinction reviewed in⁹⁸).

Selective autophagy is a receptor-mediated degradation of specific cargoes and operates both in normal vegetative (non-induced) conditions as well as in response to different stimuli (induced conditions)^{81,99}. During ER protein folding stress, parts of the ER are degraded, involving the conversion of stacked ER sheets into spherical whorls⁹⁰. Microautophagy of these whorls depends on the ESCRT machinery and is similar to general microautophagy^{100,101}. ER whorls are depleted of many transmembrane proteins, so that micro-ER-phagy entails selective degradation of special ER subdomains. How cells recognize whorls for degradation is as yet unknown. Microlipophagy takes place at liquid-ordered membrane domains rich in sterols^{102,103}, but the mechanism for vacuolar uptake of lipid droplets is unclear. Micropexophagy of peroxisome clusters occurs by means of a phagophore-like structure called the micropexophagyspecific membrane apparatus (MIPA) and requires the core autophagy machinery^{104–106}. Micronucleophagy of portions of the nucleus is mediated by the nucleus-vacuole junction¹⁰⁷, requires the core autophagy machinery, involves an intermediate stage at which detached nuclear fragments are contained within open vacuole invaginations¹⁰⁸, preferentially targets nucleolar components¹⁰⁹ and, as is the case for micropexophagy, involves a phagophore-like structure¹¹⁰). Micronucleophagic bodies consist of three membranes, which are derived from the inner nuclear membrane, the outer nuclear membrane and the vacuole membrane⁸⁸. Micromitophagy depends on the core autophagic machinery¹¹¹ and its specificity appears to be derived from Atg32^{112,113}, however, the mechanism of micromitophagy is still rather uncertain.

There is evidence for cross-talk between the autophagic and the proteasomal systems, as autophagy inhibition leads to proteasomal activation and vice versa¹¹⁴. In mammalian cells, a

ubiquitin-dependent selective autophagic pathway termed aggrephagy has been reported^{69,115}. Ubiquitinated proteasome-resistant proteins or aggregates often accumulate in the cell. These substrates can be recognized by specific adaptor proteins such as p62/SQSTM1 or NBR1, which link the ubiquitin and autophagy pathways^{116,117}. They have a UBA domain for ubiquitin conjugate binding and a distinct binding site called AIM (Atg8 interacting motif) or LIR (LC3 interacting region) domain that mediates binding to the autophagosomal protein LC3 (Atg8 in yeast). LC3, conjugated to phosphatidylethanolamine, aids in the formation of autophagosomes and serves as a central docking site for the packaging of cargo for their subsequent degradation by autophagosome-lysosomal fusion^{69,115}.

A class of Ubiquitin/Atg8 adaptors called CUET proteins has been confirmed in yeast; these target ubiquitinated substrates for autophagic degradation^{118,119}. CUET proteins such as Cue5 (human homolog TOLLIP), have a CUE binding domain instead of a UBA domain, which mediates Ubiquitin binding as well as an AIM domain that mediates binding to Atg8. Cue5 recruits the ubiquitin ligase Rsp5 and together they can promote the clearance of both PolyQ (Htt96Q) as well as starvation-induced aggregates. This indicates that Cue5 and Rsp5 connect the UPS pathway to the autophagic pathway in yeast to mediate the degradation of aggregated proteins^{118,119}.

1.2.2. Spatial quality control

When the amount of misfolded and damaged proteins exceeds the PQS capacity, such as during proteotoxic stress, aging or neurodegenerative diseases, they accumulate in aggregates at multiple cellular sites called Q-bodies, stress foci or cytoQ. These are thought to represent the same structure discovered by different laboratories and will be termed cytoQ in the following text for simplicity. Upon prolonged stress, these aggregates can cluster into deposition sites, which limits aberrant and potentially toxic interactions with other proteins. *S. cerevisiae* possesses at least three such deposition sites (see figure 2) that each harbour different types of aggregates: cytoplasmic quality control sites (cytoQ), intra- and juxtannuclear quality control site (INQ/JUNQ), and the insoluble protein deposit (IPOD). There is evidence for a mitochondrial quality control site, termed IMiQ¹²⁰.

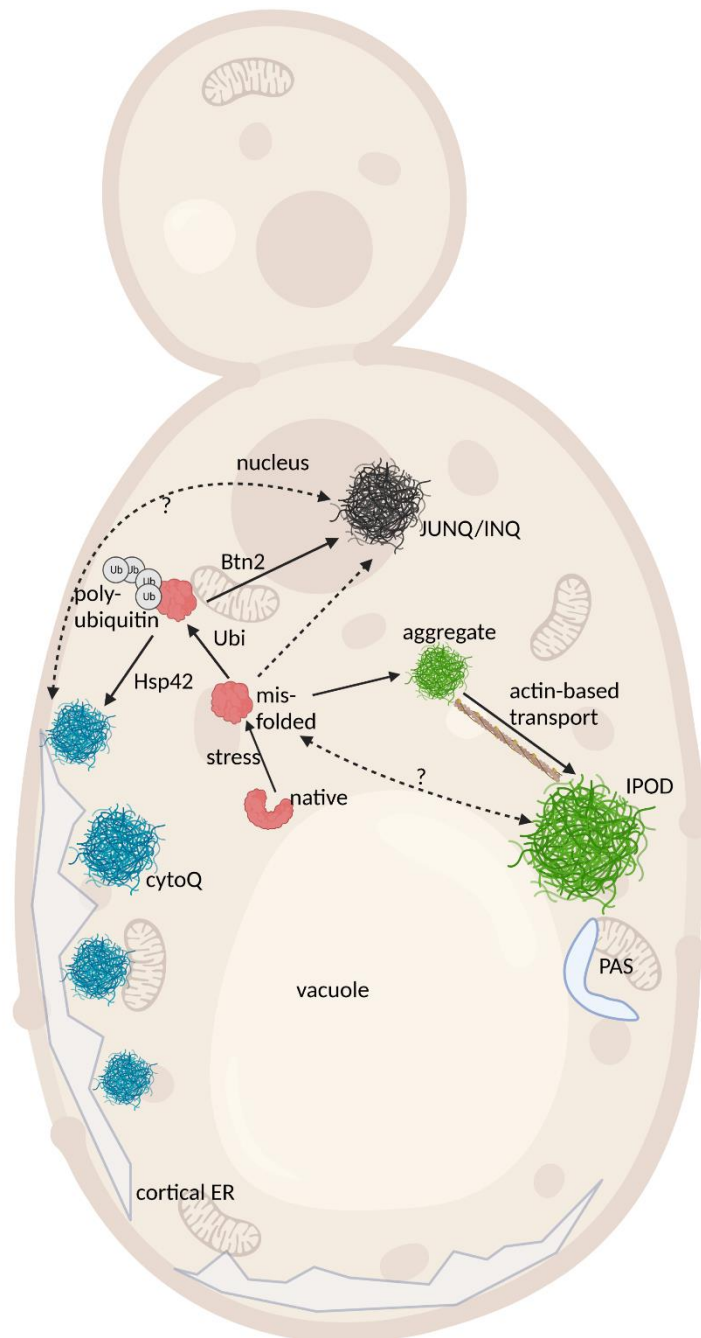


Figure 2. Overview of aggregate deposition sites in the yeast *S. cerevisiae*. Upon exposure to stress, misfolded or damaged proteins are targeted for either degradation or refolding, aided by molecular chaperones. Soluble protein aggregates are either targeted to the JUNQ/INQ compartment by the nuclear sorting factor Btn2, or to the peripherally localized Q-Bodies/CytoQ by the cytosolic Hsp42. Amyloidogenic aggregates accumulate predominantly at the perivacuolar insoluble protein deposit (IPOD) site adjacent to the Phagophore Assembly Site (PAS), targeted by an actin-based transport machinery, which has not yet been completely elucidated. Created using BioRender.com.

1.2.2.1. JUxtaNuclear Quality control compartment (JUNQ) / IntraNuclear Quality control compartment (INQ)

While the compartment called JUxtaNuclear Quality control site (JUNQ) is localized perinuclearly in an indentation of the nuclear membrane⁵⁹, the IntraNuclear Quality control compartment (INQ) is an intranuclear structure close to the nucleolus^{121–123}. Since the same

model substrates have been used in defining both JUNQ and INQ in studies, it is difficult to make a clear distinction between the two. Therefore, they will be collectively referred to as “JUNQ/INQ” in the following text.

Misfolded proteins being targeted for proteasomal degradation accumulate and are degraded at the JUNQ/INQ^{59,124}. The protein species harboured by the JUNQ/INQ are misfolded but soluble and ubiquitinated. The JUNQ/INQ is a highly dynamic structure, enriched in proteasomes^{38,59}. It was hypothesized that localization to this site was linked to the ubiquitination status of the protein and thereby recognition by the UPS. Studies have shown that blocking ubiquitination decreases the ratio of misfolded proteins that targeted to the JUNQ/INQ, whereas addition of a ubiquitin tag to the IPOD-exclusive substrate Rnq1 could partially redirect it to JUNQ/INQ⁵⁹. While this points to ubiquitination as a sorting signal, other studies have not shown a site-specific ubiquitin staining. Ubiquitination may still play a role under certain contexts, there are likely additional features of the misfolded proteins, enabling their interaction with certain sorting factors and directing them to discrete quality control sites. Under proteotoxic stress, Btn2, but not Hsp42, is required for JUNQ/INQ formation, while under genotoxic stress, both Btn2 and Hsp42 are needed^{121,125,126}.

1.2.2.2. Cytoplasmic Quality Control Sites (CytoQ)

Another class of aggregates dependent on Hsp42 are cytoQ, a term encompassing peripheral aggregates, cytosolic aggregates¹²⁵, stress foci¹²⁷ and Q-bodies¹²⁸. Co-aggregation of Hsp42 and other sHsps under different types of proteotoxic stress is a mechanism to actively control cytoQ formation and through fusion events coalesce into a smaller amount of larger-sized assemblies at specific cellular sites or even a single site^{125,128}. Therefore, cytoQ formation is thought to be an early event in protein quality control. Sequestration of amorphaously misfolded proteins at cytoQs, localized ER-adjacently, can result in their refolding using disaggregase mechanisms, or, conversely, their degradation³⁵. CytoQ formation is dependent on energy expenditure and an intact cortical ER, but independent of cytoskeletal structures.

1.2.2.3. Intramitochondrial Quality Control (iMIQ)

Recently, a PQC site in the periphery of the mitochondrial nucleus, where aggregation-prone mitochondrial proteins accumulate, has been reported¹²⁰. It has been termed intramitochondrial quality control site or iMIQ. Deposition there occurs for reporter proteins

under basal conditions as well as endogenous mitochondrial proteins under severe stress conditions¹²⁰. iMIQ formation and the sequestration of substrates at the iMIQ is dependent on Hsp78, as well as an intact microtubule network¹²⁰.

1.2.2.4. Insoluble Protein Deposit (IPOD)

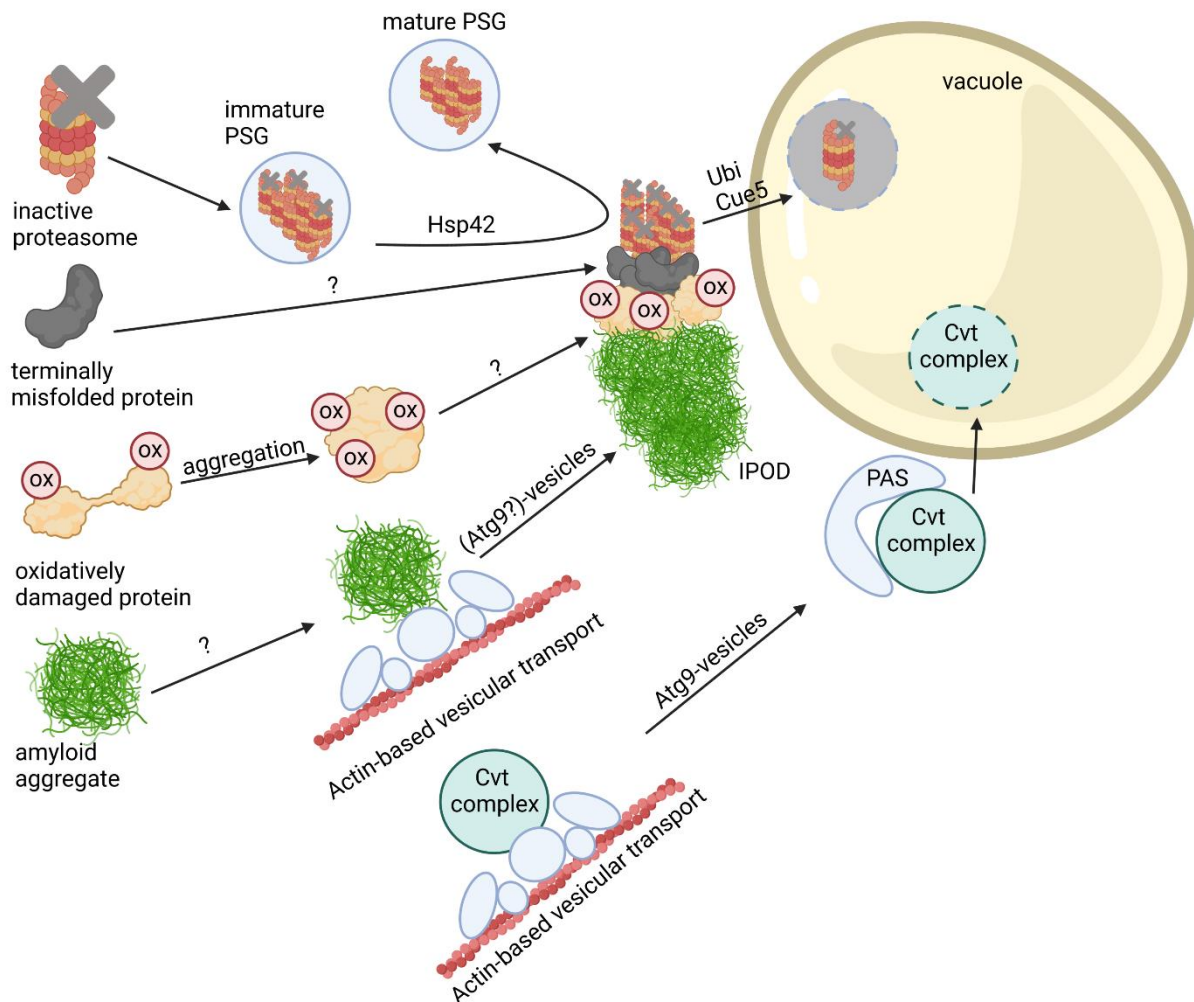


Figure 3. Deposition of damaged or inactive proteins, amyloids or protein complexes at the IPOD. Inactive proteasomes associated with Proteasome Storage Granules (PSGs) are known to accumulate at the IPOD in a Hsp42-dependent manner. Amyloid aggregates are targeted there by an actin-based transport machinery which overlaps with the recruitment machinery for vacuolar hydrolase precursors and their specific receptor (Cvt complex) to the pre-autophagosomal structure (PAS) via Atg9 vesicles, where these precursors are packaged into cytoplasm-to-vacuole vesicles for delivery to the lumen of the vacuole. It is hypothesized that large terminally misfolded proteins and oxidatively damaged proteins also accumulate at the IPOD in an as yet unknown manner. Created using BioRender.com.

S. cerevisiae has an aggregate deposition site, which has been thought to be specific for amyloid aggregates, termed the insoluble protein deposit (IPOD). The perivacuolar IPOD^{129,130} is located close to the phagophore assembly site (PAS)¹³¹, where the formation of autophagosomes and Cvt vesicles takes place in yeast cells. While the IPOD is present under

basal, non-stressed conditions, protein aggregate substrates can also be deposited specifically under different conditions of proteotoxic stress.

While it has been accepted that amyloid aggregates are the sole or most abundant substrate to be found at the IPOD, it also harbours different types of substrates (see Fig. 3)^{38,122,129,132}. It has recently been shown that immature proteasome storage granules (PSGs) transiently associated to the IPOD during their maturation, depositing damaged proteasomes there^{133–135} in a Hsp42-dependent manner. Once at the IPOD, damaged proteasomes are heavily ubiquitinated and degraded in the vacuole via a process of selective autophagy termed proteaphagy, dependent on the ubiquitin receptor Cue5¹³⁵.

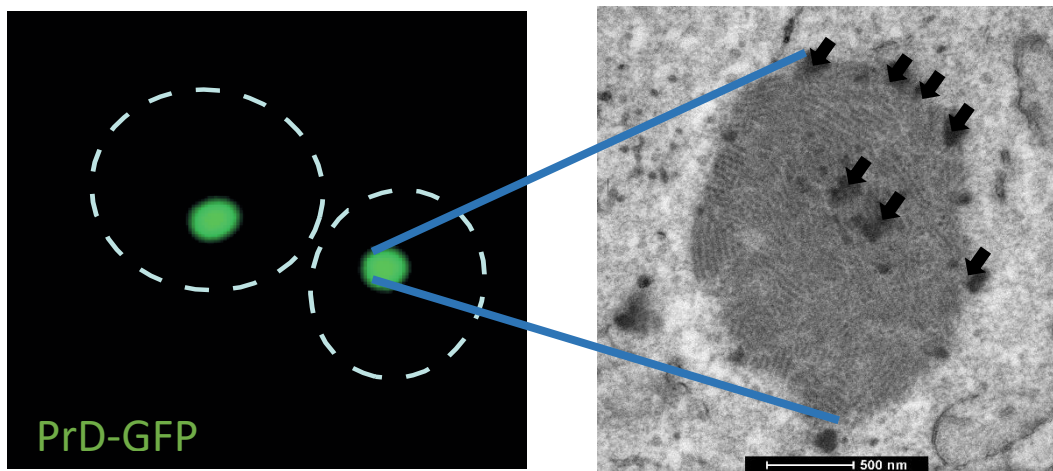


Figure 4. Correlative Light- and Electron Microscopy (CLEM) analysis of IPODs marked by PrD-GFP. Left: Fluorescent image of cells containing PrD-GFP IPODs (green). Right: Electron microscopic image of a PrD-GFP IPOD, made up of highly ordered fibres, but also containing dark dense “blobs,” indicated by arrows, of other material. Courtesy of Helen Saibil.

Other types of terminally damaged and aggregated substrates may also be deposited on the IPOD, from highly ordered to amorphous ones. This hypothesis is in part supported by electron microscopic imaging of IPODs, which shows dark, less structured “blobs” of material in between highly structured amyloid fibrils (Fig. 4)¹³⁰. In previous work by this laboratory, foci of fluorescently tagged pyruvate decarboxylase 1 (Pdc1) was observed to be localized at the IPOD occasionally, particularly under oxidative stress conditions¹³⁰.

1.2.2.5. Stress Granules (SGs)

Stress granules (SGs) are transient membrane-less organelles, which mainly consist of ribonucleoprotein assemblies which appear as part of an adaptive strategy to conserve energy and protect macromolecules in response to stress-induced alterations of mRNA metabolism, when translation is globally inhibited, which results in specific translation

machinery components being sequestered into SGs through liquid-liquid phase separation of non-translating mRNAs and RNA-binding proteins^{136–140}. Upon the end of stress and return to normal growth conditions, SGs dissolve^{141–144}. Translational repression and formation of SGs can be induced by a range of environmental stressors, including heat shock, oxidative stress, or nutrient deprivation (reviewed in¹⁴¹), which block translation initiation leading to polysome disassembly (reviewed in¹⁴⁵), resulting in the creation of a huge reservoir of RNA and related proteins that build and increase the number of SGs. Stress relief and increased translated mRNAs is associated with disassembly and reduction in the number of these granules^{146,147}.

The protein content of SGs is made up of three different groups: RNA binding proteins (RBPs), translation initiation factors and non-RBPs^{148,149}. While precise functions of SGs are yet to be determined, they appear to play a protective role during cellular stress. However, persistent and abnormal SGs may nucleate insoluble aggregates that are associated with human neurodegenerative diseases^{150–152}, such as ALS^{153–156}. RBPs that are SG resident, such as TDP-43, HNRNPA2/B1, and FUS, are encoded by genes which are mutated in ALS and also found in pathological inclusions in brain and spinal cord of ALS patients^{157,158}. The most common genetic mutation underlying ALS and frontotemporal dementia (FTD) is in C19ORF72 and is characterized by repeat-associated non-ATG (RAN) translation of C9ORF72-ALS/FTD-linked dipeptides and has been shown to influence SG formation^{159,160}.

SG formation is driven by a process of liquid-liquid phase separation (LLPS), which is itself driven by a local concentration gradient of mRNA molecules and RBPs, which contain a prion-like intrinsically disordered low-complexity domain^{161–164}. SGs evidently have properties of dense liquids^{158,165}, especially in the dynamic, RNase-sensitive outer layer (shell). However, evidence exists that they contain solid-like, RNase-resistant and protein-rich “cores”^{166,167} that are thought to represent nucleating RNPs that initiate SG assembly¹⁶⁷. It is possible that SG cores are initially as liquid-like as the shell, but then quickly harden through a molecular aging process¹⁶⁸. SGs formed upon certain stress conditions depend on different individual proteins¹⁶⁹. For example, it has been suggested that heat-induced SGs in yeast are physically and functionally interlinked with aggregates of heat-misfolded proteins and that removal of these aggregates prior SGs dissolution is required¹⁷⁰.

While RBPs are involved in SG nucleation such as yeast Pub1 and its mammalian ortholog TIA-1 and Pbp1/Ataxin-2, other proteins present in SGs are translation machinery components,

e.g. eIF4E, eIF4G, and eIF3 and other factors like signalling proteins^{171,172}. However, the SG composition depends also on the type of stress and the organism subjected to the stress. Whereas mammalian SGs are composed mainly of stalled translation preinitiation complexes¹⁷³, SG composition has been shown to be more diverse in yeast.

In mammalian cells, the formation of aggresomes, large inclusions similar to the yeast IPOD, plays an important role in linking SG clearance to autophagy (Fig. 5)¹⁷⁴. Aggresome formation is induced in cells whose clearance capacity for misfolded and damaged proteins is exceeded. Aberrant stress granules, which persist after stress removal, are targeted to the PQC and collected in a microtubule-dependent manner at the centrosome and SGs sequestered at the aggresome are selectively degraded via autophagy¹⁷⁴. In agreement with this supposition, SG-localized proteins HSPB1 and HSPB8 have also been shown to localize to the aggresome^{175,176} and the SG-localized proteins VCP/p97 and HDAC6 both play a key role in aggresome formation¹⁷⁷. Therefore, SG and aggresome formation seem to be closely linked and targeting of SGs to aggresomes may be a specific mechanism to rescue cells from excess of aberrant SGs.

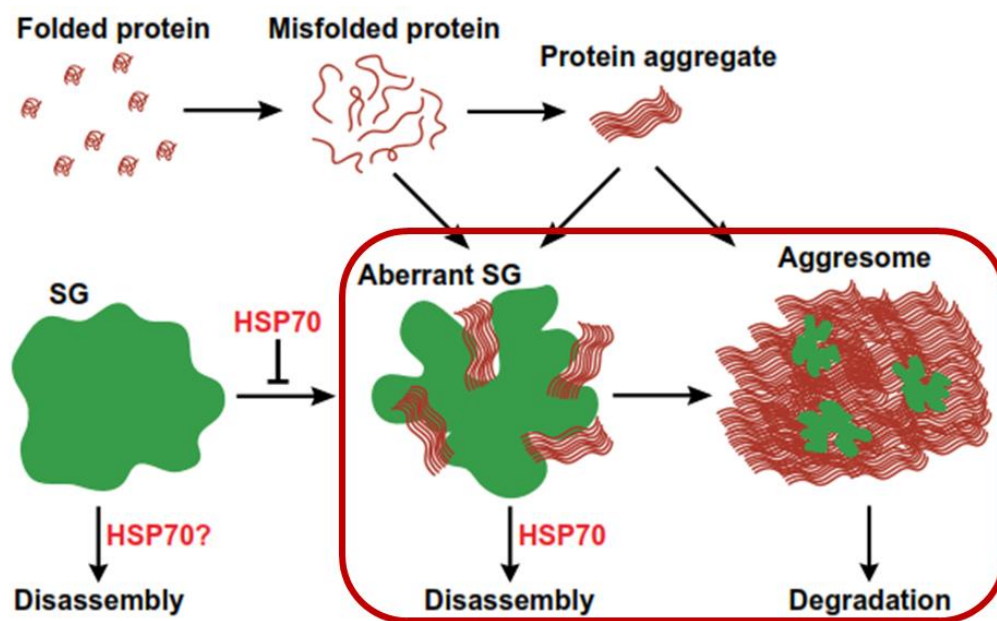


Figure 5. Interplay between stress granules and the Protein Quality Control Network. Adapted from¹⁷⁸.

SG-inducing stress conditions lead to accumulation of misfolded proteins, including defective ribosome products (DRiPs), making it likely that SGs could co-aggregate with misfolded proteins. When DRiPs and other misfolded proteins accumulate inside SGs, the biochemical

and dynamic properties of SGs are affected^{174,176}. These aberrant SGs containing misfolded proteins are less dynamic and RNase-resistant. When DRiPs and other misfolded proteins accumulate in SGs, this may lead to the formation of aggregate-like core structures inside SGs, supported by the finding that isolated core structures contain high amounts of chaperones, including the HSPB8-BAG3-HSP70 complex, perhaps because of the presence of misfolded proteins^{166,174,176}. Other chaperones are recruited as second line of defense at later time points, especially when SGs become enriched for additional misfolded proteins, to prevent conversion of aberrant SGs into irreversible aggregates^{174,176}.

Arsenite, the trivalent oxidation state of the environmental toxin and carcinogen arsenic, can damage cells in several ways, including through oxidative stress, DNA damage and mitochondrial uncoupling^{179,180}. Arsenite is also very proteotoxic not only for nascent but also susceptible native proteins, as evidenced by its rapid induction of protein aggregate accumulation, protein ubiquitinylation and SG formation^{181–184}. It also compromises the activities of key components of the proteotoxic stress response like the 26S proteasome and p97^{185,186}. It has been shown that p97 (and its yeast homolog Cdc48) and ZFAND1 (as well as its yeast homolog Cuz1), a member of a protein family containing zinc fingers of the AN1 type, associate with arsenite-stalled proteasomes^{185,187,188}. Turakhiya and colleagues showed that ZFAND1/Cuz1 is required for the efficient clearance of arsenite-induced SGs in mammalian and yeast cells, respectively¹⁸⁹. They further showed that ZFAND1/Cuz1 recruits p97/Cdc48 and the 26S proteasome to SGs, which is necessary for efficient clearance of SGs after removal of arsenite stress. Additionally, expression of ALS-causing mutant p97 and ZFAND1 depletion are epistatic with respect to SG clearance, indicating that ZFAND1 and p97 act in the same pathway mediating SG clearance¹⁸⁹. Absence of ZFAND1/Cuz1 causes formation of aberrant SGs containing DRiPs, which are targeted for autophagic degradation^{189,190}. Indeed, autophagy-deficient cells seem to accumulate SGs¹⁹¹.

1.3. Yeast Prions

Prions are self-perpetuating protein conformations that store and transmit phenotypic information independently of nucleic acids. They were first identified in the sheep disease Scrapie, but since then have been associated with pathologies in a range of different organisms, including bovine spongiform encephalopathy (BSE) in cows and Creutzfeldt-Jacob disease (or kuru kuru) in humans^{192,193}. Prion diseases are caused by the change in

conformation of the prion protein (PrP) from its endogenous form (PrP^C) to its pathological form (PrP^{SC}). The pathological PrP^{SC} is protease-resistant, insoluble, forms amyloid fibrils and can template further conversion of soluble PrP^C to its insoluble, aggregating form¹⁹⁴. Therefore, prions are considered transmissible amyloids.

Fungal prions act as protein-based hereditary elements that stably propagate their altered conformation and the associated phenotypes^{195–197}. *S. cerevisiae* possesses at least seven proteins that can undergo prion-like conformational conversion^{198,199}, namely [MOT3⁺], [OCT⁺], [SWI⁺], [URE3⁺], [PSI⁺], [ISP⁺], and [RNQ⁺], with many more proteins potentially capable of forming prions²⁰⁰. The AAA+ ATPase Hsp104 shears amyloid fibers, generating prion seeds, also referred to as propagons²⁰¹, facilitating inheritance of the prion state from generation to generation²⁰². Yeast prions can form spontaneously or by overproduction of their cellular protein determinants²⁰³. Although several prions share features, there is no single common feature defining a prion. The proteins have different molecular functions and produce different prion phenotypes. Although they share no sequence homology, their prion domains (PrDs) are enriched in asparagine and glutamine residues and can adopt self-perpetuating prion conformations that are amyloids. Fungal prions, unlike mammalian ones, are not uniformly fatal, but can be beneficial under certain conditions. The [Het-S] fungal prion, for example, is necessary for normal function and heterokaryon incompatibility²⁰⁴. Yeast prions provide a good model to study amyloid biology²⁰⁵.

Of the seven known yeast prions, [PSI⁺] is the most well characterized one²⁰⁶. It is the amyloid form of the translation termination factor Sup35^{207–210}. Sup35's PrD, also called NM, has an N-terminal amyloidogenic domain (N) and a solubilizing middle domain (M)^{195,196}. Purified Sup35 PrD can form amyloid fibrils by itself in vitro²⁰⁷. In vivo, formation of the [PSI⁺] prion causes a reduced availability of the functional, soluble Sup35 termination factor, which results in stop-codon read-through and, depending on genetic background, a range of diverse phenotypes^{195–197,211}. While [PSI⁺] propagation is well studied, spontaneous de novo formation of [PSI⁺] is rare and poorly understood. However, overexpression of Sup35, or even its PrD alone, dramatically increases the frequency of [PSI⁺] induction²¹². The AAA+ ATPase Hsp104 is essential for [PSI⁺] propagation and treatment of an [PSI⁺] *S. cerevisiae* strain with 3 to 5 mM guanidine hydrochloride leads to curing of the [PSI⁺] prion state to the non-prion form [psi⁻]. Guanidine hydrochloride inhibits the ATPase activity of Hsp104^{205,213}, hindering its

ability to generate propagons, which results in the loss of prion state after several cell divisions^{213–215}. Both de novo formation as well as induction of the $[PSI^+]$ prion by overexpression of Sup35 is possible only in the presence of another prion, $[PIN^+]$, which is a self-propagating amyloid of the Rnq1 protein²¹⁶. It also depends on Hsp104 for propagation and can therefore be cured by Guanidine Hydrochloride²¹⁷.

1.3.1. PrD-GFP as a model IPOD substrate

The Sup35 protein has 3 domains: the N-terminal Q/N-rich domain (N), the highly charged K/E-rich middle domain (M) and the C-terminal domain (C). The N domain is required for the formation and templating of the amyloid conformation, while the M domain promotes solubility in the non-prion conformation and contains Hsp104 binding sites for initiation of propagon formation, whereas the C domain is necessary and sufficient for translation termination^{218,219}. Combined, the N and M domains form the NM domain, also termed the prion domain (PrD). The Sup35 PrD is necessary and sufficient for $[PSI^+]$ induction in $[PIN^+]$ *S. cerevisiae* cells²²⁰. A fusion of Sup35 PrD with GFP confers prion properties to GFP, leading to its deposition at the IPOD, providing a visually tractable prion model for the study of $[PSI^+]$ amyloid properties in *S. cerevisiae*²²¹.

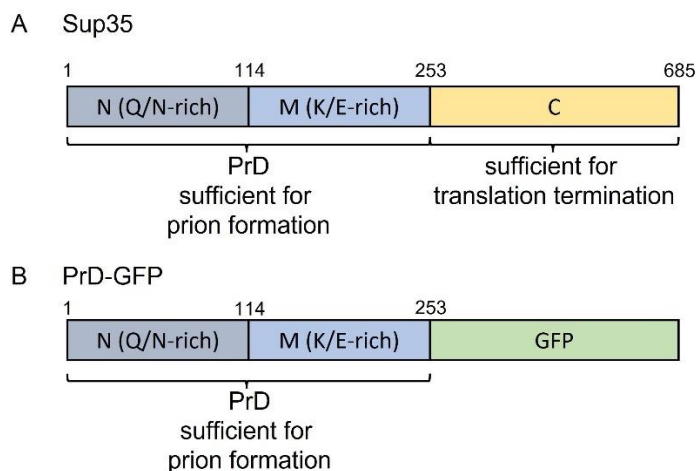


Figure 6. Domain Organization of the Sup35 and PrD-GFP proteins. **A.** The Sup35 protein contains three domains: N-terminal domain (N), middle domain (M) and the C-terminal domain (C). The C-terminal domain is necessary and sufficient for translation termination while the NM or PrD domain is sufficient for $[PSI^+]$ prion formation. **B.** Replacement of the C-terminal domain with GFP resulting in PrD-GFP serves as a visually tractable prion model to study the $[PSI^+]$ amyloid like properties in yeast¹³⁰.

1.4. Oxidative Stress

Reduction-oxidation (redox) reactions have crucial roles in mitochondrial energy production, protein quality control, as well as intracellular signal transduction. Different types of reactive molecules, including reactive oxygen species (ROS) are essential for cellular redox signalling^{222–225}. ROS include superoxide ($O_2^{\bullet-}$), hydrogen peroxide (H_2O_2), hydroxyl radical (HO^{\bullet}), as well as other reactive molecules containing oxygen, and are endogenously generated during aerobic metabolism. Perturbations in the cellular redox state play an important role in aging, but also the pathophysiology of different protein-aggregation-linked neurodegenerative diseases, e.g. Alzheimer's disease (AD), Huntington's disease (HD), Parkinson's disease (PD), or amyotrophic lateral sclerosis (ALS)²²⁶. Signs of oxidative stress-induced damage can be found in post mortem brain tissue from patients with AD, HD, and PD^{227–229}.

Levels of ROS are usually maintained at a low level in order to ensure proper cellular redox homeostasis. Oxidative stress refers to a condition, in which levels of ROS cannot be mitigated by the cellular antioxidant defence system, ultimately causing oxidation and modification of nucleic acids, lipids, carbohydrates, and proteins^{230,231}. This can occur either due to excessive production of ROS or a loss of cellular antioxidant capacity^{232,233}, or both. An important component of the antioxidant response is glutathione (GSH), which protects against a variety of ROS, as well as classical ROS-detoxifying enzymes, e.g. superoxide dismutases, catalases, and peroxidases. Excess production of ROS under oxidative stress conditions can perturb many cellular functions^{234,235}. Due to their abundance in the cell, proteins are the major target of oxidative post-translational modifications (PTMs). ROS can interact directly with a protein or react with other molecules like lipids and sugars which generates products that then react with the protein. Both peptide bonds or amino acid side-chains can be the target of such reactions. These oxidation reactions can be very site specific²³⁶ or can modify multiple residues and result in multiple products. One global oxidative PTM that is widely studied as a marker of oxidative stress and major hallmark of oxidative damage is protein carbonylation.

1.4.1. Protein Carbonylation

Protein carbonylation is an irreversible oxidation of amino acid side chains that results in chemically reactive carbonyl groups, such as aldehydes, ketones, or lactams²³⁷. Carbonyl

groups (C=O) are introduced via direct metal-catalyzed oxidation (MCO) of amino acid side chains by ROS. Additionally, secondary reactions with reactive carbonyl compounds on carbohydrates (glycoxidation products) and advanced glycation end products (AGEs) can form carbonyl derivatives on lysine, cysteine, and histidine²³⁸. Carbonylation preferentially affects side chains of the amino acids arginine, threonine, proline or lysine²³⁹ and mostly results in loss of catalytic or structural function of the affected protein. The addition of carbonyl groups causes changes in hydrophobicity, surface charge and associated misfolding of proteins. Figure 7 shows a schematic of amino acid side-chain carbonylation by MCO.

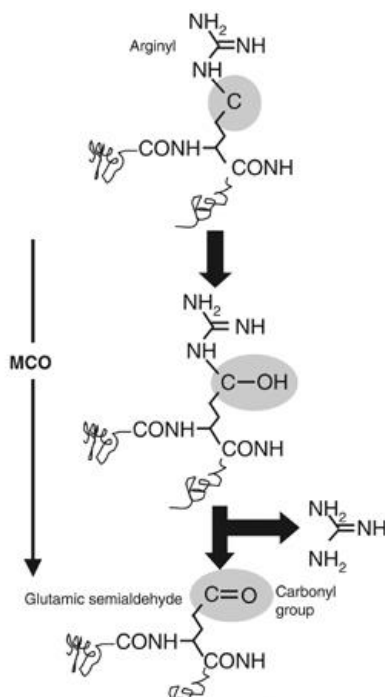


Figure 7. Carbonylation of a protein amino-acid side chain. The Formation of glutamic semialdehyde from an arginyl residue is depicted as a result of MCO. Adapted from²⁴⁰.

Oxidative stress often leads to protein carbonylation^{241,242}, which is irreversible and thus causes permanent damage^{243,244}. Therefore, protein carbonyl content is widely used as marker of protein oxidative damage²⁴⁵, including for age-related disorders²⁴⁶. Carbonylated proteins either generate cytotoxic high molecular weight aggregates or lead to abnormally high rates of protein turnover to remove them from the cell²⁴⁰.

An age-dependent increase in cellular protein carbonyl content has been observed. There are, however, multiple potentially overlapping causative factors, including a decline in the antioxidant defence system, increased ROS production, a diminished capacity for oxidized protein removal, or increased susceptibility of proteins to oxidative damage^{232,247-252}. For

instance, there has been a demonstrated decrease in catalase activity with age in certain tissues^{232,233,253}. An important factor in age- and oxidative stress-dependent ROS and protein carbonyl is the intracellular availability of free iron^{254,255}. Carbonylation levels are markedly higher in yeast mutants lacking the iron storage protein YFH1p, which can be partially rescued by expression of the human ferritin L gene that counteracts elevated carbonylation and prolongs the replicative lifespan of yeast cells²⁵⁶. Increased carbonylation has also been associated with increased tendency of aging mitochondria to produce ROS rather than a diminished activity or abundance of antioxidant defence systems^{257,258}. Furthermore, decreased proteolysis with age is a consequence of the accumulation of protease-resistant aggregates that in a sense clog up proteasomes. As a consequence of this, damaged, e.g. carbonylated, protein substrates accumulate with time²⁵⁹. Increased protein carbonylation also happens in the absence of increased ROS production or diminished ROS defence, but is rather linked to an increased production of substrates available for oxidative attack^{250,260}, which appears to be strongly associated with the production of aberrant protein isoforms²⁶⁰.

Diseases associated with increased carbonylation include Parkinson's disease, Alzheimer's disease, cancer, cataractogenesis, diabetes, and sepsis^{243,261}. Manipulations leading to extended lifespan, e.g. caloric restriction, decrease carbonylation levels in mouse mitochondria²⁶². Furthermore, levels of carbonylated proteins have been shown to be associated with the physiological age or life expectancy of an organism rather than with its chronological age²⁶³.

Aging-, starvation-, and stress-induced carbonylation does not affect the proteome uniformly²⁶¹. Studies in *E. coli* show that among the targeted proteins are the Hsp70 and Hsp60 chaperones, the histone-like protein H-NS, elongation factors EF-Tu and EF-G, glutamine synthetase, glutamate synthase, aconitase, malate dehydrogenase, and pyruvate kinase^{241,248,249}. Because some of these proteins are also specifically carbonylated in oxidatively stressed yeast cells²⁶⁴, aging flies^{252,265}, plants^{266,267} and in post mortem AD brain²⁶⁸, it can be speculated that there is a general pattern of carbonylation specificity even in distantly related organisms²⁴⁰. The molecular basis for the apparent sensitivity of some proteins to carbonylation is not well understood and some proteins, like several enzymes of the Krebs cycle and electron transport chain, may have been classified as oxidation-sensitive

because they are localised in proximity to ROS generating sites and therefore more likely to be oxidised.

The generation of a Schiff base by the reaction of a carbonyl group of one protein with an amino group from another contributes to aggregate formation of indicates that they are able to grow without further oxidation reactions²⁶⁹. While the majority of these aggregates are targeted for macroautophagy²⁷⁰, there is another storage compartment resembling the yeast IPOD in mammalian cells called the aggresome, which is aimed at specific proteins (perhaps including cytoskeletal proteins) or is an intermediate storage form^{271–273}. Furthermore, these aggregates can then contribute to oxidative stress by producing oxidants in a senescent cell²⁷⁴, supported by the presence of various metals in accumulated protein aggregates²⁷⁵.

There is, however, also evidence for a physiological role of protein carbonylation in protein quality control mechanisms. Carbonylated proteins are more susceptible to proteasomal degradation than non-carbonylated ones^{250,259,276,277}. A rapid carbonylation of an aberrant protein may direct it to the proteolytic degradation pathway rather than chaperone-mediated repair. This way, incorporation of aberrant proteins into mature complexes like ribosomes may be reduced. Another potential role of carbonylation could be in autophagy-like mechanisms, which may provide amino acids for de novo protein synthesis by targeting proteins that are no longer required or damaged. It is not clear how this process can gain specificity, but it may be that e.g. idle enzymes are more susceptible to oxidative carbonylation simply because working enzymes are protected from degradation by their substrate²⁷⁸. This would make certain enzymes more carbonylation prone in conditions with diminished substrate abundance²⁷⁸, possibly due to subtle conformational differences between the occupied working and unoccupied idle forms of the enzyme.

S. cerevisiae has evolved a Sir2p-dependent mechanism of asymmetric division that retains protein carbonyls in the mother cell during mitotic cytokinesis^{279,280}, whereby the progeny starts with a significantly reduced damage load and has full reproductive potential compared to the mother cell. In starving *E. coli* cultures, two distinct populations emerge that differ markedly in their carbonyl load²⁸¹, in which the low carbonyl cells remain reproductively competent while high carbonyl cells become genetically dead (nonculturable).

Interestingly, It has been inferred that the role of carbonylation may change over the age of an organism²⁴⁰. Originally a part of the PQS and a degradation label for aberrant, damaged or idle proteins, it can become a problem in older age by negatively influencing cellular functions like proteasomal degradation and promoting aggregation^{238,269}.

2. Materials and Methods

2.1. Materials

2.1.1. Software and Equipment

2.1.1.1. Computer software

Software	Provider
Microsoft Office	Microsoft Corp.
Excellence	Olympus Soft Imaging Solutions
ImageJ	National Institutes of Health
Image Lab v 6.0.1	Bio-Rad
Serial Cloner v 2.6.1	Frank Perez (Serial Basics)
PerseusGui v 1.6.2.3	Max Planck Institute of Biochemistry
GraphPad Prism 8	GraphPad Software Inc.
Adobe Illustrator	Adobe Systems Inc.
BioRender	https://app.biorender.com/
DAVID	Laboratory of Human Retrovirology and Immunoinformatics (LHRI)
Saccharomyces Genome Database	SGD Project. http://www.yeastgenome.org/download-data/

2.1.1.2. Equipment

Equipment	Manufacturer
pH meter	Werner Hassa GmbH
Trans-Blot Turbo™	Bio-Rad
Agarose gel chambers and trays	University Hospital workshop
T-Gradient Thermocycler	Biometra GmbH
Spectrophotometer	Eppendorf
Magnetic stirrer MR 3001 K	Heidolph
SDS gel chambers	Bio-Rad
Vortex mixer	Heidolph
Incubators	Forma Thermo Scientific
Water bath MaxQ 7000	Dinkelberg analytics
Glass ware	Schott
Centrifuges	Heraeus
Weighing Balances	Mettler
Mixer mill MM 400	Retsch
ChemiDoc Imaging Systems	Bio-Rad

2.1.1.3. Microscopes

Experiments utilizing fluorescence microscopic imaging were performed using the Olympus CellR-PointFRAP IX81 microscope at the ZMBH Imaging Core Facility, which has the following equipment features:

Feature	Details
Microscope stand	Olympus IX81, inverted microscope, motorized stage
Objectives	UPlanSApo 40x/0.95 UPlanFL N 60x/0.90 Apo N 60x/1.49 Oil UApo N 100x/1.49 Oil
Fluorescence Lamp	MT 20 illumination system with 150 W Xe or 150 W Hg/Xe arc burner
Excitation Filters	387nm/11 , 427nm/10, 470nm/40, 485nm/20, 504nm/12, 560nm/25, 572nm/35, 650nm/13
Emission Filters	Dualband CFP/YFP sbx HC filter set, Dualband GFP/mCherry sbx ET filter set, Quadband DAPI/FITC/Cy3/Cy5 sbx HC filter set
Camera	EM-CCD C9100-02 (Hamamatsu)
Software	Xcellence (Olympus)
Temperature control	Incubation Chamber (ZMBH Workshop) tempcontrol 37-2 digital and heating unit (Pecon)
Custom made heat shock stage (Olympus)	Peltier element (BelektroniG) combined with water cooling device (innovatek), Control Unit: HAT-control B-20 and Software (BelektroniG)

During a brief time this microscope could not be used, some experiments were performed using the Nikon Ni-E microscope at the Nikon Imaging Centre Heidelberg (NIC), which has the following features:

Feature	Details
Microscope stand	Upright widefield research microscope, motorized stage
Objectives	Nikon Plan Apo λ 2x NA 0.1 Nikon Plan Apo λ 10x NA 0.45 Nikon Plan Apo λ 20x NA 0.75 Nikon Plan Apo λ 40x NA 0.95 Nikon Plan Apo λ 60x NA 1.40 Oil
Fluorescence Lamp	Mercury lamp
Excitation Filters	390nm/18, 472nm/39, 543nm/22, 562nm/40, 632nm/22
Emission Filters	DAPI:460nm/60, EGFP:520nm/35, TRITC:593nm/40, TexasRed:624nm/40, Cy5:692nm/40
Camera	Nikon DS-Ri2 color camera, 24 x 36mm CMOS chip
Software	NIS-Elements AR 4.30.01

2.1.2. Expendable items

Item	Provider
Cover slides	Thermo Scientific Inc.
Cover slips, 20 x 20 mm	Menzel-Gläser (Thermo Scientific Inc.)
Cuvettes	Sarstedt AG & Co.
Falcon tubes 15, 50 ml	Greiner
Petri dishes	Greiner
Microcentrifuge tubes, 1.5 ml, 2 ml	Sarstedt AG & Co.
Low protein binding microcentrifuge tubes, 2 ml	Sigma Aldrich
Low protein binding microcentrifuge tubes, 1.5 ml	Eppendorf
PCR tubes, 200 µl	Kisker Biotech GmbH & Co.
Trans-Blot Turbo RTA Mini Nitrocellulose Transfer Kit	BioRad
Sterile filters, 0.2 µM	GE Healthcare
Whatman paper, 3 mm	Schleicher & Schuell
Costar 96-well plate	Greiner
PolarSafe Label Strips	Sigma Aldrich
PolarSafe Label Dots	Sigma Aldrich
reinforced bead mill tubes 2ml	VWR
Ampule breakers	Thermo Fisher
Disposable SteriStoppers, 20mm, 28mm and 32mm	neolab

2.1.2.1. Chemicals

If not mentioned differently, all chemicals were purchased from Roth, Sigma Aldrich, Invitrogen, AppliChem or Merck.

Enzymes and protease inhibitors

Reagent	Provider
100X Protease Inhibitor Cocktail (#5871S)	CST
Leupeptin (microbial, >90%) (#L2884)	Sigma Aldrich
Pepstatin A	Pepta Nova GmbH
Aprotinin	AppliChem
Phenylmethylsulfonyl Fluoride (PMSF)	Sigma-Aldrich Co.
OptiTaQ DNA Polymerase (#E2600-03)	roboklon
MyTaQ Red DNA Polymerase (#21109)	Bioline
Velocity DNA polymerase (#21098)	Bioline
AmpliTaQ Gold (#4311806)	Thermo Scientific
Restriction Enzymes	NEB
Zymolyase 100T	Amsbio

Standards and Kits

Reagent	Provider
Proteo Silver silver stain kit (#PRTOSIL1)	Sigma Aldrich
Pierce BCA Protein Assay kit (#23227)	Thermo Fisher
peqGOLD Plasmid Miniprep Kit (#13-6943-02)	PeqLab
QIAquick Gel Extraction Kit	QIAGEN GmbH
GeneRuler 1 kb Plus DNA Ladder (#SM1331)	Thermo Scientific Inc.
PageRuler Prestained Protein Ladder (#26616)	Thermo Scientific Inc

Media Components

Reagent	Provider
Bacto Agar	BD Biosciences
Bacto Peptone	BD Biosciences
Bacto Tryptone	BD Biosciences
Bacto Yeast extract	BD Biosciences
Difco Yeast Nitrogen Base w/o amino acids	BD Biosciences
Complete Supplement Mixture (CSM) (amino acids for drop out media)	MP Biomedicals, LLC

Antibiotics

Only final concentrations are listed here. All stock solutions were filter sterilized.

Reagent	Final conc.	Provider
G418 sulfate (#ALX-380-013-G005)	200 µg/ml	Enzo life sciences
Ampicillin	100 µg/ml	Sigma-Aldrich Co.
ClonNAT (Nourseothricin) powder(#AB-102XL)	200 µg/ml	Jena Bioscience
Hygromycin B	250 µg/ml	Carl Roth

Other Chemicals and Reagents

Reagent	Provider
D(+) Galactose	Roth
D (+) Raffinose (#R0250)	Sigma Aldrich
Bromphenol blue	Sigma Aldrich
Guanidine hydrochloride	Sigma Aldrich
poly(ethylene glycol) (#P4338)	Sigma Aldrich
Tween™ 20 Surfact-Amps™ Detergent Solution (#85113)	Thermo Fisher
Lithium Acetate Dihydrate (#L4158)	Sigma Aldrich
DMSO (sterile, cell-culture grade) (#D2650)	Sigma Aldrich
di-Potassium hydrogen phosphate	Sigma Aldrich
Potassium dihydrogen phosphate	Sigma Aldrich
GFP-Trap magnetic agarose beads (#gtma-20)	Chromotek
Amersham ECL Western Blotting Detection Reagent (#RPN2106)	GE Life Sciences
Quick Coomassie Stain (#GEN-QC-STAIN)	ProteinArk
4-20% mini-PROTEAN TGX precast gels, 15µl,30µl and 50µl wells	BioRad
Ponceau S solution (#P7170)	Sigma Aldrich
Gel Red Nucleic Acid Stain (#41003)	Linaris / Biotium
salmon sperm ssDNA (#D9156-5X)	Merck
RT-PCR-grade water (Invitrogen) (#AM9935)	Thermo Fisher
Paraformaldehyde (PFA)	Sigma Aldrich
DH5alpha competent E.coli (20 X 50µl) (#C2987H)	NEB
Agarose	Sigma Aldrich
dNTP mix (5mM each) (#AB0196)	Thermo Fisher
Valinomycin (#V3639)	Sigma Aldrich
MG132 (Z-Leu-Leu-Leu_al) in DMSO (#M7449)	Sigma Aldrich
Menadione sodium bisulfate (#M5750)	Sigma Aldrich

2.1.2.2. Media and Buffers

Growth media were autoclaved prior to usage. For preparation of agar plates, 2% (w/v) autoclaved agar was added to the medium prior to pouring on the plates.

Medium	Components
LB medium (Luria-Bertani)	10g/l tryptone, 5 g/l yeast extract, 10 g/l NaCl
YPD/YPGal/YPRaff	20 g/l peptone 10 g/l yeast extract 20 g/l D-Glucose /Galactose/Raffinose
YPGly	
SD (Synthetic Dropout) medium	1.7 g/l Yeast Nitrogen Base w/o amino acids and ammonium sulphate 0.7 g/l CSM mix (according to desired dropout) 5 g/l ammonium sulfate or 1 g/l glutamic acid 2% (v/v) desired sugar, added post sterilization
PBS	137 mM NaCl 2.7 mM KCl 10 mM Na ₂ HPO ₄ 2 mM NaH ₂ PO ₄ pH was adjusted to 7.4 with HCl

2.1.2.3. Plasmids and Primers

Plasmids

Name	Purpose	Markers	Resistance	Origin
O-3185 pAG415GPD:eGFP_μNS	constitutive eGFP-μNS expression		Amp	Alberti lab
O-3193 pAG304GAL:eGFP_μNS	inducible eGFP-μNS expression		Amp	Alberti lab
pMaM44	3xmCh tag	HygB	Amp	Knop lab
pYM25	GFP tag	HygB	Amp	Knop lab
pFA6a-KanMX	deletion cassettes	G418	Amp	Knop lab
pFA6a-hphNT1	deletion cassettes	HygB	Amp	Knop lab
pFA6a-natNT2	deletion cassettes	CloNA T	Amp	Knop lab
pBS35	mCh tag	HygB	Amp	Knop lab

p425 Gal1 Rnq1-mCh	inducible Rnq1-mCh expression		Amp	Bukau lab
p303 Gal1 Rnq1-mCh	inducible Rnq1-mCh expression	His	Amp	Bukau lab, modified
pMaM45	3xmCh tag	CloNA T	Amp	Knop lab
pMaM12	3xmCh tag	G418	Amp	Knop lab
pFA6a-neon-HA-natNT2	mNeonGreen-HA tag	CloNA T	Amp	Schuck lab

Primers

Gene	Type	Sequence
OM45	Forward	TAAGGGTGATGGTAAATTCTGGAGCTCGAAAAAGGACTAGGGTCGACGGATCCCGGG
	Reverse	ATGTTATGCGGGAACCAACCCTTTACAATTAGCTATCTAAATCGATGAATTCGAGCTCG
	check	CAACTTTCCAAGGACGAAATG
Pex11	Forward	ATCTATCCTTGGTATGCAAGACATGTGGAAAGCTACATAGGGTCGACGGATCCCGGG
	Reverse	GCGGAGAATAGCCAAATAAAAAAAAAAAGATGAAAAGAAAGATCGATGAATTCGAGCTCG
	check	AAAGTGATTCCTGTAACCGTTC
RPL25	Forward	CGATGCTTTGGACATTGCTAACAGAATCGGTTACATTTAAGGTCGACGGATCCCGGG
	Reverse	GAAAAATTTAAAAATAATATTTAAATTTATTAATTAACCAATTAGAATCGATGATTCGAGCTCG
	check	GCTCCAAAATATGCTTCCAAGG
Pre6	Forward	GCAGCAAGAGCAGGACAAAAAGAAAAATCTAACCATTAAGGTCGACGGATCCCGGG
	Reverse	AAACGGCGATATATATTGGGCATAAAACCTATATAAAATAATCGATGAATTCGAGCTCG
	check	GCTTTACCAGACCGAGCCAAG
Atg32	S1	CCTAATCACAAAAGCAAAAAAATCTGCCAGGAACAGTAAACATATGCGTACGCTGCAGGTCGAC
	S2	GTAAAAAAGTGAGTAGGAACGTGTATGTTTGTGTATATTGAAAAAGGTTAA TCGATGAATTCGAGCTCG
	delta check	AGACGGCTGAAGGGACGACATC
Lys2	S1	CTGCTAATTATAGAGAGATATCACAGAGTTACTACTAATGCGTACGCTGCAGGTCGAC
	S2	TTATTGTACATGGACATATCATAACGTAATGCTCAACCTTAATCGATGAATTCGAGCTCG
	delta check	CGGACGGTGTTCGTCAAGGGC
	upstream	CCTTGTGATCTTCACAGGTCG
	downstream	GAATATAGACGTAACAAAGGCAC
Pex3	S2	GCTATATATATATATATTCTGGTGTGAGTGTCAGTACTTATTCAGAGATTAATCGATGAATTCGAGCTCG

	S3	GTATACAGCAACTTTGGCGTCTCCAGCTCGTTTTCTTCAAGCCTCGTACGCTG CAGGTCGAC
OM45	S2	GTATATATGTTATGCGGGAACCAACCCTTTACAATTAGCTATCTAACTAATCGA TGAATTCGAGCTCG
	S3	GAATGGAATGATAAGGGTGATGGTAAATTCTGGAGCTCGAAAAAGGACCCTGA CGCTGCAGGTCGAC
	check	CAACTTTCCAAGGACGAAATG
Pex11	S2	CATAAGCGGAGAATAGCCAAATAAAAAAAAAAAGATGAAAAGAAAGCTAATCG ATGAATTCGAGCTCG
	S3	GGTGTGTGCATCTATCCTTGGTATGCAAGACATGTGGAAAGCTACACGTAC GCTGCAGGTCGAC
	check	AAAGTGATTCTGTAAACCGTTC
RPL25	S2	GAAAAATTTAAAAATAATATTAATTTATTAATTAACCAATTAGATTAATCGA TGAATTCGAGCTCG
	S3	GCTGACTACGATGCTTTGGACATTGCTAACAGAATCGGTTACATTCGTACGCT GCAGGTCGAC
	check	GCTCCAAAATATGCTTCCAAGG
UBP3	S1	GCTACCATCATCCAGGTACCGCTTTCCTTCCATCATCATTAATAAAAAATGCGT ACGCTGCAGGTCGAC
	S2	CTATATTATTTTTATGTATTTTGTCTATAATACCACCCCGTCTTAATCGATGA ATTCGAGCTCG
	delta check	GATCACTCTCCCACCAGCGTAC
BRE5	S1	GCATTTGAAGTCATACCCCTCGAATAGAAGTATCAAATAAAAGAAAATGCGTAC GCTGCAGGTCGAC
	S2	CAAATTTTTTATTATTTTTCAATTTTTCTTTTTAAAAGGCTTGTGGTTGACTAA TCGATGAATTCGAGCTCG
	delta check	CGAAGACTGTACAAGTGGTAGTAC
Erg6	S1	
	S2	
	delta check	GCATCCATCAGTTGCCACCCTCC
Pre6	S2	
	S3	
	check	GCTTTACCAGACCGAGCCAAG
Pre10	S2	
	S3	
	check	CAGCAAGAGAGGCCGTTAAAC
Rpn5	S2	
	S3	
	check	GGTGGAGAAGCTAATAAGCATC
KanB		CTGCAGCGAGGAGCCGTAAT
Rev_m Ch		CTCGAAGTTCATCACGCGCTC
Pdc1	S1	<i>CTCATAACCTCACGCAAATAACACAGTCAAATCAATCAAAAATGCGTACGCTGC AGGTCGAC</i>
	S2	GCTTATAAACTTTAACTAATAATTAGAGATTAATCGCTTAATCGATGAATTC GAGCTCG
	S3	GGTTGAACAAGCTAAGTTGACTGCTGCTACCAACGCTAAGCAACGTACGCTGC AGGTCGAC
	check	CATGATCAGATGGGGCTTGAAG

Hsp42	S1	GTCCATATCCCACACAAATTAAGATCATACCAAGCCGAAGCAATGCGTACGCTGCAGGTCGAC
	S2	CGCTTATTATAAATAAATGTATGTGTGTATAAACAGATACGATATTCAATCGATGAATTCGAGCTCG
	delta check	CATACTTCAATTCAGCTTTCCC
Tsa1	S1	CGTTCAATTGCTCACAACCAACCACAACACTACATACACATACATACACAATGCGTACGCTGCAGGTCGAC
	S2	GTGAATTTTAAATAAGTAGTCATTTAGACAACGCAAGCGTCTTATATCGATGAATTCGAGCTCG
	S3	GCCAACCGTTGAAGACTCCAAGGAATACTTCGAAGCTGCCAACACGTACGCTGCAGGTCGAC
	check	GGCATGGACCAATATCCCAAG
Atg7	S1	GATAACTAAAGTTCATTATATTTCAACAAATATAAGATAATCAAGAATAAAATGCGTACGCTGCAGGTCGAC
	S2	GGAAAGTGGCACCACAATATGACCAATGCTATTATATGCAAAATATTAATCGATGAATTCGAGCTCG
	delta check	CACCAAAGAATGGAGAGTAG
Ndi1	S2	CGGTGCCTACCACCTTTTTCTTTTTCCAGAAAAGGGCATGTTAATTTTCATCTATCGATGAATTCGAGCTCG
	S3	CTTTTTCGACTGGATTAATAGCATTTCAAAAGAGACTTTTTTAAAGGATTACGTACGCTGCAGGTCGAC
	check	CAAGAATTTTGATAAAATGGCTC
Qcr2	S2	CTATATATATATTTGCCTTTTCGTTTTTCGTTTTGTACAAATACTTTCTCTTAATCGATGAATTCGAGCTCG
	S3	CAACTATGTAGCCGTCGGTGATGTTTCCAACCTGCCATATTTGGACGAATTGCGTACGCTGCAGGTCGAC
	check	CTCTGCCCTATCCGAGCTTTCC
Fas1	S2	GGAGTTTCAAAGTTAAATATTTCTTACGGTTATATAATCACTTAAGAAATTAATCGATGAATTCGAGCTCG
	S3	GGCTCCGAACCTATCAAGGAAATCATCGACAACGTTGGAAAAGTATGAACAATCCCGTACGCTGCAGGTCGAC
	check	CATTGACGAAGCTTCCAAGAAATC
Eno1	S2	GACAAAAAACGTGTTTTTGGACTAGAAGGCTTAATCAAAGCTTTAATCGATGAATTCGAGCTCG
	S3	GGTGACAACGCTGTTTTTCGCTGGTGAAAACCTCCACCACGGTGACAAATTACGTACGCTGCAGGTCGAC
	check	GCTACCGCTATCGAAAAGAAGG
Cuz1	S1	GATATAAAAAAAGGACCATCAACTAATTTTTGCTATATTTAAGAATGCGTACGCTGCAGGTCGAC
	S2	CGCTTGACGTTCCGCGGATTGTTTGTATTTATAGTGCCTTCTTAATCGATGAATTCGAGCTCG
	delta check	CCTTGCTTTCATATTTTAAATG
Snx4	S1	CTTTATTTACGGTATACCACAATACTGCTCTTTTTGTTGAGGATATGCGTACGCTGCAGGTCGAC
	S2	CGTAGTGCCCAAGGTATTATCAGTAATGGGAAAACATTAAGAGCACCCTAATCGATGAATTCGAGCTCG
	delta check	CACCCTATAAAATCTATATGC
Pab1	S2	GATGATAAGTTTGTGAGTAGGGAAGTAGGTGATTACATAGAGCATTAAATCGATGAATTCGAGCTCG

	S3	GCCTATGAGTCTTTCAAAAAGGAGCAAGAACAACAACTGAGCAAGCTCGTA CGCTGCAGGTCGAC
	check	CCCAATGGGCGGTATGCCAAAG
Fas1	S2	GGA GTT TCA AAG TTA AAT ATT TCT TAC GGT TAT ATA ATC ACT TAA GAA ATT AAT CGA TGA ATT CGA GCT CG
	S3	GGC TCC GAA CCT ATC AAG GAA ATC ATC GAC AAC TGG GAA AAG TAT GAA CAA TCC CGT ACG CTG CAG GTC GAC
	check	CAT TGA CGA AGC TTC CAA GAA ATC
KanB		CTG CAG CGA GGA GCC GTA AT
mCherry	reverse	CTC GAA GTT CAT CAC GCG CTC
Dnm1	S1	CAT TAA GTA GCT ACC AGC GAA TCT AAA TAC GAC GGA TAA AGA ATG CGT ACG CTG CAG GTC GAC
	S2	CGC CCG CAA TGT TGA AGT AAG ATC AAA AAT GAG ATG AAT TAT GCA ATT AAT CGA TGA ATT CGA GCT CG
TRX1	reverse	CAG TAT AGA AAC ACA ATA TAT CGG TCA TTG GGT GAG TTT AAT CGA TGA ATT CGA GCT CG
	forward	CAA CCC AGC GGC TAT TAA GCA AGC CAT TGC TGC TAA TGC TGG TCG ACG GAT CCC CGG G
	check	ATG GTT ACT CAA TTC AAA AC
TRS33	forward	CAA GGG AGT TAG CTT CCA TGT TCA AGT CAC AAT GCC GCA GGG TCG ACG GAT CCC CGG G
	reverse	TCG ATG TAC ATT CTT AGA ACA AAA ATC TGT CGG ACC TTT AAT CGA TGA ATT CGA GCT CG
	check	GTC TGG AAA CAA ATA TTT GG
FRE7	reverse	GAA TGA TAT TTC ACA TGG TGG ATG CCA TCT GTT TCC TAC TAA TCG ATG AAT TCG AGC TCG
	forward	TGT CGA AGA GTG CTA TTT ACA CAG CGA GAG TTT TGG CTA CGG TCG ACG GAT CCC CGG G
	check	CAA TAG ACA CCG CCA GTG ACC
CYC1	forward	CAG AAA CGA CTT AAT TAC CTA CTT GAA AAA AGC CTG TGA GGG TCG ACG GAT CCC CGG G
	reverse	CTA ATT ACA TGA TAT CGA CAA AGG AAA AGG GGC CTG TTT AAT CGA TGA ATT CGA GCT CG
	check	GGT TCT GCT AAG AAA GGT GC
Sod2	forward	CTG GAA AGA AGC ATC CAG AAG ATT CGA TGC TGG CAA GAT CGG TCG ACG GAT CCC CGG G
	reverse	GTG GAA AAA AAA AGG TAT TTT CTT TCT TTC TTT CTT CAG ATC GAT GAA TTC GAG CTC G
	check	CGC TTT GGC AAA GGC AAT CGA C
GOR1	forward	CAA AAT GAA GAC TGG CCC AAT GAA TCT AAG CCA TTA GTT GGT CGA CGG ATC CCC GGG
	reverse	CAT TTC GAA AGG AAG AAT AAA ACT ATG GAT CTT GTA GTC AAT CGA TGA ATT CGA GCT CG
	check	GAT GGT GTA GTT ATT GTT AAC

2.1.2.4. Yeast strains

Strain	Genotype	Origin
Y8505	MAT α can1 Δ ::STE2pr-SpHIS5 lyp1 Δ ::STE3pr-LEU2 his3 Δ 1 leu2 Δ 0 ura3 Δ 0	282
Y8205 ΔNM	Y8205 Δ PrD (SUP35)::URA3	Tyedmers lab
Y8205A	Y8205 Δ PrD (SUP35) [<i>PrD-GFP</i>] ⁺ ::URA3	Tyedmers lab
SZ1	Y8205A	This study
SZ2	Y8205A OM45-GFP::hphNT1	This study
SZ3	Y8205A Pex11-GFP::hphNT1	This study
SZ4	Y8205A Rpl25-GFP::hphNT1	This study
SZ5	Y8205A atg7 Δ ::natNT2	This study
SZ6	Y8205A pab1-mCh::hphNT1	This study
SZ7	Y8205A pab1-mCh::hphNT1 cuz1 Δ ::natNT2	This study
SZ8	Y8205A Eno2-mCH::hphNT1	This study
SZ9	Y8205A Tdh3-mCh::hphNT1	This study
SZ10	Y8205A Hsp30-mCh::hphNT1	This study
SZ11	Y8205A hsp30 Δ ::natNT2	This study
SZ12	Y8205A hsp42 Δ ::natNT2	This study
Y8205B	Y8205 Δ PrD (SUP35)::URA3 [<i>PrD-GFP</i>] ⁺ @Sup35C::hphNT1	Tyedmers lab
Y8205A cured	Y8205 Δ PrD (SUP35) [<i>prd-gfp</i>] ⁻ ::URA3	Tyedmers lab
BY4741	MAT α his3 Δ 1 leu2 Δ 0 met15 Δ 0 ura3 Δ 0	283
SZ13	BY4741 pAG415GPD-EGFP- μ NS	This study
SZ14	BY4741 pAG304GAL-EGFP- μ NS	This study
SZ15	BY4741 OM45-GFP::hphNT1	This study
SZ16	BY4741 Rpl25-GFP::hphNT1	This study
SZ17	BY4741 Pex11-GFP::hphNT1	This study
SZ18	BY4741 Pre6-GFP::hphNT1	This study
SZ19	BY4741 Pre6-GFP::hphNT1 cue5 Δ ::natNT2	This study
SZ20	BY4741 Rpn55-GFP::hphNT1	This study
SZ21	BY4741 Pab1-GFP::hphNT1	This study
SZ22	BY4741 Pab1-GFP::hphNT1 cuz1 Δ ::natNT2	This study
SZ23	BY4741 OM45-GFP::hphNT1 erg6 Δ ::natNT2	This study
SZ24	BY4741 Rpl255-GFP::hphNT1 erg6 Δ ::natNT2	This study
SZ25	BY4741 OM45-GFP::hphNT1 atg7 Δ ::natNT2	This study
SZ26	BY4741 Rpl255-GFP::hphNT1 atg7 Δ ::natNT2	This study
C-SWAT general	MAT α leu2 Δ 0::GAL1pr-NLS-Scel-natNT2 can1 Δ ::STE2pr-SpHIS5 lyp1 Δ ::STE3pr-LEU2 his3 Δ 1 ura3 Δ 0 met15 Δ 0 ORF::mNeongreen-hph	284
C-SWAT 1	C-SWAT Ndi1-mNG-hph	284

C-SWAT 2	C-SWAT Qcr2-mNG-hph	284
C-SWAT 3	C-SWAT Tom20-mNG-hph	284
C-SWAT 4	C-SWAT Adh3-mNG-hph	284
C-SWAT 5	C-SWAT Adh6-mNG-hph	284
C-SWAT 6	C-SWAT Ald6-mNG-hph	284
C-SWAT 7	C-SWAT Eno1-mNG-hph	284
C-SWAT 8	C-SWAT Fas1-mNG-hph	284
C-SWAT 9	C-SWAT Tsa1-mNG-hph	284
C-SWAT 10	C-SWAT SCP160-mNG-hph	284
C-SWAT 11	C-SWAT FKS-mNG-hph	284
C-SWAT 12	C-SWAT Hsp60-mNG-hph	284
C-SWAT 13	C-SWAT Pgk1-mNG-hph	284
C-SWAT 14	C-SWAT Rpl25-mNG-hph	284
C-SWAT 15	C-SWAT Rpl6B-mNG-hph	284
C-SWAT 16	C-SWAT Cdc19-mNG-hph	284
C-SWAT 17	C-SWAT Snq2-mNG-hph	284
C-SWAT 18	C-SWAT Pdc1-mNG-hph	284
BY4742	MAT α his3 Δ 1 leu2 Δ 0 lys2 Δ 0 ura3 Δ 0	283
BY4742 Pdc1-mCh	BY4742 Pdc1-mCh::hphNT1	Tyedmers lab
74D ΔNM	74D-694- Δ PrD (SUP35)::TRP1	Tyedmers lab
74D ΔNM GPD-GFP-μNS	74DdeltaNM pAG415GPD-EGFP- μ NS	This study
LT1a	74D-694- Δ PrD (SUP35) [<i>PrD-GFP*</i>]::TRP1	Tyedmers lab
SZ27	LT1a lys2 Δ ::natNT2	This study
SZ28	LT1a OM45-3xmCh::hphNT1	This study
SZ29	LT1a Pex11-3xmCh::hphNT1	This study
SZ30	LT1a Rpl25-3xmCh::hphNT1	This study
SZ31	LT1a atg7 Δ ::natNT2	This study
CT1b	74D-694- Δ PrD (SUP35) [<i>PrD-YFP*</i>]::TRP1	Tyedmers lab
CT1b Pdc1-CFP	CT1b Pdc1-CFP::hphNT1	Tyedmers lab
MT1b	74D-694- Δ PrD (SUP35) [<i>prd-gfp-</i>]::TRP1	Tyedmers lab
SZ32	MT1b lys2 Δ ::natNT2	This study
SZ33	MT1b OM45-3xmCh	This study
SZ34	MT1b Pex11-3xmCh	This study
SZ35	MT1b Rpl25-3xmCh	This study
SZ36	MT1b atg7 Δ ::natNT2	This study

2.1.2.5. Antibodies

Antibody	Provider
mouse anti-GFP clones 7.1 and 13.1 (#11814460001)	Roche
rabbit anti-DNP-KLH (#A-6430)	Invitrogen

mouse anti-HA clone 16B12 (#901514)	BioLegend
anti-mouse IgG, HRP-linked Antibody (#7076)	Cell Signaling
rabbit anti-RFP (polyclonal) (#ab6556)	Chromotek
donkey anti-rabbit Alexa 594 (#A32754)	Thermo Fisher
goat anti-mouse Alexa488 (#A-11001)	Thermo Fisher
donkey anti-mouse Alexa594 (#A-21203)	Thermo Fisher
goat anti-rabbit Alexa488 (#A-11008)	Thermo Fisher

2.2. Methods

2.2.1. Molecular Biology Methods

2.2.1.1. Agarose gel electrophoresis

In order to prepare 1% agarose gels, agarose was boiled in 0.5X TBE, 1X GelRed (from 10000X stock from Biorline) was added when the molten agarose had cooled to handwarm. The molten agarose was poured into a flat-bed tray with combs and left to solidify. The gel was transferred to an electrophoresis chamber filled with 0.5X TBE. Samples were prepared with Orange loading dye (Thermo Scientific), loaded onto the gel and electrophoresis was carried out at a constant voltage of 100 – 140V until the dye reached the bottom part of the gel. The gel was visualized under UV trans-illumination using the GelDoc XR+ (BioRad) system's GelRed programme.

2.2.1.2. Restriction digestion of DNA

Restriction digestion of plasmid DNA was carried out to linearize a plasmid before either genomic integration or PCR reaction. About 1U of restriction enzyme/ μ g DNA was used to digest the plasmid in a 50 μ l reaction, which was carried out as per the manufacturer's instructions.

2.2.1.3 Purification of DNA fragments

Linearized plasmid DNA or PCR products were separated via agarose gel electrophoresis, the band corresponding to the required DNA fragment was excised from the gel using a sterile scalpel and transferred to a fresh 2ml reaction tube. The DNA was then extracted from the gel and purified using the QIAquick Gel Extraction and PCR purification kit (Qiagen) as per the manufacturer's instructions.

2.2.1.4. Polymerase Chain Reaction (PCR)

PCR was used to amplify fusion or knockout cassettes for the genetic manipulation of yeast as well as checking the correct genomic insertion/integration or deletion, respectively. The PCR reaction was performed with a total volume of 50 – 100µl. The PCR reaction was performed in 50-100 µl total volume containing 0.4 µM of each primer, template DNA (plasmids: 25–200ng, genomic DNA: 0.5–1µg) and 1X PCR Buffer (using the buffer recommended by the respective manufacturer). Amplification of expression or deletion cassettes was done using either OptiTaQ (using Buffer B) or AmpliTaq Gold (using PCR Gold Buffer and 6µM MgCl₂). Correct genomic integration and deletions were verified by a colony PCR using MyTaq Polymerase (in MyTaqRed Buffer). PCR programmes can be found in table below.

OptiTaQ PCR reaction mix

Reagent	Amount
10X Buffer B	10 µl
dNTP mix (5mM each)	3 µl
Forward primer (Eurofins) 100 uMol/ µl	0.4 µl
Reverse primer (Eurofins) 100 uMol/ µl	0.4 µl
Template DNA	20-50 ng
OptiTaQ DNA Polymerase, 5 U/µl	1 µl
ddH ₂ O	adj 50 µl

PCR cycling conditions

PCR steps	Temperature	Time	Cycles
Initial denaturation	95 °C	3 min	1
Denaturation	95 °C	30 s	33
Annealing	55 °C	30 s	
Extension	72 °C	1 min/1 kb	
Final Extension	72 °C	7 min	1

Colony PCR reaction mix

Reagent	Amount
5X MyTaq red reaction buffer	10 µl

Forward primer (Eurofins) 100 uMol/ μ l	0.2 μ l
Reverse primer (Eurofins) 100 uMol/ μ l	0.2 μ l
MyTaq red DNA polymerase	0.3 μ l
ddH ₂ O	adj 50 μ l

Colony PCR cycling conditions

PCR steps	Temperature	Time	Cycles
Initial denaturation	95 °C	1 min	1
Denaturation	95 °C	20 s	33
Annealing	55 °C	20 s	
Extension	72 °C	30 s/1 kb	
Final Extension	72 °C	7 min	1

2.2.2. Bacterial methods

2.2.2.1. Transformation of competent *E.coli*

A 50 μ l aliquot of competent *E. coli* cells was thawed on ice, after which 1-2 μ l (~100ng) DNA was added and mixed by pipetting. The mixture was incubated on ice for 30min, then heat shocked for 30s at 42°C. 950 μ l of SOC outgrowth medium was added to the cells and the tube was placed at 37°C with vigorous shaking (300rpm) on a heat block for 1h. Selection plates of antibiotic containing LB agar were warmed to 37°C. 50-100 μ l of the cell-DNA-mixture were spread onto plates, which were incubated over night at 37°C. A positive control transformed with pUC19 DNA (Thermo Fisher) and a negative control “transformed” with water were added in order to assess protocol success, background colony formation as well as transformation efficiency.

2.2.2.2. Plasmid isolation

Transformed *E. coli* colonies were picked and grown in 8ml antibiotic containing liquid LB media over night at 37°C and 160rpm. 1ml of culture was kept at 4°C for potential glycerol stock preparation of successful transformants. Plasmid DNA was extracted using the standard peqGOLD plasmid miniprep kit (PeqLab, VWR) and stored at -20°C. A test restriction digestion was performed on miniprep products with appropriate restriction enzymes and resulting DNA fragments were separated alongside undigested plasmid using agarose gel electrophoresis. DNA concentrations of the samples were measured using the Nanodrop 2000 system.

2.2.3. Yeast Methods

2.2.3.1. Yeast transformation

Yeast cells were transformed using a standard lithium acetate (LiOAc)/single stranded salmon testes carrier DNA (ssDNA)/polyethylene glycol (PEG) method. A 30ml over night pre-culture of the desired yeast mother strain was inoculated the evening before transformation and grown at 30°C and 150rpm. The next morning, stationary phase cultures were diluted into 30ml of YPD and grown at 30°C and 150rpm. The 30ml of liquid culture of yeast cells in logarithmic growth phase (OD600 of 0.5 to 1.3) in YPD were pelleted by centrifugation for 5min at 5000rpm at RT, washed once with 50ml sterile H₂O and resuspended in 1ml of transformation buffer (100mM LiOAc, 10mM Tris-HCl pH 7.6, 1mM EDTA). Fresh 1.5ml reaction tubes were prepared with 10µl ssDNA and the DNA to be transformed (10µl of PCR product or 1µl of linearized plasmid). To this DNA mixture, 100µl competent yeast cells were added and the mixture was vortexed briefly to mix it. The mixture was vortexed again after addition of 600µl of plate buffer (40% PEG, 100mM LiOAc, 10mM Tris-HCl pH 7.6, 1mM EDTA). The transformation mix was then incubated for 30min at 30°C and 300rpm on a heat block. DMSO was added to 10% and the transformation mix was heat shocked for 15min at 42°C in a heat block. The cells were pelleted by centrifugation for 30s at 13 000rpm, the supernatant discarded and the cells were resuspended in 100µl sterile water, then spread on appropriate selective plates. The plates were incubated at 30°C for several days until colonies appeared. Positive clones were confirmed by colony PCR, microscopy and/or western blot.

2.2.3.2. Spotting Assay

A serial dilution spotting assay was performed in order to check cell viability after application of different stressors. These stressors were as follows: nitrogen starvation, 0.5mM menadione, 1mM H₂O₂, 4µM valinomycin, 5mM NaAsO₂, 8µM MG132, or change of carbon source. A pre-culture of yeast was grown over night at 30°C and 150rpm, then diluted to an OD600 of 0.15 into 30ml YPD and grown to an OD600 of 0.4. Cells were further grown in the absence and presence of the stressors for 2h. The OD600 was adjusted to 0.5. These cells were further 5-fold serial diluted and spotted onto YPD plates. Plates were incubated 30°C for 2-3 days and imaged.

2.2.3.3. Preparation of yeast cell lysates for western blot

Yeast cells were grown to mid-log phase. A volume of culture with equivalent to OD600 of 1.0 was centrifuged, resuspended in 500 µl of 0.2 M NaOH and incubated on ice for 15min. Cells were again centrifuged, and the pellet was resuspended in 100 µl of 5X sample buffer, then boiled at 95°C for 15 min. For analysis by SDS-PAGE and western blot, 10µl protein extract was loaded.

2.2.3.4. Preparation of yeast cell lysates for IPOD enrichment using a bead mill (Cryolysis)

50 ml of a yeast culture in logarithmic growth phase at an OD600 ~ 0.6 – 1.0 were harvested by centrifugation at 3500rcf for 10min in a 50ml conical tube. The pellet was resuspended in 200µl cryolysis buffer and transferred to a safe-lock 2ml tube and centrifuged at 13000rpm for 2min. The supernatant was discarded and the pellet resuspended in 100µl cryolysis buffer. These samples were frozen in liquid nitrogen for several minutes, then thawed on ice. In the meantime, fresh 2ml safe-lock tubes were placed into an adaptor for a Retsch Mixer Mill MM 400, a 7mm stainless steel bead was added to each tube and the set-up was submerged in liquid nitrogen. The thawed sample was dripped into the prepared tubes containing liquid nitrogen using a P200 pipette to make small enough drops. After boiling out the liquid nitrogen, the tubes were closed and placed back into the adaptor, which was secured into a Retsch Mixer Mill MM 400 and agitated three times for 2 min at 30 Hz. The samples were cooled in liquid nitrogen in between the two rounds of agitation. The resulting powder of lysed cells was transferred into a fresh safe-lock 1.5 ml tube and resuspended in 500 µl of cryolysis buffer, spun at 7500rpm and 4°C for 5min to remove the cellular debris. The resulting supernatant was transferred to a fresh tube and spun down again at 13000 rpm for 1h at 4°C to separate the insoluble fraction from the soluble fraction.

Cryolysis buffer

Reagents	0.5mM EDTA pH 8, 150mM NaCl, 10mM Tris, 0.2% NP40, adjust to 50ml with ddH ₂ O
Directly before use:	add 100X protease inhibitor cocktail to a final concentration of 1X

2.2.4. Biochemical methods

2.2.4.1. BCA Assay

To determine the samples' protein concentration, a microplate Pierce BCA Protein Assay (Thermo Fisher Scientific) was performed according to manufacturer's instructions.

2.2.4.2. SDS -polyacrylamide gel electrophoresis (SDS-PAGE)

Separation of proteins by molecular weight was achieved by SDS-PAGE under denaturing conditions. The protein samples were diluted to the same concentration of total protein in SDS sample buffer and incubated at 95°C for 20-30 min. The samples were then loaded into 4-20% mini-PROTEAN TGX precast gels (Bio-Rad). Electrophoresis was performed at 150-200V until the dye front reached the bottom of the gel. These gels were then used for Coomassie/silver staining or western blot.

Buffer	Reagents
5X SDS Loading buffer	0.25% (w/v) Bromophenol Blue, 50% (w/v) Glycerol, 10% (w/v) SDS, 0.25M Tris HCl pH 6.8
10X Running Buffer	30.3 g Tris, 144 g Glycine, 10 g SDS, adj. to 1l with ddH ₂ O

2.2.4.3. Coomassie-Silver staining

SDS-PAGE gels were stained with Coomassie brilliant blue for 45min at room temperature on a rocker. The gels were then destained twice for 15min with fast destaining solution (40% (v/v) methanol, 10% (v/v) acetic acid in ultrapure H₂O) on a rocker at room temperature. Further, the gels were incubated in slow destaining solution (10% (v/v) methanol, 5% (v/v) acetic acid in ultrapure H₂O) overnight at 4°C on a rocker. A further incubation with fast destaining solution for 15min on a rocker at room temperature followed. The Coomassie stained gels were then subjected to a silver staining using the ProteoSilver Silver Stain Kit from Sigma Aldrich according to manufacturer's instructions.

2.2.4.4. Western blot

Samples separated by SDS-PAGE gels were transferred to nitrocellulose membranes by semidry transfer using the Trans-Blot®Turbo™ system (Bio-Rad). The membranes were

blocked with 5% milk in TBST for 1 hour at room temperature and then incubated with primary antibodies overnight at 4°C. After three TBST washes, each lasting 10min, horseradish peroxidase (HRP)-conjugated secondary antibodies were applied for 1.5-2h. After washing with TBST, the membrane was incubated with Amersham ECL Western Blotting Detection Reagent (#RPN2106) for 1min before development of the blot with the ChemiDoc Imaging Systems (Bio-Rad).

Buffer	Reagents
1X Transfer buffer	200ml 5X Transfer buffer (Bio-Rad) + 600ml nanopure H ₂ O + 200ml ethanol
10X TBS	0.2 M Tris-HCl, 1.5 M NaCl, pH 7.5
TBST	100ml 10X TBS+ 900 ml ddH ₂ O+0.5 ml Tween 20
Blocking solution	TBST with 5% milk powder
Primary antibody solution	TBST with 5% milk powder
Secondary antibody solution	TBST with 5% milk powder
Western blotting Substrate	Amersham ECL Western Blotting Detection Reagent (#RPN2106)

2.2.4.5. Oxyblot for detection of protein carbonyls

Protein carbonyls were detected using the Abcam Protein Carbonyl Assay Kit for Western Blot detection (ab178020) according to manufacturer's instructions.

2.2.4.6. Immunoprecipitation from yeast lysates

Yeast cell lysates obtained by cryolysis were cleared of debris by centrifugation and the entire soluble fraction was used for immunoprecipitation experiments. Immunoprecipitation was carried out using GFP-Trap_MA beads (ChromoTek, gtma#20) to isolate the model amyloid IPOD substrate PrD-GFP along with all its interaction partners in vivo in specific yeast mutant cultures. 25µl of bead slurry was used per reaction. Beads were washed once with ice-cold lysis buffer and magnetically separated until a clear supernatant was obtained. The supernatant was discarded, and the wash was repeated once more. Yeast cell lysates equivalent to 2-3µg of total protein extract (post debris clearing) were mixed with equilibrated GFP-Trap_MA beads and the total volume was normalized to 300µl with the lysis

buffer. The reaction was incubated at 4°C for 2 hour in a end-over-end tumbling tube. Beads were magnetically separated, washed with 300ul lysis buffer and again magnetically separated till a clear supernatant was obtained. The supernatant was discarded and the wash step was repeated two more times. Post this, the beads were resuspended in 50µl 2X SDS sample buffer and boiled for 30 min at 98°C to dissociate immunocomplexes from the beads. The eluted fraction was further analysed by SDS-PAGE and Western blotting using anti-GFP antibodies.

2.2.5. FACS-based approach for IPOD enrichment

Cleared and concentrated IPOD samples after cryolysis were diluted in lysis buffer and subjected to FACS sorting at the ZMBH Flow Cytometry and FACS Core facility using a BD FACSDiva cytometer equipped with a 488nm laser. The correct size gating of the sort protocol was adjusted to include species of the observed approximate size range of IPODs (between 0.5µm and 1µm in diameter), using control samples with intact cells, lysates from cells containing IPODs and diffuse GFP. A 4way purity tube sorting (1.5/5ml) setting was employed using a 70µm nozzle and a flow rate of 10µl/min. Thresholding settings include an 488-B SSC of 200 and and FSC ASF of 0.83. The sorted samples were concentrated by centrifugation and used for further experiments.

2.2.6. Microscopy

2.2.6.1. Fixation of yeast cells for standard epifluorescence microscopy

For image acquisition by fluorescence microscopy, 10 ml of culture was harvested by centrifugation at 3500rpm for 5min. 5ml of the supernatant was removed, and the pellet was resuspended in remaining 5ml of medium, then mixed with 5 ml of 8% PFA (paraformaldehyde) and incubated immediately for 10 min at room temperature. The fixed cells were pelleted by centrifugation at 3500rpm for 5min and washed once with 5 ml of 0.1M potassium phosphate buffer (pH 6.5). The cell suspension was pelleted by centrifugation at 3500rpm at 5 min, resuspended in 1ml PBS and then transferred into a fresh 1.5ml tube. After one centrifugation at 13000rpm for 1min, cells were resuspended in 15-20 µl of PBS and subjected to fluorescence microscopy.

2.2.6.2. Microscopy image acquisition, processing, and data interpretation

Images of fixed cells were acquired using the Xcellence IX81 Olympus microscope at the ZMBH imaging core facility. Unless specified differently, optical sections of 0.2 μm were acquired to image the whole cell volume using the specified widefield system and a Plan-Apochromat 100x /NA 1.45 oil immersion objective. All images were acquired with a Hamamatsu ORCA-R2 camera. Acquired z-stacks were deconvolved using Xcellence software (Olympus) using the Wiener Filter. Further digital image processing was performed with ImageJ by a linear adjustment of brightness and contrast.

2.2.7. In-gel tryptic digestion and LC-MS/MS analysis

Protein samples were separated by SDS-PAGE, and stained with Coomassie Brilliant blue. Stained bands were cut out and processed as described previously²⁸⁵. The samples were reduced, alkylated and subjected to digestion with trypsin. Peptides were extracted from the gel pieces, concentrated in a speedVac vacuum centrifuge and diluted to a total volume of 30 μl with 0.1% TFA. 25 μl of the sample was analyzed by a nanoHPLC system (nanoAcquity, Waters) coupled to an ESI LTQ Orbitrap XL mass spectrometer (Thermo Fisher). Sample was loaded on a C18 trapping column and separated on an analytical column (75 μm x 250mm) with a flow rate of 300nl/min in an acetonitrile-gradient (3%-40%). One survey scan (res: 60000) was followed by 5 information dependent product ion scans in the ion trap. The uninterrupted MS/MS spectra were searched against "The Swissprot_2014_04 Saccharomyces Cerevisiae Database."

2.2.8. Individual modification site statistics in carbonyl proteomics

These statistic analyses were the result of an extensive collaboration with bioinformaticians at the Proteomics core facility.

All contrasts for each modification within lysate and eluate were calculated. For the modification site analysis, the site intensities of each multiplicity were used independently (e.g. Intensity Sample01___1, Intensity Sample01___2, Intensity Sample01___3). The data was analysed with the R package limma. Site intensities were normalized via quantile normalization. Quantile normalization could initially not be performed for some modification in some samples due to too many NA values. To overcome this issue, 0 values were added but

this will distort the results for these sites. For the imputation of missing values, we were restricted to the down shifted normal distribution method due to too many missing values for some modifications. This method assumes missingness due to limit of detection, so values with a very low intensity are imputed. The down shifted normal distribution was applied with a down shift of 2.2 and a narrowed width of 0.3 of the samples standard deviation. The p-values were adjusted with the Benjamini–Hochberg method for the multiple testing. For the sites intensities the MaxQuant Andromeda search score, which describes how well the measured spectra fits to a modified peptide in the database, was used. The scores were mapped to 0-1, by using an upper bound of 150.

2.2.9 Statistical analysis

Statistical analysis was performed for experiments with at least three independent replicates using the GraphPad Prism 6.0 software (GraphPad, USA). Results are expressed as mean \pm standard deviation (SD). Unpaired student's *t*-test was used for two-group comparisons and one sample *t*-test for values expressed as relative to a control sample. For data encompassing three groups or more, one-way ANOVA with Tukey's multiple comparisons test was employed. P-values < 0.05 were considered statistically significant.

3. Aims

The Insoluble Protein Deposit (IPOD) has been initially described as a deposition site for amyloid aggregates in yeast^{59,130,286}, but more recently it has been suggested that the IPOD may also harbor other endogenous types of substrates, such as oxidatively damaged proteins¹³⁰ and inactive/damaged proteasomes or subunits thereof^{133,134,287}. Interestingly, many of these potential substrate classes can form high molecular weight aggregates²⁴⁰ or represent large protein complexes, respectively. Directly adjacent to the IPOD, the cell accumulates large multimeric complexes of vacuolar precursor hydrolases at the Pre-Autophagosomal Structure (PAS) for translocation into the vacuolar lumen via the CVT-pathway^{288–290}. Furthermore, it has been shown that aberrant stress granules transiently associate with the aggresome on their way to autophagic degradation in mammalian cells¹⁷⁸. It was hypothesized that the IPOD may play a similar role to the aggresome in yeast in this regard. Therefore, it was postulated that the perivacuolar IPOD may represent a sorting center for aggregates and larger protein complexes destined for autophagic turnover.

The long-term goal is to reveal the biological significance of depositing different types of aggregates and damaged macromolecules at the IPOD. This study aimed at uncovering and characterizing novel IPOD substrates, first and foremost oxidatively damaged proteins. The main aims of this study can be summarized as follows:

- Isolate or enrich IPODs under unstressed or stress conditions known to damage proteins, protein complexes or cellular organelles to identify structural components and endogenous IPOD substrates by a large-scale unbiased mass spectrometric analysis.
- Candidate-based tests to identify new substrates of the IPOD under unstressed and different stress conditions
- Further characterize the presence of carbonylated proteins at the IPOD
- Find a visually tractable marker for proteins susceptible to oxidative stress at the IPOD
- Investigate the possible interaction of aberrant stress granules with the IPOD

4. Results

4.1. Methods for the enrichment of IPODs

One long-term goal of this laboratory's studies was to reveal the biological significance of depositing different types of aggregates and damaged macromolecules at the IPOD. Therefore, it was important to characterize which kinds of substrates can be found at the IPOD. Previously it has been described to represent a specific deposition site for terminally misfolded proteins including amyloid aggregates^{59,221,286}. More recently however, additional studies suggest that the IPOD also harbors other endogenous types of substrates, such as oxidatively damaged proteins²²¹ and inactive/damaged proteasomes or subunits thereof^{133,134,287}. Interestingly, many of these potential substrate classes can form high molecular weight aggregates²⁴⁰ or represent large protein complexes, respectively. In order to further characterize IPOD substrate composition, a method to efficiently enrich IPODs from yeast cells needed to be established. For this purpose, two approaches were tested, namely FACS- and IP-based enrichment of IPODs.

4.1.1. Fluorescence Activated Cell Sorting (FACS)-based enrichment of IPODs

Other experiments of this lab had previously utilized immunoprecipitation of the IPOD model substrate PrD-GFP to isolate IPODs from yeast cell lysates. However, it was hypothesized that perhaps not only IPODs had been isolated, but also other soluble species, like fragments due to lysis or propagons, which could interact with other protein species than intact IPODs. Therefore, the background from other unrelated proteins may be high in further experiments. It was previously demonstrated that differently sized aggregates from yeast cell lysates²⁹¹, as well as in mammalian cells²⁹², can be characterized by flow cytometry. Furthermore, IPOD load and pattern have previously been characterized in living yeast cells by this lab²⁹³. On this principle a method of enrichment by FACS was tested that allows the isolation of PrD-GFP aggregates a specific size range and study their composition by mass spectrometry. In pilot experiments a gating was defined that would allow for collection of fluorescent particles below the size of intact cells, but above the size of diffuse PrD-GFP molecules, for which lysates from yeast cultures with diffuse PrD-GFP and control lysates from cells which did not express any GFP-tagged proteins were used. Observed GFP species in the size range between

0.5 μ m and 1 μ m in diameter were categorized as IPOD aggregates and sorted by FACS at the ZMBH Flow Cytometry Core Facility.

Cells expressing PrD-GFP in logarithmic growth phase were harvested at an OD of approximately 0.6, pelleted by centrifugation and cryo-lysed by bead milling. The lysates were cleared from debris and larger particles including the majority of PrD-GFP present in IPOD depositions were pelleted, resuspended in cryolysis buffer and fluorescent particles of a particular size range were sorted by FACS.

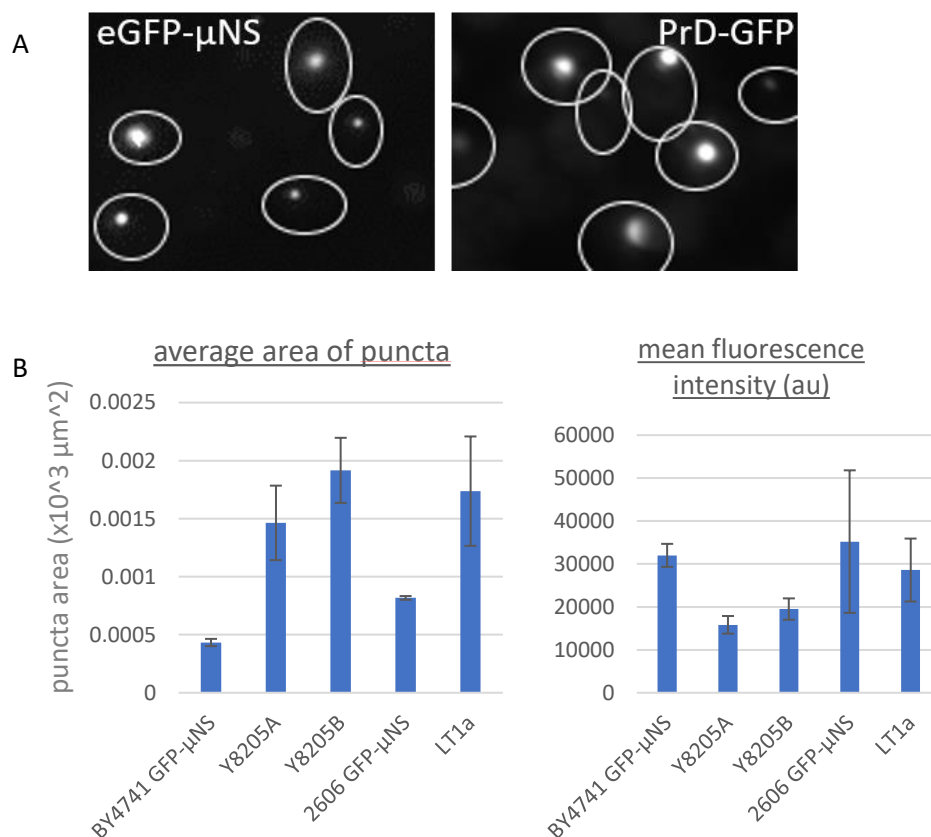


Figure R 2. Comparison of IPODs (PrD-GFP) and eGFP- μ NS particles. Cells expressing either PrD-GFP (strain Y8205 Δ PrD+PrD-GFP) or eGFP- μ NS (Y8205 Δ PrD+eGFP- μ NS) were grown in YPD media to an OD600 of 0.8, fixed with 4% paraformaldehyde and observed at 60X magnification. Images were processed using ImageJ software. (A) shows representative images of PrD-GFP in the [PSI⁺] strain Y8205A and eGFP- μ NS particles expressed in the non-PrD-GFP expressing strain BY4741, which is a parent strain of Y8205A. (B) shows an analysis of average size and fluorescent intensity of the observed puncta in the aforementioned yeast strains as well as the other BY4741-derived PrD-GFP expressing strain Y8205B, the PrD-GFP expressing strain LT1a, as well as the eGFP- μ NS expressing strain 2606, which is a parent strain of LT1a. N=3 biological replicates. Data shows Mean \pm SD.

As an additional control to reveal which proteins may be co-sorted unspecifically, lysates from BY4741 and 2606/74D yeast cells that do not express PrD-GFP but eGFP- μ NS were used. eGFP- μ NS is a fusion of the genetically encoded orthoreovirus capsid protein μ NS with GFP, that can be expressed in yeast and self-assembles into distinct particles of a similar size range

as IPODs in the yeast cytoplasm²⁹⁴ (see Fig. R1). Because it is not an endogenous yeast protein and has no known interactors in the yeast proteome, proteins co-sorting with eGFP- μ NS would represent a more random, unspecific background. Figure R1 shows an analysis of size and fluorescence intensity of eGFP- μ NS and PrD-GFP puncta observed in different yeast strains, either BY4741 (Y8205A/B)- or 2606/74D-based (LT1a). While the fluorescence intensity is similar between the particles, IPODs vary more in size and can be bigger than eGFP- μ NS assemblies.

In initial experiments intending to analyse IPOD composition by mass spectrometry, the lysates obtained by cryolysis from yeast cells in logarithmic growth, were cleared of debris by low-speed centrifugation at 4500rpm for 5min, resulting in the fractions pellet 1 (P1), containing the cellular debris and supernatant 1 (S1). S1 was further subjected to ultracentrifugation at 80,000rpm for 60min at 4°C to pellet the PrD-GFP aggregates along with their interaction partners in the pellet fraction P2. The P2 fraction was resuspended in cryolysis buffer and further used for FACS and subsequent mass spectrometric analysis. The entire workflow is visualized in Figure R2.

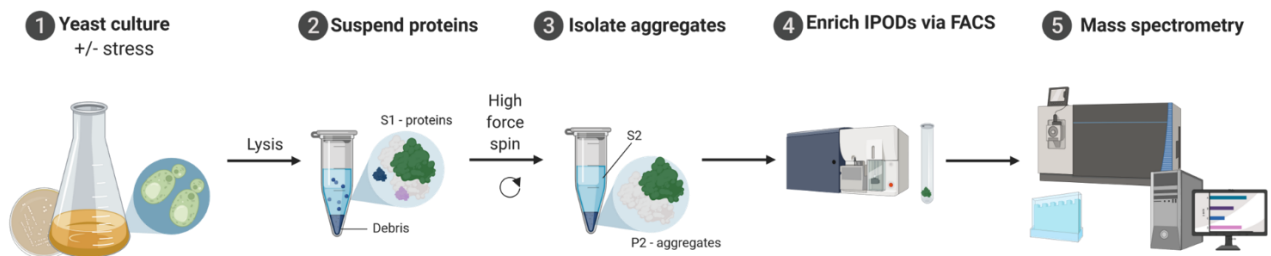


Figure R 3. Workflow of sample preparation and analysis in FACS-MS experiments. 1. Yeast cultures were grown to an OD of approximately 0.6 in the presence or absence of stressors in the growth medium. 2. Cells were cryolysed and the lysates cleared by a low speed centrifugation, resulting in a debris pellet (P1) and the supernatant S1. 3. Aggregates in the supernatant (S1) were pelleted by high speed centrifugation in the pellet P2. 4. P2 fractions were further resuspended and IPODs containing PrD-GFP were enriched from this fraction via FACS. 5. The sorted fractions were adjusted for PrD-GFP content and subjected to mass spectrometric analysis. Created using BioRender.com.

In order to increase the stringency of the FACS sorting approach, the gating was optimized repeatedly with control samples of Y8205A treated with 5mM guanidine hydrochloride, which led to the loss of PrD-GFP aggregates through curing from the prion state, resulting in a diffuse cytoplasmic PrD-GFP localization. Further, samples of BY4741, a yeast strain not expressing PrD-GFP, were used to increase the strictness in the size of particles accepted. This way, small particles outside the IPOD size range of around 1 μ m, as well as intact cells and cellular debris were sure to be excluded.

Because μ NS should not interact with many cellular proteins, one would expect a specific band for eGFP- μ NS with not many other bands in silver staining. However, as seen in figure R3, the original protocol yielded samples which showed many bands in silver staining, indicating a high background of unspecifically co-sorted proteins. It was further attempted to increase sorting stringency by using settings usually intended for doublet discrimination to exclude the co-sorting of unwanted close-by large particles. This, however, did not appear to bring much of a change as seen in silver staining of the samples after SDS-PAGE (Fig. R3). However, subjecting PrD-GFP samples to two rounds of FACS sorting with strict criteria appeared to reduce background, as bands became more distinct (Fig. R3).

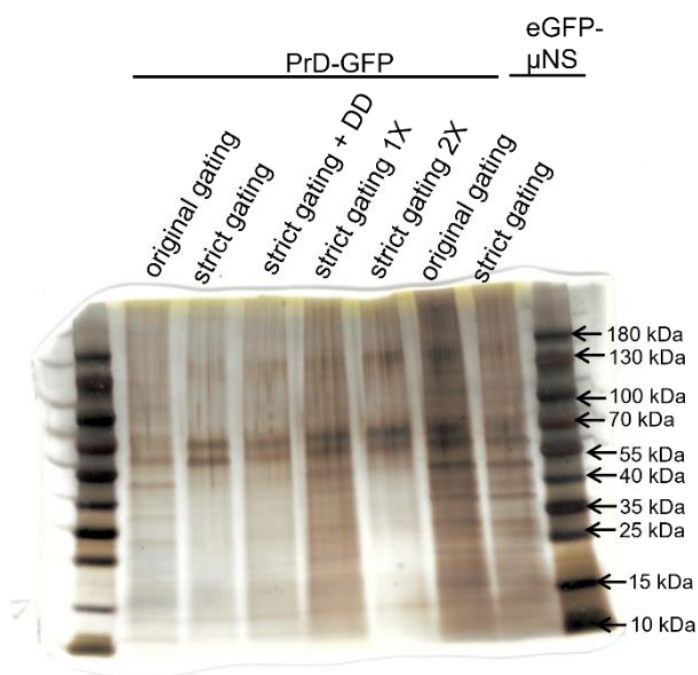


Figure R 3. Representative image of silver staining of FACS-sorted fractions of PrD-GFP and eGFP- μ NS samples subjected to different sort protocols, including different gating settings, doublet discrimination settings (DD), as well as one or two rounds of sorting (1X and 2X). Samples were adjusted for the same total protein concentrations.

For further analysis, the yeast strains Y8205A, which expresses the model IPOD substrate PrD-GFP and as a control its parent strain BY4741, transformed to express the viral capsid protein eGFP- μ NS, were used. Only samples sorted twice with strict criteria were processed further. Before the sorted samples originating from these cultures were subjected to mass spectrometric analysis, they were separated using SDS-PAGE and Coomassie staining followed by silver staining. The band pattern in the gel was analysed to ensure that the PrD-GFP pattern was sufficiently different from the eGFP- μ NS one, which would indicate a more specific co-sorting of proteins.

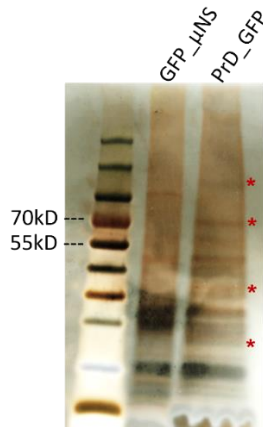


Figure R 4. Representative image of Coomassie-silver staining of FACS-sorted fractions of eGFP- μ NS and PrD-GFP. PrD-GFP is expected to run at a molecular weight of about 70kD, where there is a distinct band in the corresponding sample but not in the eGFP- μ NS sample. Protein bands only appearing in PrD-GFP samples are indicated with red asterisks.

As shown in figure R4, there was a visually different pattern of bands in the silver-stained gels, which indicated more protein bands seen in the PrD-GFP samples that were distinct from those observed in the eGFP- μ NS samples. A prominent band at 70kDA only present in the PrD-GFP but not the eGFP- μ NS sample represents PrD-GFP, which was confirmed by Western blot. The presence of distinct additional bands only in the PrD-GFP sample indicates that likely PrD-GFP containing particles that also contain specific other proteins were isolated successfully. Based on these indications, these samples were used for mass spectrometric analysis identify whether the co-sorted proteins may be structural elements or other substrates of the IPOD.

The model substrate PrD-GFP was among the most abundant proteins in the sorted IPOD-enriched sample (confirmed by iBAQ and fold-enrichment over the control sample), confirming that the FACS approach can indeed be used to enrich IPODs from the aggregate fraction of yeast cell lysates. Via a mass spectrometric analysis of the IPOD-enriched sorted samples, possible candidates of substrates or structural components of the IPOD could be identified. An initial 991 proteins were found, of which 229 met the criteria for analysis (peptide count ≥ 2). A peptide count of 2 is very low, indicating a low peptide recovery. Because total protein content in the FACS sorted samples was very low, resulting in a low coverage rate, these criteria were used nonetheless. These candidates were further filtered quantitatively based on LFQ enrichment ratio (≥ 2 -fold enrichment in the PrD-GFP compared to the eGFP- μ NS control), reducing the list of possible candidates to 186 proteins. Several highlighted proteins found enriched in PrD-GFP sorted fractions compared to those obtained

from eGFP- μ NS samples are listed in Table R1. Various proteins found to be much more abundant in PrD-GFP samples than eGFP- μ NS samples by fold-change enrichment are known to play roles in IPOD formation, like Myo2²⁹⁵ which is involved in the transport of amyloid aggregates to the IPOD. Or the peroxiredoxin Tsa1, which is involved in recruitment of chaperone proteins like Hsp104 and Ssa1 to peroxide stress-induced aggregates, that accumulate at inclusions sites like the IPOD⁵². Ssa1 has previously been identified highly abundant in [PSI+] aggregates and the IPOD^{296,297}.

Rank	Protein names	Gene names	PrD-GFP/GFP- μ NS ratio
1	Inorganic phosphate transporter PHO84	PHO84	31.516
2	Homocitrate synthase, cytosolic isozyme	LYS20	11.456
3	Pleiotropic ABC efflux transporter of multiple drugs	PDR5	8.7691
6	Eukaryotic peptide chain release factor GTP-binding subunit	SUP35	6.3206
13	60S ribosomal protein L28	RPL28	4.919
14	Peroxiredoxin TSA1	TSA1	4.8264
17	Ribosomal RNA-processing protein 12	RRP12	4.3235
19	Protein SNQ2	SNQ2	4.2205
20	Myosin-2	MYO2	4.2012
30	Protein SIS1	SIS1	3.6685
34	Vacuolar transporter chaperone 4	VTC4	3.5932
44	60S ribosomal protein L4-A	RPL4A	3.3369
46	Heat shock protein SSA2	SSA2	3.2188
47	Myosin-5	MYO5	3.1956
48	60S ribosomal protein L25	RPL25	3.1811
56	Glyceraldehyde-3-phosphate dehydrogenase 3	TDH3	3.0554
85	Alcohol dehydrogenase 3, mitochondrial	ADH3	2.7811
90	Mitochondrial import receptor subunit TOM70	TOM70	2.7043
109	Heat shock protein 104	HSP104	2.5093
149	[NU+] prion formation protein 1	NEW1	2.2225
150	Pyruvate decarboxylase isozyme 1	PDC1	2.2222
173	Enolase 2	ENO2	2.0781

Table R 1. Proteins which are significantly enriched in FACS sorted IPOD containing fraction compared to GFP- μ NS containing fraction. Marked in green is Sup35, representing the model substrate PrD-GFP. Marked in yellow are proteins expected to be at the IPOD based on previous studies.

A gene ontology (GO) term analysis of co-isolated proteins in the sample with PrD-GFP revealed a strong enrichment for ribosomal subunits (enrichment score ES = 12.38), specific chaperones, vacuolar membrane proteins, proteasomal subunits and mitochondrial proteins, among others (Fig. R5). The enrichment score was determined using the DAVID Functional Annotation algorithm tool²⁹⁸. Interestingly, proteins involved in protein degradation

(autophagy, ubiquitin-dependent catabolic processes) were also enriched, which may reflect the IPOD's location close to the PAS as well as hint at a turnover of potential substrates. The identification of vacuolar proteins co-isolated with IPODs may reflect its localization at the vacuolar rim, next to the assembly site for autophagosomes^{59,286}. Other interesting findings in this first analysis of IPOD components include cytosolic proteins known to be susceptible to oxidative damage (carbonylation), for example Pyruvate decarboxylase 1 (Pdc1)²⁶⁴. These two proteins have been shown previously to form foci when the cells were subjected to oxidative stress by treatment with 0.1mM menadione for 4h^{38,130}.

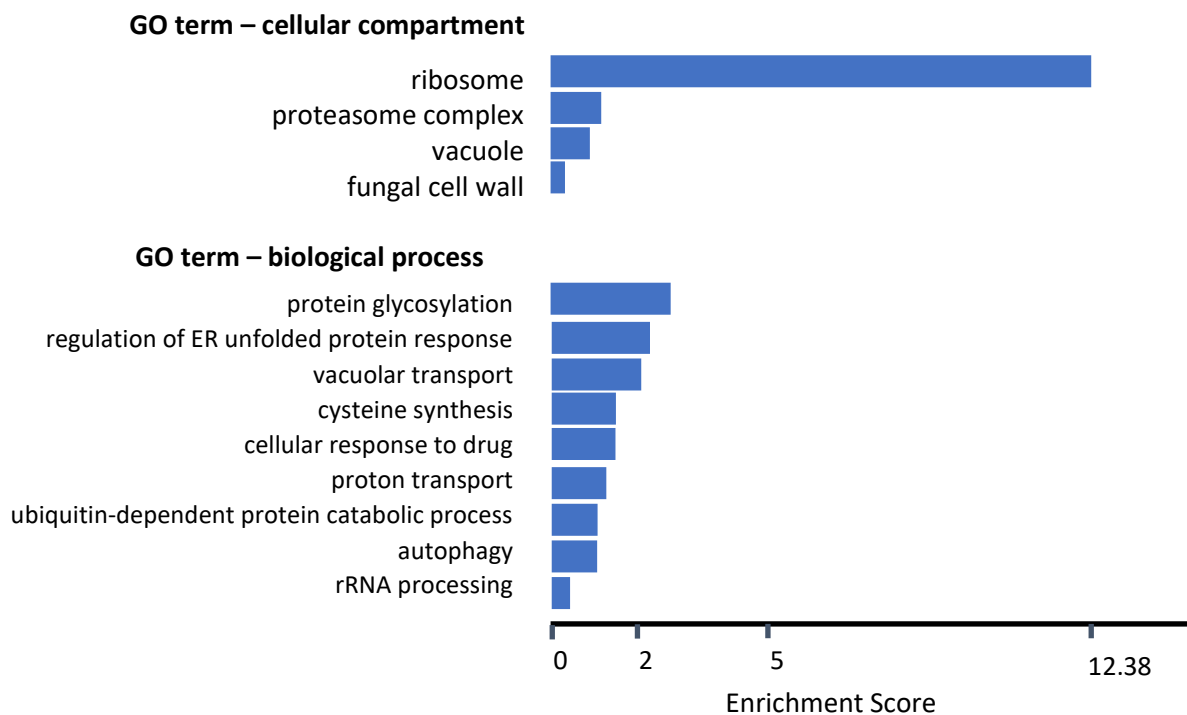


Figure R 5. GO-Term analysis of proteins found enriched in PrD-GFP as compared to eGFP- μ NS samples. Enrichment score shows the over-representation of term clusters as compared to the total genome frequency. The analysis was performed using the DAVID (Database for Annotation, Visualisation and Integrated Discovery) Functional Annotation algorithm tool (david.ncifcrf.gov/home.jsp) first described in ²⁹⁸.

The immense over-representation of ribosomal proteins and to a smaller degree also that of vacuolar and cell wall proteins was concerning. While these types of proteins were more prominent in the PrD-GFP samples, they were also very abundant in eGFP- μ NS samples. It was rationalized that it seems possible that the tight P2 pellet after ultracentrifugation not only contained PrD-GFP aggregates and their interaction partners, but also captured unspecific interactions of the “sticky” PrD-GFP aggregates with other macromolecular structures and storage granules through unspecific post-lysis interactions (illustrated in Fig. R6).

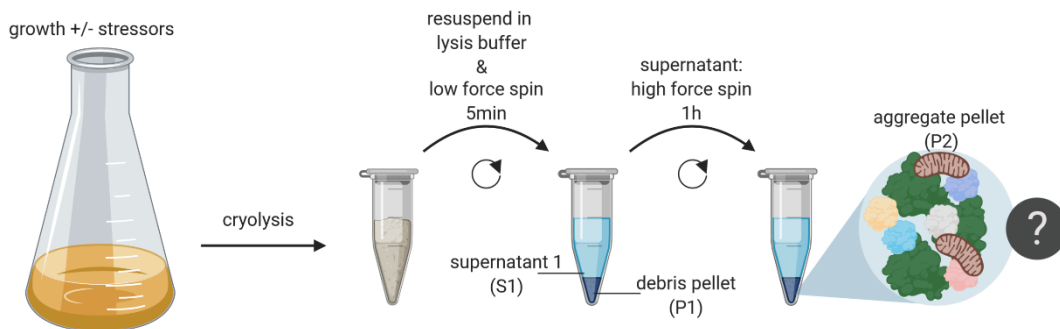


Figure R 6. Flowchart highlighting the possibility of non-specific interactions of sticky PrD-GFP aggregates with other macromolecular structures. Created using BioRender.com.

One possibility to avoid this problem was to directly dilute and sort PrD-GFP aggregates from the S1 fraction of sample preparation without further pelleting of the aggregate fraction of the cleared lysate. However, mass spectrometric analysis of these sorted fraction still brought with it a high amount of possibly unspecific interactions, indicated by the very similar extremely high enrichment of ribosomal proteins and many metabolic enzymes and a cross-reference of the dataset with the CRAPome tool (Contaminant Repository for Affinity Purification Mass Spectrometry Data²⁹⁹). Because of the problem of possibly unspecific background due to post-lysis interactions, another approach using the immunoprecipitation-based enrichment of IPODs from this fraction was therefore employed.

4.1.2. Immunoprecipitation (IP)-based enrichment of IPODs

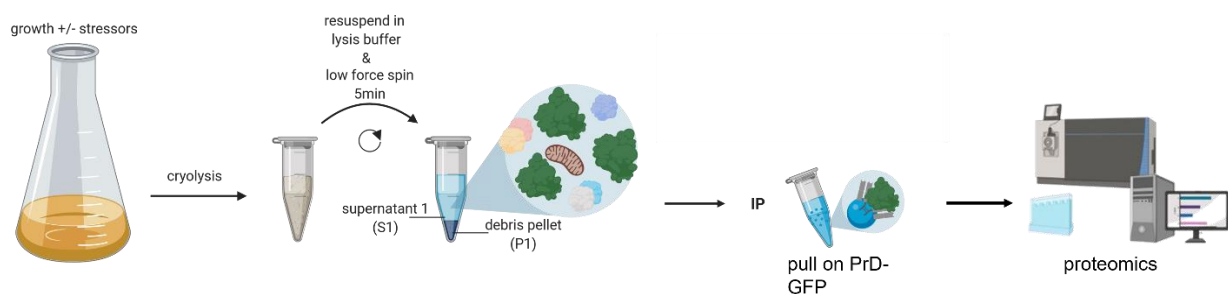


Figure R 7. Workflow of sample preparation and analysis in IP-MS experiments.

Due to the problem of a possible unspecific background due to post-lysis interactions and low total protein yield in the FACS-based IPOD enrichment approach, a second approach to enrich IPODs containing PrD-GFP from yeast cell lysates consisted of an immunoprecipitation (IP) pulling on PrD-GFP in cleared lysates using GFP-Trap magnetic beads (an overview of the workflow is depicted in Figure R7) was employed. Using the manufacturer's GFP pull-down protocol, PrD-GFP could be precipitated efficiently (Fig. R8). Lysates from cells with a cured

IPOD were used as control. Samples were further processed, adjusted to equal levels of PrD-GFP and used for mass spectrometric analysis. Eluate over load ratios were formed in order to find proteins enriched in the eluate fractions compared to the loaded cleared lysate.

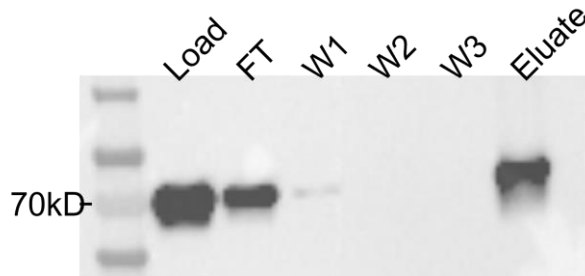
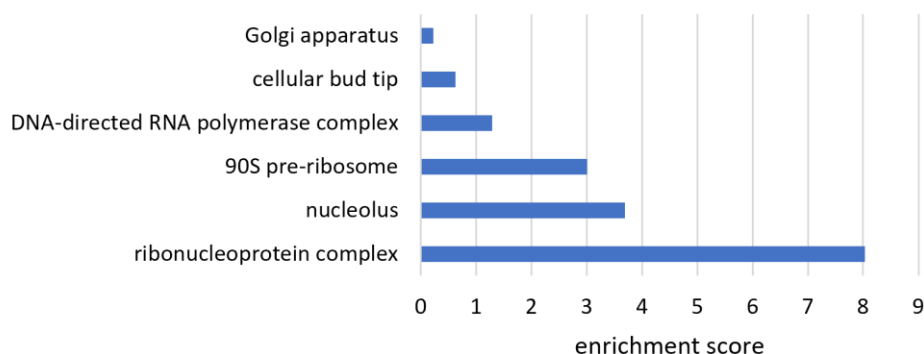


Figure R 8. Western blot with IP fractions from cleared lysates of Y8205A cells grown under basal, unstressed conditions. FT= flow-through, W= wash. PrD-GFP could be precipitated efficiently from the sample.

An initial 2489 candidate proteins were found. These candidates were further filtered quantitatively based on LFQ enrichment ratio (peptide count ≥ 2 , ≥ 2 -fold enrichment in the eluate compared to the load), resulting in 122 valid candidates.

A GO-term analysis (Fig. R9) suggests again a high enrichment of proteins involved in translation (enrichment score of 8.03) like ribosomal proteins, but also proteins involved in protein folding (enrichment score of 0.46), phosphorylation (enrichment score of 0.40) and transport (enrichment score of 0.22), as well as metabolic proteins (enrichment score of 1.33). While this is still a large enrichment of ribosomal proteins, there are more groups of proteins found in the GO-term analysis of these samples. Importantly, Myo2 and Rnq1, another prion protein, which is an IPOD substrate^{130,297,300}. At a lower abundance, proteins susceptible to oxidative damage, like Pdc1 were also found in this approach.

GO term - Cellular Compartment



GO term - Biological Process

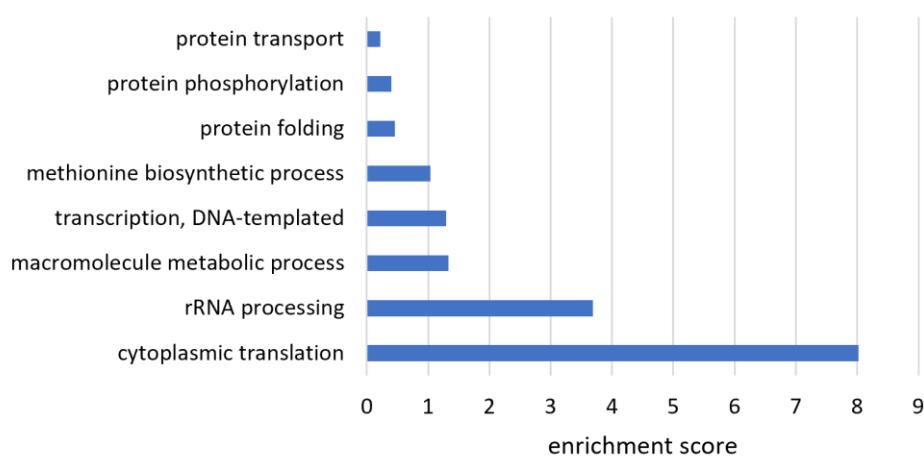


Figure R 9. GO term analysis of proteins found enriched in unstressed PrD-GFP IP eluate samples compared to cleared lysate. Enrichment score shows the over-representation of term clusters as compared to the total genome frequency. The analysis was performed using the DAVID (Database for Annotation, Visualisation and Integrated Discovery) Functional Annotation algorithm tool (david.ncifcrf.gov/home.jsp) first described in ²⁹⁸.

While both datasets overlap particularly with respect to the abundance of ribosomal proteins and the finding of several proteins which are known to be susceptible to oxidative damage, there are more known IPOD resident proteins in the IP-derived data, for instance Rnq1. Furthermore, with the IP-based approach, the total protein amount in the eluate sample was higher than the FACS-based approach yielded, which might give a better peptide recovery and coverage rate. Based on these considerations coupled with the remaining concern for unspecific co-sorting even with the FACS based approach, it was decided to use the IP-based approach in subsequent experiments.

4.2. Proteomic analysis of IPOD composition under different conditions

Via a mass spectrometric analysis of IPOD-enriched, FACS sorted, as well as IP-enriched samples, possible IPOD substrate candidates could be identified (see section 4.1). In order to test the hypothesis that the IPOD is a sorting hub for aggregates and damaged larger protein complexes, I first enriched IPODs marked by PrD-GFP from yeast cells grown under standard conditions and analysed their contents by mass spectrometry. Since many proteins which are susceptible to oxidative damage as well as mitochondrial and ribosomal proteins were found, I asked whether represent putative new IPOD substrate classes. It was hypothesized that the deposition of the protein classes may be a consequence of their damage by, for example, oxidative stress, defective mitochondria, aberrant ribosomes or aberrant stress granules. To follow up on this, my goal was to enrich IPODs after applying different stressors, which lead to protein damage and aggregation, as well as the possible accumulation of different putative new substrate classes at the IPOD. The contents of these enriched IPODs were then analysed by mass spectrometry. In these mass spectrometric analyses of IPODs an enrichment of certain proteins after oxidative stress (2h 0.5mM menadione or 1mM H₂O₂), as well as mitochondrial stress (2h 4μM valinomycin), was observed when compared to samples from unstressed cells. Many of these were known to be susceptible to modifications by oxidative stressors like menadione or H₂O₂. Additionally, many proteins involved in the oxidative stress response were found under these conditions.

4.2.1 IPOD composition after oxidative stress

An IP-based strategy to enrich IPODs from crude yeast cell lysates from unstressed and oxidatively stressed cells was further employed, utilizing magnetic agarose beads coupled to camelid anti-GFP antibodies (GFP-Trap), to pull on PrD-GFP and therefore the IPOD. PrD-GFP was among the most abundant proteins in the enriched samples, confirming that this approach can indeed be used for IPOD enrichment from crude lysates. Via a mass spectrometric analysis of these IP samples, it was possible to identify IPOD substrate candidates.

In a previous analysis of IPOD contents under basal conditions (see section 4.1), a variety of proteins which are known to be susceptible to oxidative damage, particularly carbonylation, were found even under unstressed conditions. It was hypothesized that these proteins may

be oxidatively damaged by carbonylation to a degree under steady state conditions and are found at the IPOD for this reason. Therefore, I asked whether these proteins could be enriched under oxidatively stressed conditions.

Rank	Protein	Ox/Uns	Function
3	PET9	12.87	mitochondrial transport, aerobic respiration
6	VMA2	5.39	proteasome storage granule assembly, vacuole mitochondria membrane contact
10	QCR2	4.67	mitochondrial oxidoreductase
15	ADH1	4.03	alcoholic fermentation, methylglyoxal reductase
16	OLA1	3.94	hydrolase, part of stress granules
28	TDH3	2.49	glycolysis, gluconeogenesis, apoptosis, ROS metabolism
40	PDC1	1.88	alcoholic fermentation
48	ENO1	1.59	glycolysis and gluconeogenesis
49	TIF1	1.45	helicase and translation initiation factor, localizes to stress granules and P-bodies upon starvation
58	ARB1	1.32	disaggregation, ribosome biogenesis, nucleo-cytoplasmic shuttling
60	YHB1	1.30	oxidative and nitrosative stress responses

Table R 2. Proteins enriched at the IPOD after 2h oxidative stress by 1mM H₂O₂. Results show the mean of 3 replicate oxidatively stressed (Ox)/Unstressed(Uns) sample pairs.

2h of oxidative stress by addition of 1mM H₂O₂ or 0.5mM menadione were applied to a yeast culture before lysis and compared the IPOD composition in these cells to unstressed cells (Table R2). Indeed, an enrichment of known carbonylation-sensitive proteins was found, including Pyruvate decarboxylase 1 (Pdc1), Enolase 2 (Eno2), and Glyceraldehyde-3phosphate dehydrogenase 3 (Tdh3). While other proteins were even more highly enriched after oxidative stress, these particular proteins had been found in previous mass spectrometry analyses of IPOD co-enriched proteins (see section 4.1.). Significantly enriched hits of 3 oxidatively stressed (ox)/unstressed (uns) sample pairs were analysed. Initially, 2396 candidate proteins were found, of which 446 fit the analysis criteria (peptide count ≥ 2 , ≥ 2 -fold enrichment in ox compared to uns, $p \leq 0.05$).

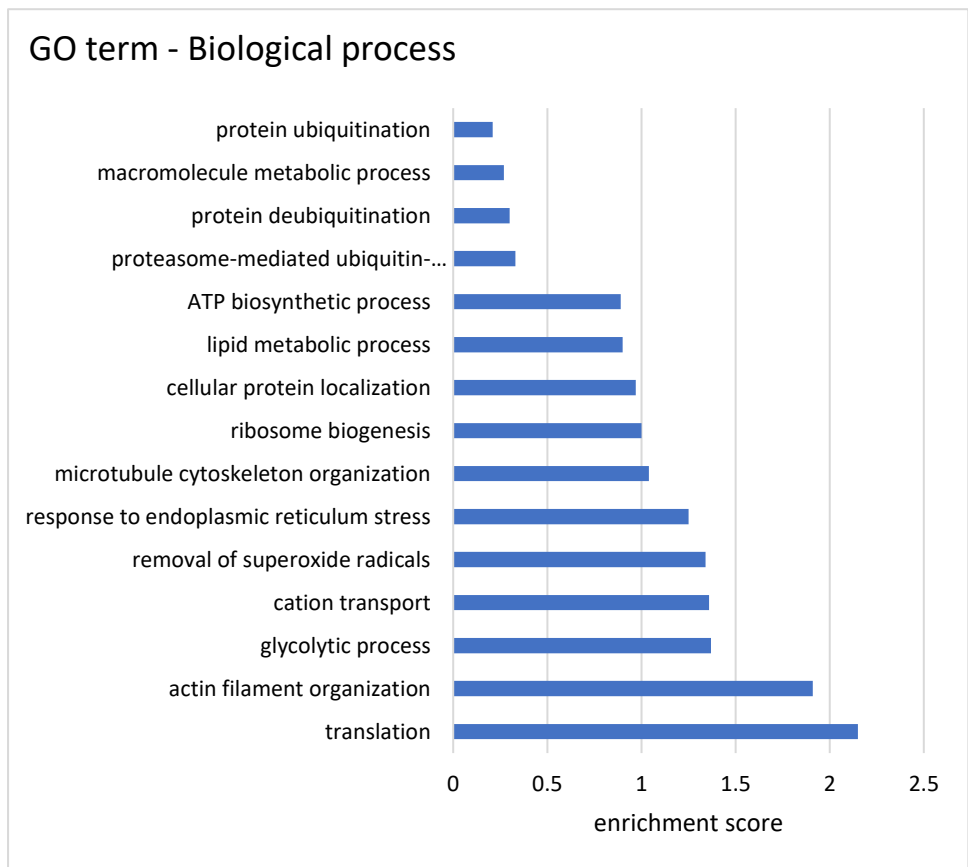
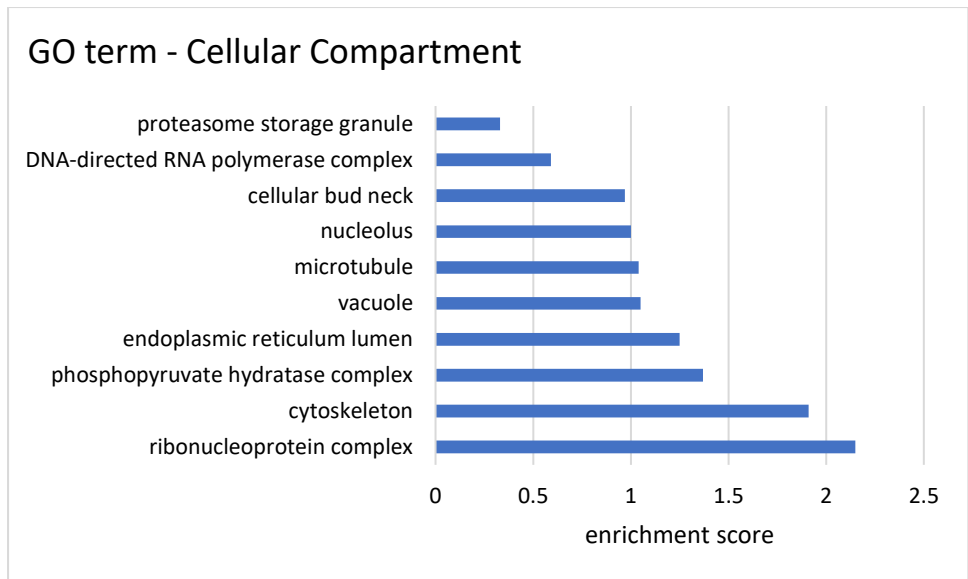


Figure R 10. GO Term analysis hits significantly enriched in enriched IPODs after oxidative stress compared to unstressed. Enrichment score shows the over-representation of term clusters as compared to the total genome frequency. The analysis was performed using the DAVID (Database for Annotation, Visualisation and Integrated Discovery) Functional Annotation algorithm tool (david.ncifcrf.gov/home.jsp) first described in ²⁹⁸.

A GO-term analysis of IPOD substrates co-isolated with PrD-GFP under oxidative stress (Fig. R10) revealed a strong enrichment as compared to unstressed cells for ribosomal subunits, specific chaperones, vacuolar membrane proteins, proteasomal subunits, and mitochondrial proteins as well as some metabolic enzymes, among others. The enrichment score was

determined using the DAVID Functional Annotation algorithm tool²⁹⁸) The identification of vacuolar proteins co-isolated with IPODs may reflect its localization at the vacuolar rim next to the assembly site for autophagosomes. Finding proteins expected to be in proteasome storage granules is consistent with a study of Marshall and colleagues (2016)²⁸⁷, according to which immature proteasome storage granules transiently associate with the IPOD during their maturation. During this process, damaged components are degraded in the vacuole in a process termed proteaphagy¹³³.

4.2.2. IPOD composition after mitochondrial stress

Since many mitochondrial proteins were found in previous mass spectrometric analyses of IPOD components both under unstressed and oxidatively stressed conditions (see sections 4.1 and 4.2.1.), it was investigated whether these proteins might be enriched after mitochondrial stress and damage, potentially accumulating in the process of mitophagy. This condition was of interest, as the hypothesis of the IPOD as a sorting hub for damaged or inactive macromolecules as well as large aggregates, could also make it a midway station for proteins destined to be degraded via microautophagy, as has been shown for proteasome storage granules. Therefore, one would expect to find more mitochondrial proteins at the IPOD in conditions of elevated mitophagy.

For this purpose, Y8205A yeast cells expressing PrD-GFP were grown under basal conditions as well as under conditions of mitochondrial stress. Mitochondrial stress was induced by treatment with 4 μ M valinomycin for 2h. Valinomycin is a naturally occurring neutral ionophore which transports K⁺ ions across membranes, leading to mitochondrial depolarization and uncoupling of oxidative phosphorylation, ultimately inducing mitophagy³⁰¹. Cells were grown in YPglycerol growth medium to increase mitochondrial stress. Spotting assays were performed in order to assess cell viability under these conditions. Cells were cryolysed and IPODs enriched from the lysates by IP as described above. Significantly enriched hits of 3 mitochondrially stressed (MS)/unstressed (uns) sample pairs were analysed. Initially, 2396 candidate proteins were found, of which 112 fit the analysis criteria (peptide count ≥ 2 , ≥ 2 -fold enrichment in MS compared to uns, $p \leq 0.05$). A selection of interesting hits is shown in table R3.

Rank	Gene names	MS/uns	function
1	YPR010C-A / MIN8	26894668	unknown
2	CET1	16172668	subunit of mRNA capping enzyme
3	COQ4	13930001	ubiquinone (Coenzyme Q) biosynthesis
5	RPN13	10655768	ubiquitin receptor for the proteasome
6	RPL36B	8992934	ribosomal 60S subunit
7	CYC1	7931634	electron carrier of mitochondrial intermembrane space
8	TDH2	7474168	involved in glycolysis and gluconeogenesis
9	TDH3	7045534	involved in glycolysis and gluconeogenesis
10	COX1	6807268	subunit I of cytochrome c oxidase (Complex IV), mitochondrial inner membrane electron transport chain
24	SSC1	5.803	Hsp70 family ATPase; constituent of the import motor component of the Translocase of the Inner Mitochondrial membrane (TIM23 complex)
44	MAS1	3.413	Beta subunit of the mitochondrial processing protease (MPP)
45	SSA1	3.344	Hsp70 ATPase involved in protein folding and NLS-directed nuclear transport; required for ubiquitin-dependent degradation of short-lived proteins
100	MSS116	2.092	Mitochondrial transcription elongation factor

Table R 3. Proteins enriched at the IPOD after 2h mitochondrial stress (MS) by 4 μ M valinomycin. Results show the mean of 3 replicates mitochondrially stressed (MS)/Unstressed(Uns) sample pairs. Marked in yellow are proteins uniquely found after mitochondrial stress. Instead of a ratio, the LFQ intensity is given.

Interestingly, several proteins were found only in IPOD samples of mitochondrially stressed cells. Most of these, like for example Cyc1 or Cox1, are mitochondrial proteins, which one would expect to find elevated in conditions of elevated mitophagy, if the IPOD is indeed a midway-station on the ways to mitophagic degradation at the vacuole. For this its close perivacuolar localization would be an advantage. A GO term analysis of co-enriched proteins in the samples with PrD-GFP under mitochondrial stress, revealed a strong enrichment as compared to unstressed cells for vacuolar transport proteins, proteins involved in peptide metabolism, mitochondrial proteins, as well as ribosomal subunits.

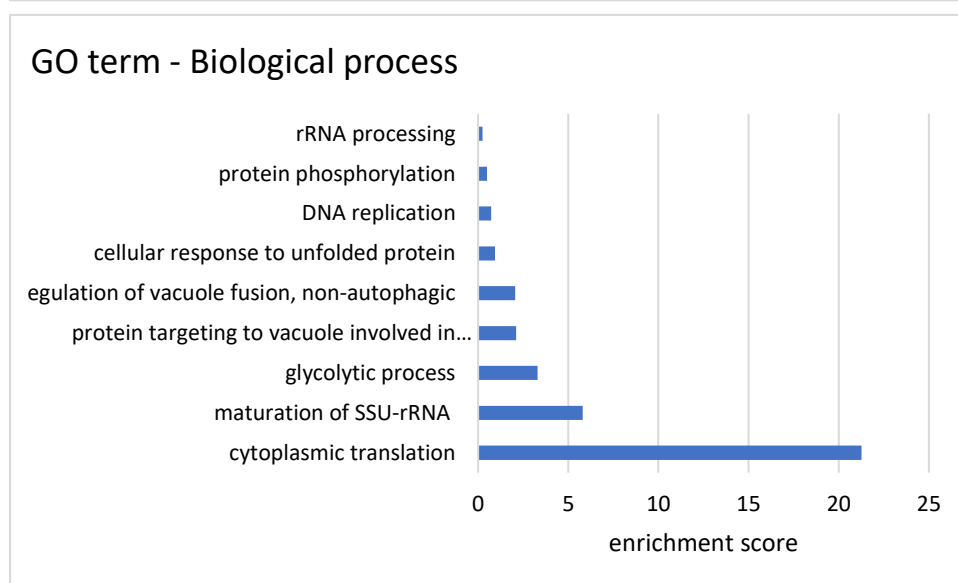
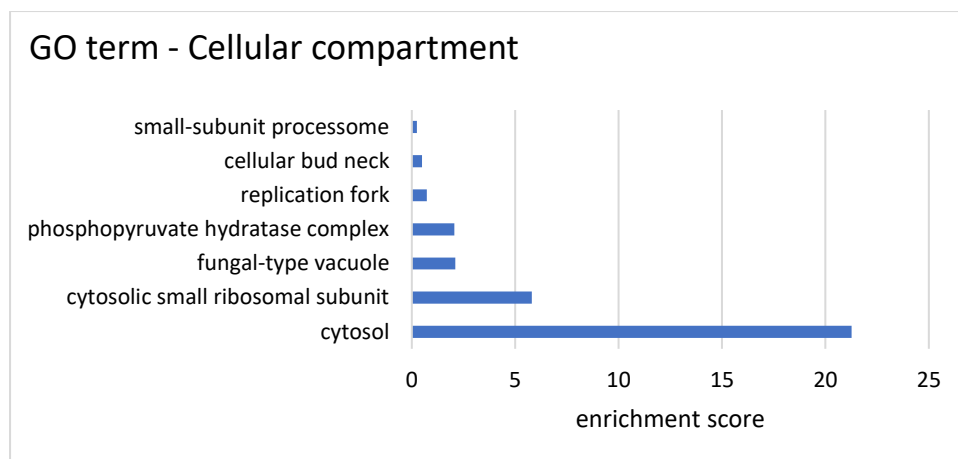


Figure R 11. GO Term analysis of protein hits significantly enriched in enriched IPODs after mitochondrial stress compared to unstressed. Enrichment score shows the over-representation of term clusters as compared to the total genome frequency. The analysis was performed using the DAVID (Database for Annotation, Visualisation and Integrated Discovery) Functional Annotation algorithm tool (david.ncifcrf.gov/home.jsp) first described in ²⁹⁸.

Mitochondrial protein-related terms did not cluster significantly when using the DAVID bioinformatics tool, however, several GO terms relating to mitochondria were found in the datasets (Table R4) which are nonetheless interesting, because some of the proteins were among the most abundant or even unique to the MS dataset.

GO term	# Proteins found	Examples
Mitochondrion	28	ARO3, MSS116, SSA1, STI1, SAM35, TDH2, TDH3, COQ4
Respiratory chain	3	CYC1, COX1, COX2
Oxidoreductase activity	7	HOM2, CTA1, GCY1, HMG2

Table R 4. GO terms which did not significantly cluster in DAVID analysis, but are relevant to this study. Some of the proteins recognized were among the most abundant in the MS/uns dataset.

4.2.3. Comparing IPOD composition of oxidatively and mitochondrially stressed cells

When comparing the datasets for proteins found at the IPODs of oxidatively stressed cells (see section 4.2.1.) to those found at mitochondrially stressed cells (see section 4.2.2.), there is a significant overlap of 110 proteins which were found under both conditions. These include for example Cyc1, Tdh2, Ssc1, Cox1, Cox2, and Cet1, as well as many ribosomal proteins. An overlap between enriched proteins in these two conditions is perhaps not surprising, as conditions of mitochondrial stress also favour the production of reactive oxygen species (ROS), which can lead to oxidative stress and oxidative damage of proteins. 97 proteins were unique to the mitochondrially stressed dataset, for example the mitochondrial heat shock protein Ssc1, as well as proteins like Sam35, Mas1, Pol1, Hmg2, Hom2, Gcy1 and Aro3. Some of these proteins are highly abundant in the samples of mitochondrially stressed cells. 316 proteins were unique to the oxidatively stressed cells, including many of the proteins previously known to be susceptible to carbonylation, like Sod1, Sod2, Eno1, Eno2, Pdc1, and Pdc5. This was a further hint to the hypothesis that irreversibly oxidatively damaged, especially carbonylated, proteins may be deposited at the IPOD either for permanent storage or until their degradation.

4.3. Oxidatively damaged proteins are enriched at the IPOD

In mass spectrometry analyses of proteins co-enriched with the IPOD, many proteins which are known to be susceptible to oxidative damage by carbonylation are consistently found (see sections 4.1, 4.2). In order to validate this putative new IPOD substrate class, I decided to determine whether protein carbonyls are enriched at the IPOD and further, whether markers of different potential macromolecular IPOD substrates form foci in the cells, esp. after the corresponding stress, e.g. oxidative stress or mitochondrial stress.

4.3.1. Carbonylated proteins are enriched at the IPOD

When cells are oxidatively stressed by treatment with stressors like H₂O₂ or menadione, this causes extensive carbonylation of parts of the cellular proteome^{241,242}, which is irreversible and therefore causes permanent damage to proteins^{244,246}. Therefore, protein carbonyl content is widely used as a marker of protein oxidative damage²⁴⁵. This led to the question whether carbonylated proteins are enriched at the IPOD after oxidative stress by 2h 1mM H₂O₂. In order to assess this, an oxyblot was performed with IP eluate and lysate samples from

unstressed (uns), oxidatively stressed (H_2O_2) and mitochondrially stressed (vali) cells. Figure R12 shows a representative image of an oxyblot. In this method, samples are treated with 2,4-dinitrophenylhydrazine (DNPH). The reaction of DNPH derivates carbonyl groups in protein side chains to 2,4-dinitrophenylhydrazone. The DNP-derivatized protein samples are separated by polyacrylamide gel electrophoresis followed by Western blotting using a primary antibody specific to the DNP moiety of the protein, BSA-DNP in specific concentrations was used as a positive control. The samples were adjusted to the same amount of PrD-GFP, which was confirmed by western blot.

It can be seen even by eye, that although the amounts of protein carbonyls are similar in the lysate load fractions, the amounts of protein carbonyls detectable in the eluate fractions differs significantly: while there is almost no visible signal from the mitochondrially stressed sample, there is slightly more signal in the unstressed sample, but much more in the oxidatively stressed one. This leads to the conclusion that an increased amount of carbonylated proteins at the IPOD after oxidative stress can indeed be detected.

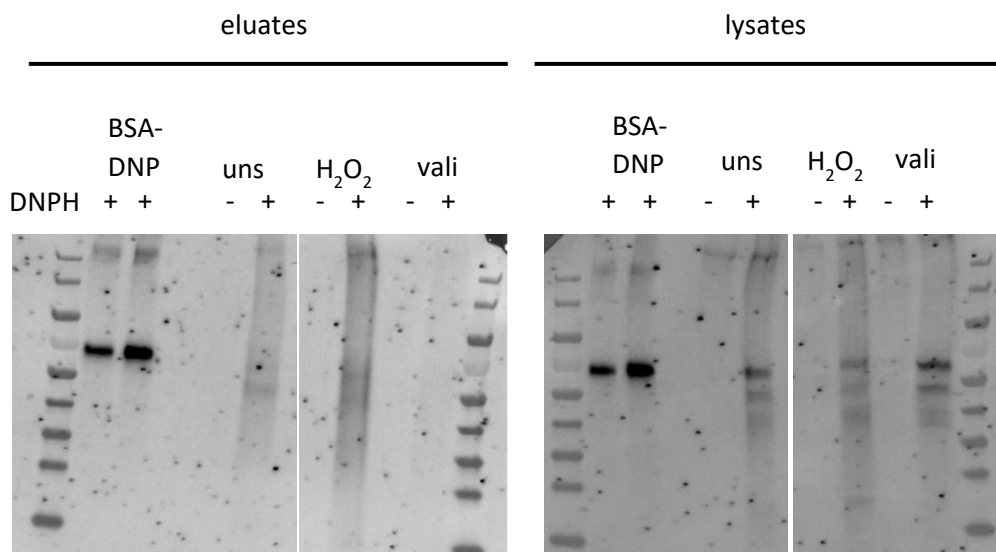


Figure R 12. Oxyblot for detection of protein carbonyl content in IP load (lysate) and eluate samples of different conditions. BSA-DNP was used as a positive control in a 1:20 and 1:10 dilution according to manufacturer's instructions. An un-derivatized negative control was run for each sample. The cut represents an empty lane (only sample buffer) and further unstressed sample.

4.3.2. Carbonyl Proteomics

In order to gain a better understanding of carbonyl species enriched at the IPOD after oxidative stress (see section 4.3.1), I endeavoured to find a large-scale approach of identifying carbonyl species at the IPOD. Since protein carbonyls are the most common markers of

protein oxidation, different methods have been developed for the detection and quantification. Carbonylation-prone sites are chiefly located in regions enriched for the susceptible amino acids arginine, lysine, proline or threonine, probably due to the fact that carbonylation increases the reactivity of neighbouring carbonylatable sites³⁰².

The most commonly used method of detection involves the derivatization of carbonyl groups in protein side chains to 2,4-dinitrophenylhydrazone (DNP) using 2,4-dinitrophenylhydrazine (DNPH) and the following detection of these adducts using different assays like oxyblot or ELISA. However, this method of marking protein carbonyls has also been used to detect protein carbonyls in mass spectrometry approaches.

Amino acid	Carbonylation product	Predicted mass shift
Arginine	Glutamic 5-semialdehyde	-43.05 Da
Lysine	Allysine	-1.03 Da
Lysine	2-aminoadipic acid (double oxidation of lysine)	+14.96 Da
Proline	Glutamic 5-semialdehyde	+15.99 Da
Proline	Pyroglutamic acid	+13.98 Da
Threonine	2-amino-3-oxobutanoic acid	-2.02 Da

Table R 5. Carbonyl modifications of amino acid side chains and predicted mass shifts caused by these.

Due to the possibility of creating artefacts during the derivatization reaction, the large mass shift and therefore difficulty in accurate detection caused by the DNP adduct, as well as concerns regarding the reactivity of traces of DNPH that might remain in the samples and therefore contaminate the system, this method was not used. Instead, with the collaboration of the DKFZ Proteomics core facility, an approach was tested in which un-derivatized samples were subjected to mass spectrometry analysis and the detection of carbonyls based on the mass shift, a carbonylation reaction causes in the peptides. This approach was based on previous experience of the facility in handling and discriminating similar types of samples (e.g.³⁰³). A list of variable modifications used for database search always included oxidation of Met as well as, direct carbonylation on Lys (aminoadipic semialdehyde), Arg and Pro (glutamic semialdehyde), and Thr (amino-ketobutyric acid) (full list see table R5).

Unstressed Y8205A cells as well as oxidatively stressed ones (2h 1mM H₂O₂) and ones which were cured of the [PSI⁺] prion using 5mM guanidine hydrochloride resulting in diffuse PrD-GFP were cryolysed. The cleared lysates and eluates from PrD-GFP targeted immunoprecipitation on these lysates were submitted to mass spectrometry analysis, to search for carbonylated proteins in triplicates. All samples had been equilibrated to equal PrD-GFP amounts. Among all proteins found, with and without modifications, PrD-GFP was the most abundant by iBAQ rating. An initial analysis could confirm the presence of an increased amount of protein carbonyls in the samples from oxidatively stressed cells (Fig. R13). Especially when one compares lysate to eluate fractions, it appears that oxidatively modified proteins are slightly more abundant in the IPOD enriched samples from oxidatively stressed cells. Comparing the total number of modified peptides found in the different groups of samples, in the eluates from unstressed cells (fourth box, Fig. R13) can be found approximately 30% the number of modified peptides as in the corresponding lysates (first box, Fig.13). In the oxidatively stressed samples, this percentage was higher at approximately 50% (third and sixth boxes, Fig. R13), while in the cured control with diffuse GFP it was only at approximately 25% (second and fifth boxes, Fig. R13). The main decrease is found in the modifications of N-terminal acetylation and methionine oxidation (Fig. R13).

Figure R14 shows a quantification of the frequency of the found carbonyl modification sites by sample. Overall, the distribution of a particular modification site between samples is similar to that of modified peptides found seen in figure R13. However, it is striking that indeed not all carbonyl modifications appear in similar amounts, but rather certain modifications are much more common in the samples than others, notably that of Threonine to 2-amino-3-oxobutanoic acid and direct proline oxidation appeared to be much more common in this dataset than the other possible modifications. It is possible that the results were slightly distorted due to the constraints of the bioinformatic analysis (see section 2.2.5). While there might be specific modifications leading to enrichment at the IPOD, it might also be that aggregates of heavily modified proteins are deposited because of the structural alterations caused by extensive carbonylation.

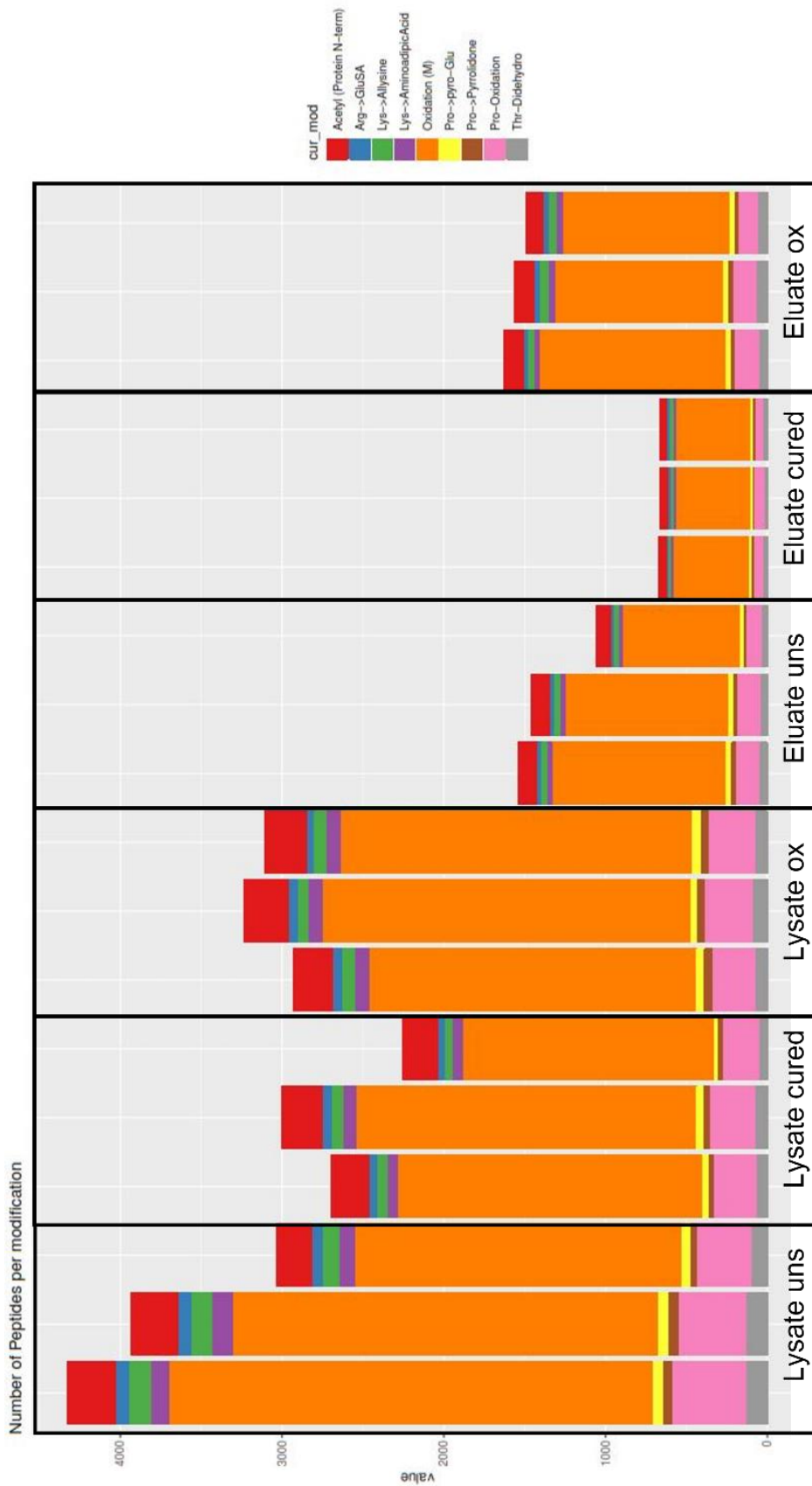


Figure R 13. Quantification of the number of peptides carrying oxidative modifications in lysates and eluates, each with $n=3$ biological replicates, of the indicated samples by modification. While lysate samples appear similar overall, with samples from unstressed cells being more variable, there are differences between the eluate fractions, with eluates from oxidative stress samples containing a higher number of modified peptides.

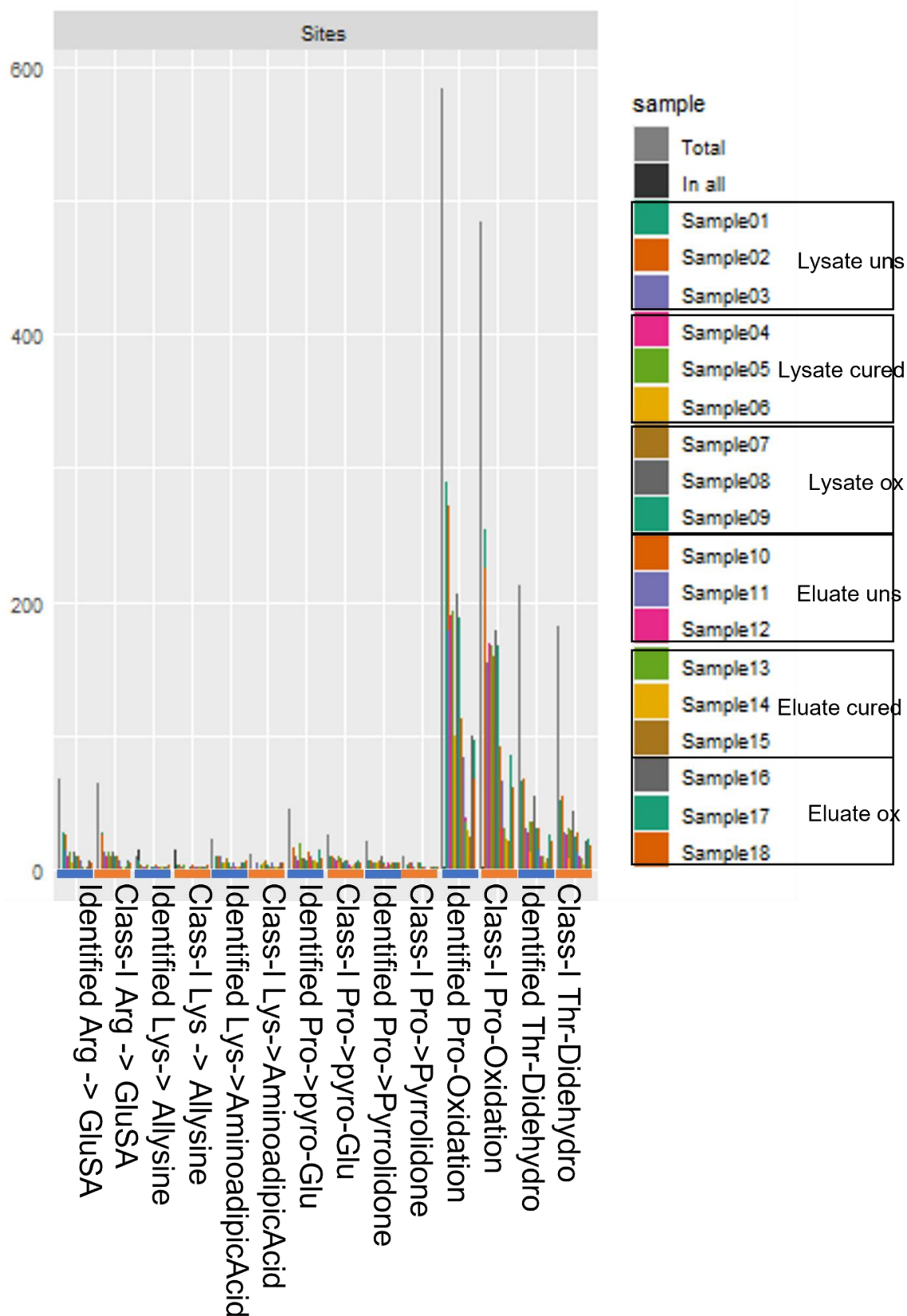


Figure R 14. Quantification of the frequency of found carbonyl modification sites by sample. The number of found sites per sample is shown for each modification using two different analysis settings (named here "identified" and "class-I", whereby class-I represents more stringent settings in the database search). Sample groupings are indicated by blue or orange colour block underneath.

Rank	Protein names	Gene names	logFC
1	40S ribosomal protein S22-B;40S ribosomal protein S22-A	RPS22B;RPS22A	9.9935E+14
3	Polyadenylate-binding protein, cytoplasmic and nuclear	PAB1	9.8821E+14
4	U3 small nucleolar ribonucleoprotein protein IMP3	IMP3	9.8704E+14
11	Adenylate cyclase	CYR1	9.6591E+14
17	Isocitrate dehydrogenase [NAD] subunit 1, mitochondrial	IDH1	9.4085E+14
19	Enolase 1	ENO1	9.2901E+14
20	Glyceraldehyde-3-phosphate dehydrogenase 1	TDH1	9.2855E+14
24	Myosin-4	MYO4	9.167E+14
32	Proteasome-interacting protein CIC1	CIC1	8.948E+14
33	Nucleolar GTP-binding protein 2	NOG2	8.904E+14
41	Vacuolar protein sorting-associated protein 35	VPS35	8.5499E+14
43	Ribosome quality control complex subunit 2	RQC2	8.4398E+14
98	Protein TOM71	TOM71	6.7976E+14
99	Glyceraldehyde-3-phosphate dehydrogenase 3	TDH3	6.7467E+14
122	Malate dehydrogenase, mitochondrial	MDH1	6.1219E+14
204	Pyruvate dehydrogenase E1 component subunit alpha, mitochondrial	PDA1	3.7963E+14
208	Cytochrome b-c1 complex subunit 1, mitochondrial	COR1	3.6668E+14
221	Heat shock protein 104	HSP104	3.4803E+14
234	Nuclear and cytoplasmic polyadenylated RNA-binding protein PUB1	PUB1	3.3223E+14
239	[PIN+] prion protein RNQ1	RNQ1	3.2808E+14
264	Cytochrome c oxidase subunit 2	COX2	2.7939E+14
290	Alcohol dehydrogenase 4	ADH4	2.4532E+14
293	Heat shock protein 42	HSP42	2.3838E+14
366	Superoxide dismutase [Mn], mitochondrial	SOD2	1.569E+14
497	Pyruvate decarboxylase isozyme 1	PDC1	3.5599E+13

Table R 6. Interesting oxidatively modified proteins enriched in IPOD-enriched samples of oxidatively stressed cells when compared to unstressed cells.

This is a preliminary dataset and requires further exploration, keeping in mind specific modification sites and proteins of interest and is more of a guide for further proteomic experiments. Nevertheless, several noticeable, modified proteins were found enriched in samples from oxidatively stressed cells overall (see table R6). Proteins of interest in this sample include mitochondrial proteins like Tom71, Mdh1 or Cox2, stress granule marker proteins like Pub1 and Pab1, proteins known to be at the IPOD like Rnq1 and Hsp104, some

ribosomal proteins, as well as several proteins known to be susceptible to oxidative damage³⁰⁴, like Eno1, Tdh1, Tdh3, Sod1, and Pdc1.

In general, this analysis has to be seen as a guide to find potentially interesting sites and not as a proof of specifically modified sites and further exploration is needed. However, this was not possible in the scope of this study due to time constraints.

A quantification of proteins found with particular modifications, either singly or multiply modified, was performed as a preliminary screening as well (see Table R7). Several of the proteins found in this analysis show more than one carbonyl modification, hinting at extensive oxidative damage. Among these are proteins known to be susceptible to oxidative damage like for example Pdc1, Eno2, and Adh2. Further experiments to validate and expand upon these findings are needed. But it is of special interest in light of the hypothesis of oxidatively damaged proteins aggregating and/or being deposited at the IPOD, that proteins with different carbonyl modifications appear to be found enriched at the IPOD. Many of these modifications were found in both unstressed and stressed samples, however more enriched in the oxidatively stressed samples.

Modification	# mod			
	proteins	single mod	multiple (2-3)	heavy mod (≥4)
Thr-Didehydro	140	105	31	4
		SSA1, RPL5	PGK1, ENO2	TDH3, PDC1
Pro-Oxidation	287	174	88	25
		ADH2, PDC5	ENO2, PAB1	PDC1, FAS1
Arg-GlutamicSemiAldehyde	53	44	9	0
		ENO1, ADH2	SRS2, KGD1	
Lys-Allysine	3	2	1	0
		SSA1, SSC1	TY4B-H	
Lys-AminoadipicAcid	14	7	7	0
		ARE1, SRB8	VPS13, IWR1	
Pro-PyroGlutamicAcid	23	11	11	1
		ADH1, SSA1	SUP35, SSC1	TEF1
Pro-Pyrrolidone	12	8	4	0
		PDR15, IWR1	SSC1, MVP1	

Table R 7. Sum of modified proteins found per modification. The number of total proteins found in the dataset with the modification is counted as well as the number of those which are singly, multiply or heavily modified, depending on how many putative modification sites were found. Example proteins are listed underneath these numbers.

4.3.3. Oxidative stress-induced foci formation

The previous mass spectrometric experiments confirmed the possible enrichment of proteins prone to oxidative damage at the IPOD (see section 4.1 and 4.2) and the enrichment of protein carbonyls in IPOD enriched samples supports this hypothesis (see sections 4.3.1 and 4.3.2). However, the mass spectrometry experiments are all *ex vivo* analyses and due to the potential for unspecific co-enriched proteins due to post-lysis interactions, it was needed to confirm that carbonylation-prone proteins are indeed IPOD-resident *in vivo*. A method that would have lent itself to help answer this question is the *in situ* detection of protein carbonyls in intact cells, which functions similarly to an oxyblot (see section 4.3.1): cells are fixed, treated with DNPH, and the carbonyl-DNP adducts are detected with a DNP-specific antibody. However, this approach was technically difficult to optimise and no clear structures could be seen, as signals were either very grainy or uniform throughout the cell (data not shown). This may have been a sensitivity problem. Therefore, it was chosen to validate the candidate proteins by colocalization experiments using fluorescence microscopy. Since Pdc1 had previously been seen to form foci in response to oxidative stress¹³⁰, this protein was investigated further to see whether how many cells shows this phenotype and whether the observed foci colocalize with the IPOD. For this purpose, a BY4742 strain expressing Pdc1-mCherry (Pdc1-mCh) stably integrated into the genome was used to screen for oxidative stress-induced foci formation and a 74D PrD-YFP strain expressing Pdc1-CFP was utilized to screen for colocalization of these foci with the IPOD.

In order to verify whether Pdc1, which under unstressed conditions is localized to the nucleus, forms foci, BY4742 Pdc1-mCh cells in logarithmic growth phase were subjected to 2h of oxidative stress by either a range of concentrations of H₂O₂ or menadione for 2h, 4h or 6h. Under both conditions of oxidative stress, Pdc1-mCh showed increased formation of extranuclear foci (Fig. R15). Under H₂O₂ stress, between 10% and 20% of all cells show a formation of foci under all concentrations and at all timepoints tested. Under menadione stress, between 20% and 30% of all cells showed a formation of Pdc1-mCh foci at all time points. Because the number of cells showing oxidative stress induced foci did not significantly increase with time or concentration of the stressor, in following experiments the oxidative stress conditions used were either 1mM H₂O₂ or 0.5mM menadione for 2h.

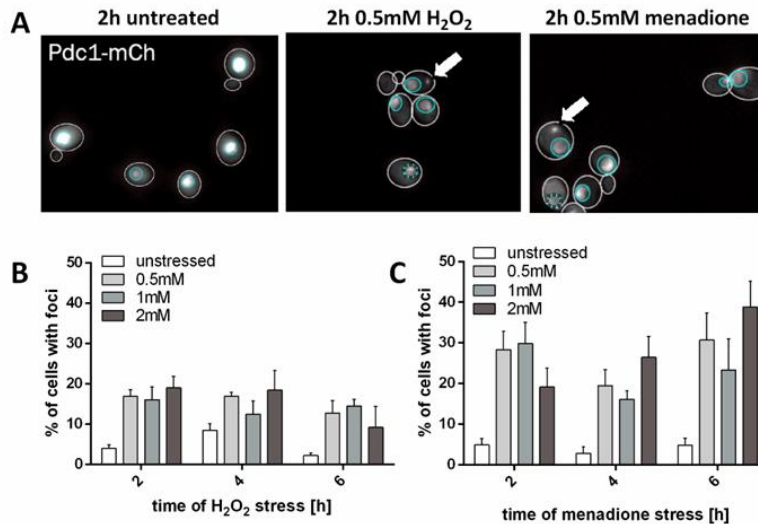


Figure R 15. Cells of the yeast strain *BY4742+Pdc1-mCh* were grown under standard conditions in YPD to an *OD600* of 0.4, then subjected to oxidative stress conditions. **A.** Representative images. Under basal conditions, Pdc1 is present in the nucleus, indicated by cyan areas. However, under conditions of oxidative stress, extranuclear foci form. Cells were then treated with 0.5mM, 1mM, or 2mM H_2O_2 over a course of 6h. Every 2h, an aliquot was withdrawn for fixation and subsequent analysis of Pdc1-mCh localization. **B.** Quantification of cells showing foci in relation to all cells. Under these conditions, approximately 20% of the cells form extranuclear foci under stress conditions. **C.** The experiment was repeated with menadione as oxidative stress-inducing agent. Upon menadione treatment, approximately 30% of cells form Pdc1-mCh foci. Images were taken at a 100X magnification and processed using ImageJ software. B: n=4 biological replicates. C: n=3 biological replicates. ≥ 100 cells per condition and replicate. Data represent mean \pm SD. Arrows indicate Pdc1-mCh foci.

Since the formation of oxidative stress-induced Pdc1 foci could be replicated and quantified, it was investigated next whether these foci colocalize with the IPOD. For this purpose, a 74D PrD-YFP Pdc1-CFP yeast strain was utilized. Liquid cultures in logarithmic growth phase were subjected to 2h of oxidative stress by treatment with 0.5mM menadione (Fig. R16). A similar number of cells showed formation of Pdc1 foci after oxidative stress, as well as a small number of cells even in unstressed conditions. The number of cells in which Pdc1 foci appear to colocalize with the IPOD was quantified in cells showing both an IPOD marked by PrD-YFP and a Pdc1 focus. In both cases, between 60% and 70% of the observed foci show a colocalization with the IPOD.

In order to test this hypothesis further, it was investigated whether candidate proteins which were found to be enriched at the IPOD of oxidatively stressed cells form foci after oxidative stress. For this purpose, strains from the mNeonGreen-tag C-SWAT BY4741-based strain library²⁸⁴ with suitable candidates found in the oxidatively stressed mass spectrometry dataset were picked. Liquid cultures in logarithmic growth phase were subjected to oxidative stress by treatment with 0.5mM menadione (mena) for 2h before fixation. Localization and

foci formation of the mNeonGreen-tagged candidate protein was assessed by fluorescent widefield microscopy and the number of cells showing foci was quantified (Fig. R17).

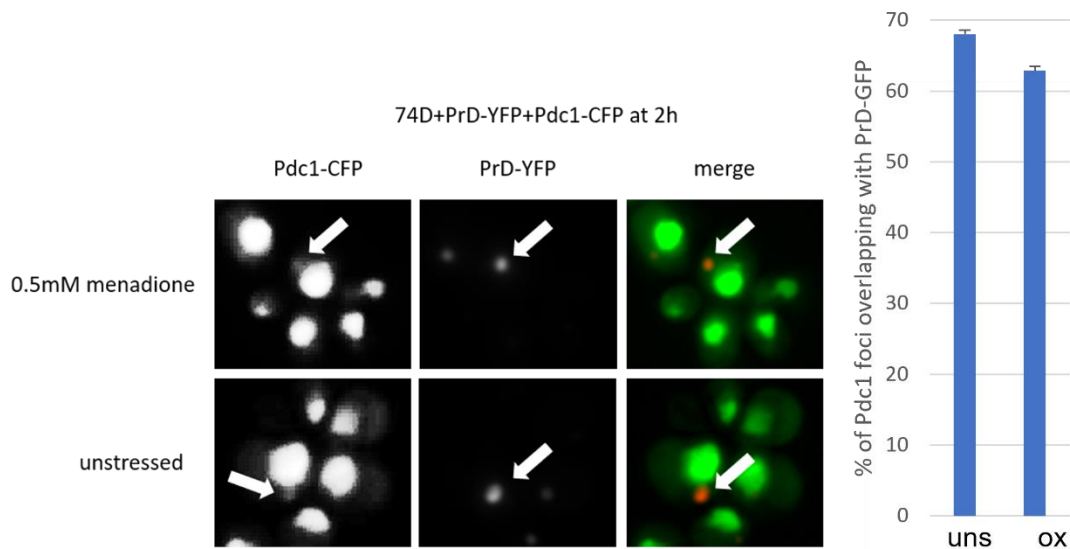


Figure R 16. PrD-YFP/Pdc1-CFP colocalization. Yeast cells were subjected to oxidative insult by 2h treatment with 0.5mM menadione or left unstressed. Cells were then fixed with 4%PFA and observed using a widefield fluorescent microscope. Images were taken at a 100X magnification and further processed using ImageJ/Fiji. When Pdc1-CFP foci could be observed, approximately 60-70% of them colocalised with the IPOD marked by PrD-YFP, as indicated by arrows. $n = 3$ biological replicates ≥ 50 cells per condition and replicate. Data represent mean \pm SD.

Most of the candidates showed a very low number of cells carrying foci both in unstressed and oxidatively stressed conditions. Candidates that showed an increase in cells showing foci in response to oxidative stress were Fks1 (unstressed (0h): 4%, 2h mena: 31%), Hsp60 (unstressed (0h): 7.5%, 2h mena: 24.1%), and Eno1 (unstressed (0h): 2%, 2h mena: 12%). However, none of these candidate proteins showed a visible localization of the formed foci close to the IPOD. It remains possible that some of these candidates do localize to the IPOD after oxidative stress-induced damage, as not all of these are highly expressed proteins and therefore foci of smaller sub-populations localizing to the IPOD may not be visible as foci.

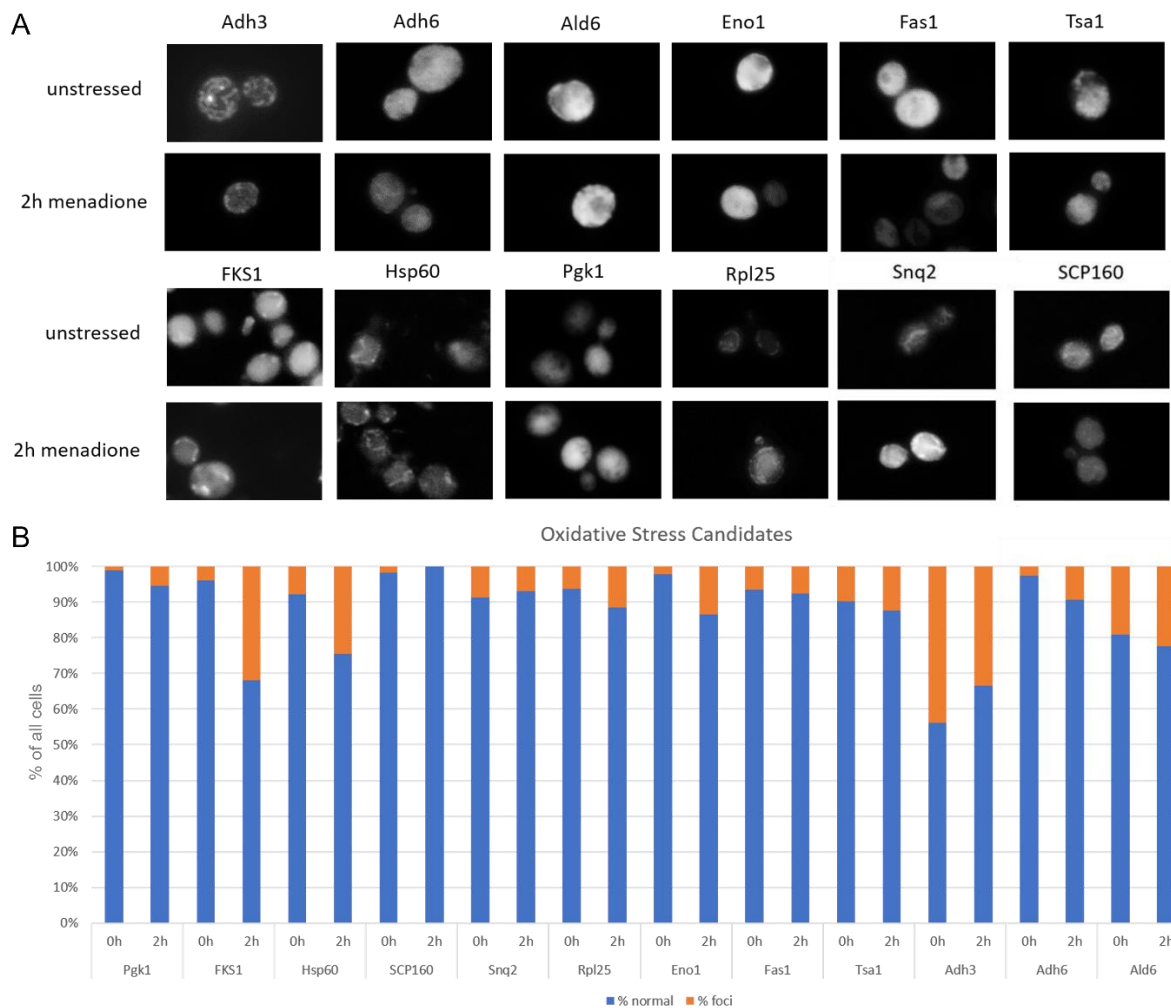


Figure R 17. Candidates picked from mass spectrometry data to check for oxidative stress induced foci formation. A. representative images. Images were taken at a 100X magnification and processed using ImageJ software. B. quantification of cells showing foci (shown in orange) and showing a native, non-stress localization of the candidate protein (shown in blue) in relation to all cells. N=200 cells per candidate.

Additionally, other candidates which have been known to be susceptible to oxidative damage and were found in the mass spectrometric analysis of enriched IPODs after oxidative stress were tested for their localization in relation to the IPOD after oxidative stress. For this purpose, Y8205A strains expressing the candidate protein tagged with mCherry were utilized. Of the candidates observed, none formed clearly defined single foci, however in some cases, the localization of some subpopulations of the candidate protein appeared to have changed to partially coincide with the IPOD after oxidative stress by 2h of 1mM H₂O₂. Where in unstressed conditions the IPOD appears separate from the candidate protein signal. Two of these candidates are shown in figure R18.

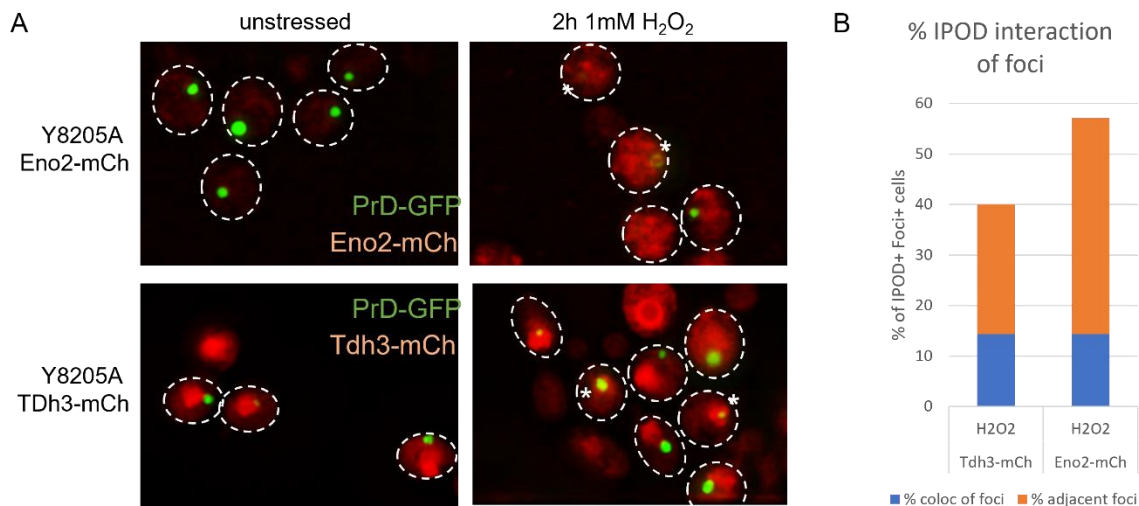


Figure R 18. Candidate protein localization after oxidative stress in relation to the IPOD. **A.** representative images. Yeast cells were subjected to oxidative insult by 2h treatment with 1mM H₂O₂ or left unstressed. Cells were then fixed with 4%PFA and observed using a widefield fluorescent microscope. Images were taken at a 100X magnification and further processed using ImageJ/Fiji. Asterisks indicate overlap of PrD-GFP and candidate-mCh signal. **B.** Localization of the candidate protein was categorized as colocalization/overlap (shown in blue) and adjacent (shown in orange) and the number of cells showing these was quantified in relation to all cells showing both an IPOD and a changed localization of the candidate protein (IPOD+ Foci+). n=407 cells for Tdh3, n= 160 cells for Eno2.

Y8205A Eno2-mCh shows a stronger signal after oxidative stress than unstressed that appears grainy, consisting of many small dots. The much stronger signal of Eno2-mCh after 2h of 1mM H₂O₂ stress may reflect an upregulation of its expression induced by increased ROS levels, which has been shown for example in Alzheimer's disease brain³⁰⁵ or mammalian cardiomyocytes³⁰⁶. After oxidative stress, some of these appear to either completely or partially overlap with the IPOD, resulting in about 57.14% of cells showing an interaction between the IPOD and Eno2-mCh signals (with 14.28% counting as overlap and 42.86% an adjacent localization). However, this cannot be classified as a real colocalization or interaction between Eno2 and the IPOD without further experiments. In the Y8205A Tdh3-mCh strain, the Tdh3-mCh signal appears to be separate from the IPOD under unstressed conditions, when it is enriched in the nucleus. Only after 2h of oxidative stress, its localization appears to change in 23% of cells, in which it becomes more compact and seems to interact with the IPOD in 40% of cells showing both an IPOD and a change in Tdh3 localization (with 14.3% counting as overlap and 25.7% counting as adjacent localization). Due to time constraints, these experiments could not be expanded upon.

4.4. Aberrant stress granules transiently colocalize with the IPOD

One protein repeatedly found in the IPOD enriched samples, albeit of lower abundance, was the stress granule marker protein Pab1, along with other stress granule markers like Pub1. It has been shown that aberrant stress granules associate with the aggresome in mammalian cells¹⁷⁸.

It was therefore hypothesized that in yeast, they may associate with the IPOD. In order to test this hypothesis, I first needed to establish a protocol to make stress granules more stable by accumulation of DRiPs, which leads to their persistence and aggregation^{178,189,307}. For this purpose, I adapted a protocol by Turakhiya and colleagues (2018)¹⁸⁹, which impairs the degradation of arsenite-induced stress granules by deleting the CDC48-associated ubiquitin-like/zinc finger protein 1, Cuz1. Generating a yeast strain which combines both PrD and the stress granule marker protein Pab1 tagged with fluorescent proteins, as well as a Cuz1 knockout (dCuz1), helped analyze whether aberrant stress granules colocalize with the IPOD. A BY4741 strain expressing Pab1-GFP (further referred to as wild type or WT) was used for this experiment, as well as the same strain carrying a knockout of dCuz1 (further referred to as dCuz1). The cells were grown to an OD of approximately 0.4, then treated for 30min with 5mM sodium arsenite (NaAsO₂). The stressor was removed by pelleting the cells via centrifugation at 1000xg for 5min and washing twice with PBS. The cells were then resuspended in growth medium and allowed to recover for 1h.

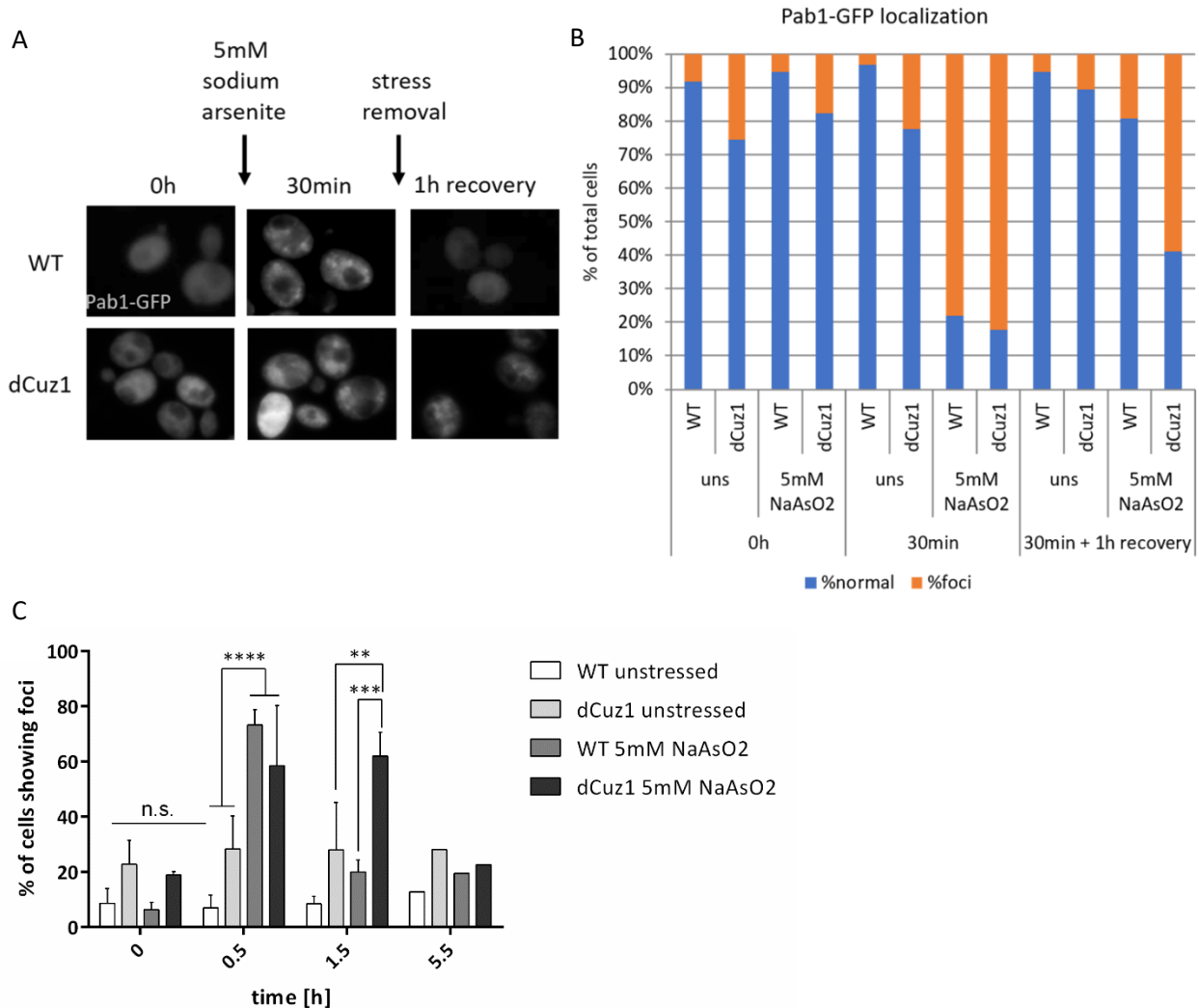


Figure R 19. Validation of a protocol for generation of persistent arsenite-induced stress granules marked by the model substrate Pab1-GFP. Wildtype (WT) and dCuz1 cells were grown under standard growth conditions in YPD to an OD600 of approximately 0.4, then subjected to 30min of arsenite stress by treatment with 5mM sodium arsenite (NaAsO₂), afterwards spun down, resuspended in fresh YPD and allowed to recover for 1h under standard conditions. **A.** Cells were then fixed with 4% PFA and observed under a widefield fluorescent microscope at a magnification of 100X. Shown are representative images of cells of both genotypes. **B. & C.** Quantified percentage of all cells showing the formation of Pab1-GFP foci representing stress granules (shown in orange) or no foci ("normal", shown in blue). n = 3 biological replicates.

A slightly higher amount of dCuz1 cells (26% of total cells) show stress granules, marked by Pab1-GFP, already under unstressed conditions compared to WT (9%) (Fig. R 21). After 30min of treatment with 5mM NaAsO₂, both WT and dCuz1 cells show a large increase in cells containing stress granules (WT: 79%, dCuz1: 82%), as expected (Fig. R19, ¹⁸¹⁻¹⁸⁴). After 1h recovery from stress, WT cells show a reduction in stress granule containing cells to almost basal levels (19.5%) (Fig. R19). This is to be expected, as stress granules are normally very dynamic and dissolve upon stress removal^{146,147}. dCuz1 cells show a much smaller reduction of the number of cells containing stress granules, as 60% of observed cells still contain stress

granules (Fig. R19B). This confirms that with this protocol, aberrant, longer-lasting arsenite stress(AS)-induced stress granules can be generated.

In order to follow the dynamics of AS-induced stress granules in this paradigm, cells were observed for a further 5h after stress removal (Fig. R20C) and the number of cells showing stress granule foci was quantified. As in the previous experiment, WT cells showed less stress granules than dCuz1 cells in response to AS, and the amount of cells is reduced to basal levels 1h after stress recovery, while the amount of dCuz1 cells showing stress granules remains high after 1h of recovery. By 5h after stress removal, the number of cells with stress granules was reduced to basal levels in both strains under unstressed and AS conditions. This leads to the assumption that aberrant stress granules may be degraded in other ways. Therefore, it was decided that for a first study of whether aberrant stress granules colocalize with the IPOD even transiently, the recovery time of 1h after stress removal should be used.

For these experiments, a Y8205A PrD-GFP strain which also expresses Pab1-mCh was generated, as well as a dCuz1 carrying variant of it. The experiment described above was repeated with this yeast strain. The amount of IPOD-containing (IPOD+) cells was counted, as was the amount of IPOD+ cells which contained also stress granules (IPOD+ SG+). In both WT and dCuz1 variants of this strain, between 30% and 40% of IPOD+ cells are IPOD+ SG+ in unstressed conditions (Fig. R20B). While the amount of IPOD+ SG+ cells increases in response to 30min AS in both strains, the increase is much more pronounced in dCuz1 cells (30% increases to 70%) than in WT cells (39% increase to 45%). This was expected, as AS-induced stress granules are not degraded properly in the dCuz1 background and are therefore more persistent¹⁸⁹.

The amount of IPOD+ SG+ cells in which a localization of stress granules indicated a complete or partial colocalization with the PrD-GFP marked IPOD, as well as a directly adjacent localization, was quantified in relation to all IPOD+ SG+ cells (Fig. R20C). In both WT and dCuz1 cells such occurrences were found, however in dCuz1 cells much more stress granules appeared to overlap completely with the IPOD after 30min of arsenite stress (WT: 19%, dCuz1: 39% of IPOD+ SG+ cells). In both WT and dCuz1, there appears to be a slight stress granule-IPOD interaction, with stress granules completely colocalizing with IPODs in approximately 5% of IPOD+SG+ cells. Some stress granules did not completely colocalize with the IPOD in these experiments, but did partially overlap. This was a very small percentage of cells overall

(WT AS: 1%, dCuz1 uns: 2.5%, dCuz1 AS: 0.76%). Furthermore, in many IPOD+ SG+ cells, stress granules appeared to be localized directly adjacent to the IPOD, but not overlap (WT uns: 22%, WT AS: 20%, dCuz1 uns: 14%, dCuz1 AS: 12.3%).

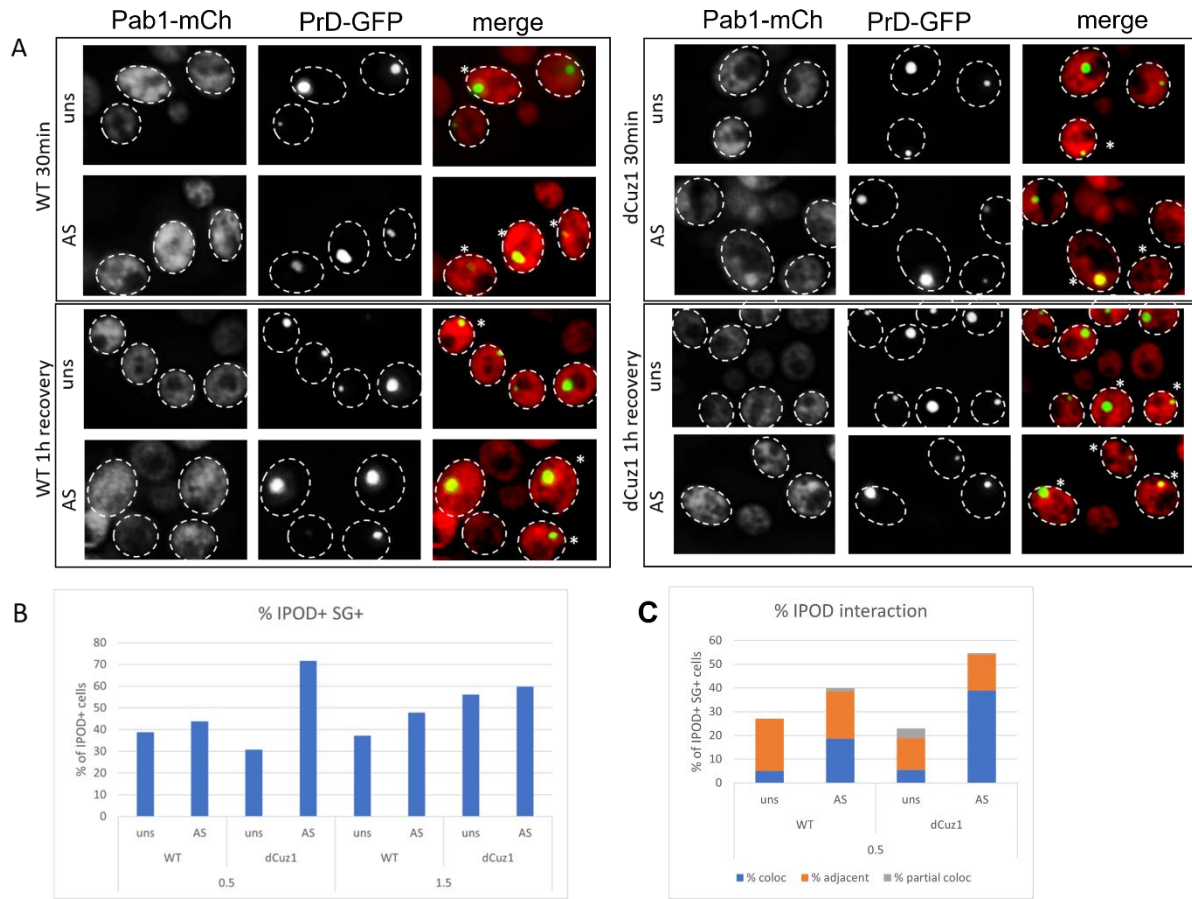


Figure R 22. Colocalization of aberrant stress granules and IPODs in Y8205A Pab1-mCh cells. Wildtype (WT) and dCuz1 cells were grown under standard growth conditions in YPD to an OD600 of approximately 0.4, then subjected to 30min of arsenite stress by treatment with 5mM sodium arsenite (NaAsO₂), afterwards spun down, resuspended in fresh YPD and allowed to recover for 1h under standard conditions. **A.** Cells were then fixed with 4% PFA and observed under a widefield fluorescent microscope at a magnification of 100X. Shown are representative images of cells of both genotypes. **B.** Quantified percentage of all IPOD containing cells showing the formation of Pab1-mCh foci representing stress granules. **C.** The percentage of IPOD+ SG+ cells in which SGs show complete colocalization (shown in blue), partial colocalization (shown in grey) or adjacent localization to the IPOD (shown in orange), was quantified. n=2 biological replicates, ≥100 cells/replicate and condition.

These results indicate that stress granules may at least transiently colocalize and interact with the IPOD and more persistent, aberrant stress granules do so in greater proportion. More experiments are needed to verify that aberrant stress granules are indeed IPOD substrates in their way to degradation, as well as the dynamics of this interactions. Unfortunately, these were outside the scope of this study due to time constraints.

4.5. Analysis of stress-induced localization changes of mitochondrial proteins

Several mitochondrial proteins were found in the mass spectrometry hit lists in datasets from stressed and unstressed cells, especially after mitochondrial stress (see sections 4.1 and 4.2). Further, it has been shown that mitophagy specifically of proteins of Complex I and II, especially the NADH:ubiquinone oxidoreductase Ndi1 and the subunit 2 of ubiquinol cytochrome-c reductase Qcr2 is increased after treatment with the potassium ionophore valinomycin compared to other mitochondrial proteins³⁰¹. Investigating this, BY4741 strains expressing these proteins tagged with mNeonGreen were analyzed for valinomycin-induced foci formation as well as the mitochondrial outer membrane protein OM45 tagged with GFP (Fig. R21).

In order to test the optimal valinomycin concentration for further experiments, a BY4741 OM45-GFP strain was subjected to 4 μ M, 6 μ M, or 8 μ M valinomycin treatment for 2h and 4h, respectively.

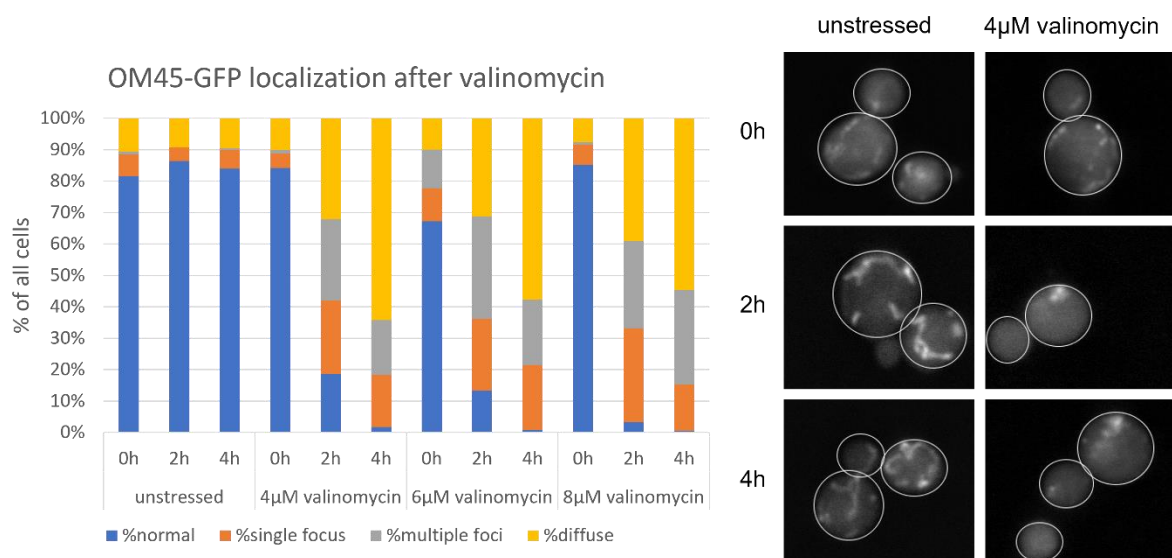


Figure R 21. BY4741 OM45-GFP localization under mitochondrial stress. Yeast cultures were grown under standard growth conditions in YPD to an OD600 of approximately 0.4, then subjected to mitochondrial stress for 2h by treatment with the potassium ionophore valinomycin. At the experimental endpoint, cells were fixed with 4% PFA and observed at a magnification of 100X using a widefield fluorescent microscope. Images were further processed using ImageJ/Fiji software. The experiment was performed in YPD, in which cells can perform fermentation. The percentage of all cells showing single foci/blob formation (shown in orange), multiple foci/blobs (shown in grey), diffuse signal (shown in yellow) or normal mitochondrial morphology (shown in blue) was quantified. n=3 biological replicates.

Under unstressed conditions, a normal mitochondrial phenotype could be observed. After treatment with valinomycin, the mitochondrial phenotype becomes disrupted and either multiple smaller foci or large “blobs” can be observed. In some cases, the OM45-GFP signal

even becomes diffuse. Since at the later time point of 4h and with increasing valinomycin concentration, the diffuse and multiple blob phenotype became more pronounced, further experiments were performed using a treatment of 4 μ M valinomycin for 2h.

As can be seen in figure R22A, in many cells, mitochondrial morphology was disrupted after valinomycin treatment and all mitochondrial proteins tested showed formation of foci or bigger assemblies I termed “blobs”. The appearance of these foci or blobs was more pronounced in cells growing in the YPGlycerol medium, also used during the mass spectrometry experiments (see figure R22B), in which the cells rely on respiratory metabolism as opposed to YPDextrose, in which they can perform fermentation of their carbon source.

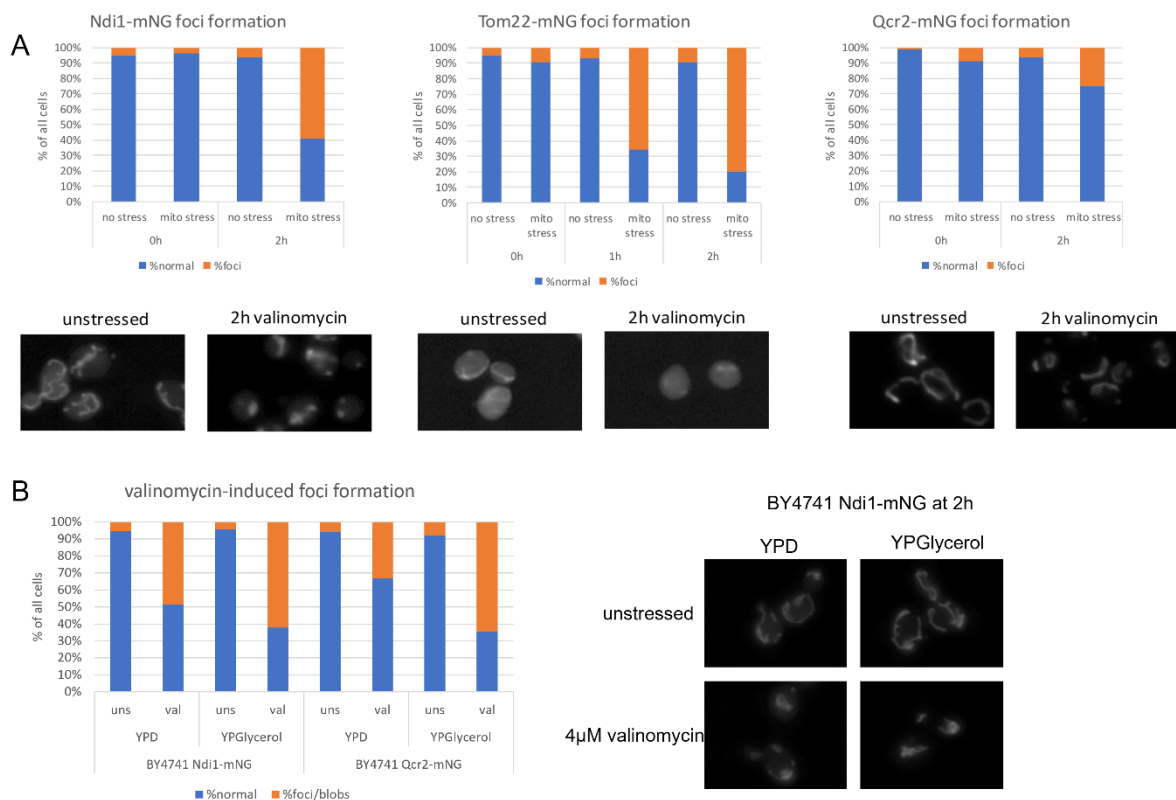


Figure R 20. BY4741 expressing IPOD substrate candidates tagged with mNeonGreen (mNG) under mitochondrial stress. Yeast cultures were grown under standard growth conditions in YPD to an OD600 of approximately 0.4, then subjected to mitochondrial stress (mito stress) for 2h by treatment with 4 μ M of the potassium ionophore valinomycin. **A.** At the experimental endpoint, cells were fixed with 4% PFA and observed at a magnification of 100X using a widefield fluorescent microscope. Images were further processed using ImageJ/Fiji software. The experiment was performed either in YPD, in which cells can perform fermentation or YPGlycerol under respiratory growth conditions. **B.** The percentage of all cells showing foci/blob formation (shown in orange) or normal mitochondrial morphology (shown in blue) was quantified. N=2 biological replicates. The foci/blob phenotype appears more pronounced when cells are growing under respiratory growth conditions.

Since Ndi1 and Qcr2 are known to undergo mitophagy after valinomycin treatment and were also found as candidates in the mass spectrometry of IPOD co-enriched proteins after both oxidative and mitochondrial stress, along with Tom22, which was also among candidate

proteins, these were tested. Tom22 and Ndi1 showed a pronounced “blob” phenotype after 1h and 2h valinomycin treatment. Qcr2 shows a less pronounced phenotype, but also an increase in cells showing “blobs”.

The change in mitochondrial morphology indicated by the different studied marker proteins, do not show a classical IPOD structure. It was decided to prioritize the investigation of oxidatively damaged proteins as initial results appeared to be more promising (see section 4.3). Nevertheless, the morphological changes are interesting and worth mentioning. They might indicate a possible IPOD interaction, however due to time constraints, it remains to be analysed whether these blobs or foci colocalize with the IPOD at any stage.

5. Discussion and Outlook

5.1. Discussion

The Insoluble Protein Deposit (IPOD) has been initially described as a deposition site for amyloid aggregates^{59,130,286}. However, more recently it has been suggested that the IPOD may also harbor other endogenous types of substrates, such as oxidatively damaged proteins¹³⁰ and inactive/damaged proteasomes or subunits thereof^{133,134,287}. Interestingly, many of these potential substrate classes can form high molecular weight aggregates²⁴⁰ or represent large protein complexes, respectively. Directly adjacent to the IPOD, the cell accumulates large multimeric complexes of vacuolar precursor hydrolases at the Pre-Autophagosomal Structure (PAS) for translocation into the vacuolar lumen via the CVT-pathway^{288–290}. Therefore, it was hypothesized that the perivacuolar IPOD may more generally represent a sorting center for aggregates and larger protein complexes destined for autophagic turnover (refer to Fig. 4, section 1.2.2.4).

This study focuses on the enrichment of IPODs visualized with PrD-GFP under different conditions, including oxidative stress, to help characterize other IPOD substrates through an unbiased mass spectrometry approach. This strategy identified several proteins that were co-enriched with the IPOD, mainly after oxidative stress. Among these, Pdc1, a protein susceptible to carbonylation³⁰⁴ which has been previously hypothesized to be present at the IPOD after oxidative insult¹³⁰, has also been found.

For a Pdc1-mCh fusion protein, it was observed that the number of cells which formed Pdc1-mCh foci was increased after different forms of oxidative stress such as H₂O₂ or menadione treatment (refer to Fig. R15, chapter 4.3.3). Other proteins found enriched at the IPOD after oxidative stress through co-isolation of IPODs include Enolase 2 (Eno2) and Glyceraldehyde-3-phosphate dehydrogenase isozyme 3 (Tdh3) (see table R2, section 4.2.1). Along these lines, by staining for carbonylated proteins using the Oxyblot method, it was found that the overall levels of carbonylated proteins co-enriching with IPODs was much higher after application of oxidative stress (refer to Fig. R12, section 4.3.1). This supports the hypothesis that aggregates of oxidatively damaged proteins are another substrate group for the IPOD.

Furthermore, it has been shown that aberrant stress granules transiently associate with the aggresome on their way to autophagic degradation in mammalian cells¹⁷⁸. It was

hypothesized that the IPOD may play a similar role to the aggresome in yeast in this regard and indeed, in a dCuz1 background that hinders proteasomal degradation of stress granules and makes them aberrant and more persistent, a proportion of aberrant arsenite-induced stress granules marked by Pab1-mCh colocalized with the IPOD after 30min of arsenite stress (refer to Fig. R20, chapter 4.4).

5.1.1. Strategies for IPOD-enrichment

It has been demonstrated that differently sized aggregates from yeast cell lysates²⁹¹ as well as in mammalian cells²⁹² can be characterized by flow cytometry. Furthermore, IPOD load and pattern have previously been characterized in living yeast cells by my research group²⁹³. On this principle a method of enrichment by FACS was tested that allows the isolation of PrD-GFP aggregates a specific size range and study their composition by mass spectrometry. This method was attractive, but technically challenging. It was theorized that this way of isolating IPODs by FACS instead of IP would reduce the amount of IPODs fragmented due to lysis conditions and propagons, which might cause a background of unspecific proteins because of post-lysis interactions. As a control, the self-assembling viral particle eGFP- μ NS²⁹⁴ was used. This viral protein does not have any known interactors in the yeast proteome, therefore it was hypothesized that no specific proteins would be co-sorted with this particle. While indeed the pattern of proteins co-sorted with eGFP- μ NS was different than those co-sorting with PrD-GFP (refer to Fig. R4, section 4.1), a lot of ribosomal proteins still appeared. Ribosomal proteins were among the most enriched proteins found in enriched IPODs (see sections 4.1 and 4.2). Because this abundant group of proteins was found in each approach and also appears in the CRAPome tool (Contaminant Repository for Affinity Purification Mass Spectrometry Data²⁹⁹), it is possible that ribosomal and other abundantly found proteins like metabolic enzymes may not be specifically co-sorted but the result of unspecific post-lysis interactions. However, it was still important to note that among proteins found at the IPOD by mass spectrometry in all approaches (see section 4.1., 4.2), the model substrate PrD-GFP and known IPOD resident proteins like Ssa1 were among the highly enriched proteins. Furthermore, the total protein content of FACS-sorted IPOD fractions was very low, resulting in poor peptide recovery and proteome coverage (section 4.1). Due to the remaining problem of a possible unspecific background due to post-lysis interactions and low total protein yield in the FACS-based IPOD enrichment approach, a second approach to enrich IPODs containing

PrD-GFP from yeast cell lysates consisted of an immunoprecipitation (IP) pulling on PrD-GFP in cleared lysates using GFP-Trap magnetic beads. This does not completely solve the possibility of unspecific post-lysis interactions but appears to slightly reduce it (see section 4.2) and results in a higher total protein yield and therefore better peptide recovery and coverage.

The FACS and IP datasets overlap, particularly with respect to the abundance of ribosomal proteins and the finding of several proteins which are known to be susceptible to oxidative damage, there are more known IPOD resident proteins in the IP-derived data, for instance Rnq1. These considerations led to the employment of the IP-based approach in further experiments. Furthermore, since the mass spectrometry experiments are by design *ex vivo* and there is the possibility of post-lysis interactions confounding the results, it was needed to validate the results in intact cells. Especially, I wanted to know whether particular carbonylation-sensitive proteins accumulate at the IPOD in their carbonylated state. A method that would have lent itself to help answer this question is the *in situ* detection of protein carbonyls in intact cells, which functions similarly to an oxyblot (see section 4.3.1). However, this approach was technically difficult to optimise, and no clear structures could be seen, as signals were either very grainy or uniform throughout the cell (data not shown). This may have been a sensitivity problem. Therefore, it was chosen to validate the candidate proteins by colocalization experiments using fluorescence microscopy.

5.1.2. Carbonylation-prone proteins accumulate at the IPOD

In the literature, it has been identified that during aging, which is associated with an increase of oxidative stress, protein carbonylation increases^{232,247-250,308,309}. However, not the entire proteome is equally at risk, or susceptible, for carbonylation damage, but rather specific proteins are more susceptible to oxidative damage^{261,304}. When comparing the protein carbonyl content of IPODs enriched from oxidatively stressed cells with that of IPODs from unstressed cells, the overall levels of co-enriching carbonylated proteins was visibly higher after application of oxidative stress (refer to Fig. R12, section 4.3.1). These results were confirmed with results from an initial attempt at carbonyl proteomics (see figure R13, chapter 4.3.2). Addition of carbonyl groups causes changes in hydrophobicity, surface charge and associated misfolding of proteins. It has been theorized, that carbonylated proteins either generate cytotoxic high molecular weight aggregates or lead to abnormally high rates of

protein turnover to remove them from the cell²⁴⁰. Furthermore, decreased proteolysis with age is regarded as a consequence of the accumulation of protease-resistant aggregates that in a sense clog up proteasomes. Consequently, damaged, e.g., carbonylated, protein substrates accumulate with time²⁵⁹. Interestingly, the role of carbonylation may change over the age of an organism. Originally a part of the PQS and a degradation label for aberrant, damaged or idle proteins, it can become a problem in older age by negatively influencing cellular functions like proteasomal degradation and promoting aggregation^{240,269}. It is possible that resulting aggregates of carbonylated proteins are targeted to the IPOD for storage or later degradation.

When comparing results of mass spectrometry analyses of IPOD contents after oxidative stress, many overlaps with proteins that are more susceptible to carbonylation³⁰⁴ can be found, including proteins which were hinted to be heavily modified by carbonylation in initial carbonyl proteomic screens (an overview can be seen in table D1, see also table R6 and Table R7, chapter 3.4), including for example Pdc1, Eno2, Tdh3, Adh2, and Sod1. Some of these proteins were also found at the IPOD under unstressed conditions, though in lower abundance (see sections 4.1.1 and 4.1.2). Therefore, a subpopulation of highly carbonylated proteins may aggregate and subsequently be deposited at the IPOD. A mechanism for spatial sequestration of protein carbonyls exists in yeast in the context of asymmetric cell division, whereby the daughter cell carries a markedly reduced load of carbonyls compared to the mother cell^{279,281}.

Interestingly, the deposition of aggregates at the IPOD has been hypothesized to facilitate asymmetric aggregate inheritance^{59,130,286,310,311}, since the IPOD remains in the mother cell upon cell division. Furthermore, Myo2, which is a factor involved in transport of amyloid aggregates to the IPOD²⁹⁵, is also involved in asymmetric inheritance of different types of aggregates including the Huntington's disease protein Htt103Q in yeast^{312,313}. It is therefore conceivable that mechanisms exist which favour the transport of aggregated protein carbonyls to the IPOD.

Category	Enzyme	References for relation to aging
Glucose metabolism	HXKA, Hexokinase-1	314
	Glyceraldehyde-3-phosphate dehydrogenase (TDH3)	280,314,315
	Enolase 1 (alpha enolase) (ENO1)	315
	Enolase 2 (ENO2)	280,315
	Pyruvate decarboxylase (PDC)	280,315,316
	Alcohol dehydrogenase I (ADH1)	280,314–316
PDH and Tricarboxylic acid cycle	Isocitrate dehydrogenase (IDH)	314
Electron transport chain and ATP metabolism	ATP synthase subunit beta (ATP2)	280,315
Amino acid and protein metabolism	Methionine synthase (MET)	280
	Elongation factor 1-alpha (EF1A)	314
Antioxidant defense systems	Catalase T (CTT)	315
Heat shock proteins/Chaperones	Heat shock protein 60 (Hsp60)	315
	Ssa1 (Hsp70 family)	280,314,315
	Ssa2 (Hsp70 family)	280,314,315
	Ssb1 (Hsp75)	280
	Ssc1 (Hsp70) mitochondrial	280
	Hsp82 (Hsp90 family)	315
Cytoskeleton	Actin (ACT1)	280,315
Membrane transport	Voltage dependent anion channel protein 1 (VDAC1)	314
Miscellaneous	Alcohol dehydrogenase 2 (ADH2)	314
	Malate synthase 1 (MLS1)	314
	Potassium-activated aldehyde dehydrogenase (ALDH4)	314

Table D8. Carbonylated proteins during aging in *S. cerevisiae* adapted from³⁰⁴. Shown is a selection of carbonylation susceptible proteins which also frequently appear in mass spectrometry analyses of enriched IPODs after oxidative stress when compared to unstressed ones.

Indeed, looking at patterns of carbonylation-prone protein categories that appear similar in aging in different species (reviewed in³⁰⁴, see Fig. D1), might support the finding of many proteins involved in cytoplasmic translation, mitochondrial proteins, metabolic enzymes, as well as cytoskeletal proteins and chaperones in analyses of IPOD contents after oxidative and mitochondrial stress as well as in parts also under unstressed conditions, as members of these protein groups appear to be more susceptible to carbonylation damage.

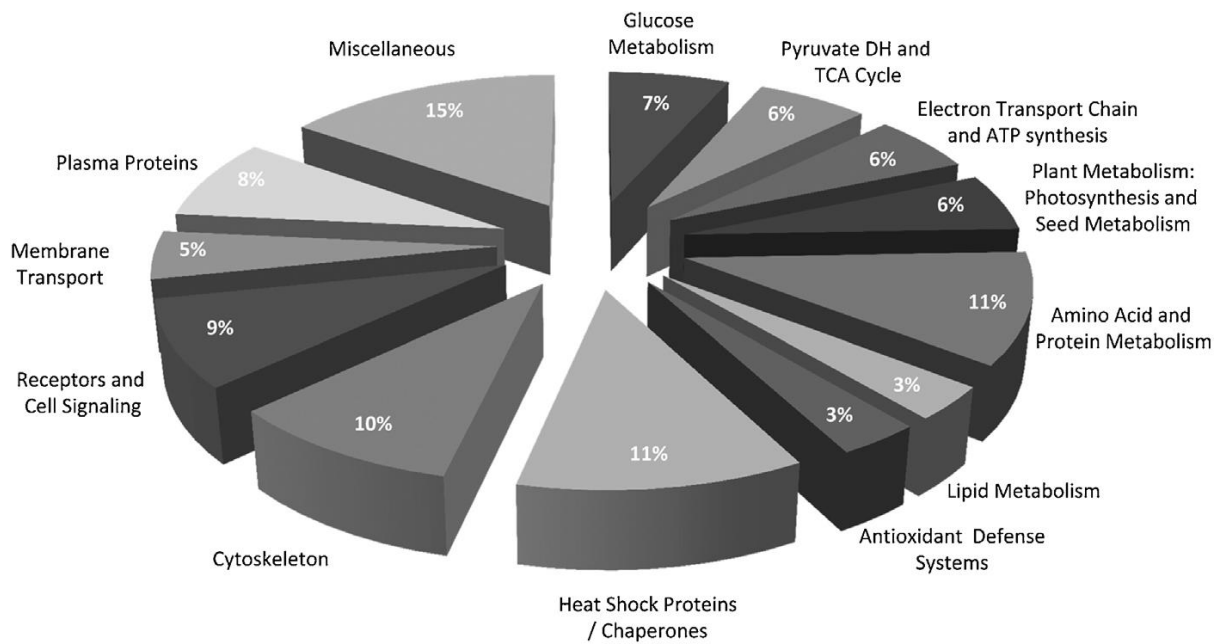


Figure D4. Pattern of carbonylation-prone protein categories that are similar in different species (*s. cerevisiae*, *e. coli*, *r. norvegicus*, *m. musculus*, *a. thaliana* and *h. sapiens*), from ³⁰⁴.

One aim of this study was the generation of a visually tractable marker for the for oxidatively damaged proteins by fusion of the carbonylation sensitive Pdc1 to mCherry. In only a minor fraction of cells (approximately 30% of all observed cells), the enzyme formed foci upon oxidative stress (refer to figure R14, chapter 3.3.2). Of these foci, however, a majority colocalized with the IPOD (refer to chapter 3.3.2). Other candidate proteins did not yield better result, as most of them showed a very low number of cells carrying foci both in unstressed and oxidatively stressed conditions (section 4.3.3). It may be that these proteins are not IPOD substrates after all as the mass spectrometry analyses suggest, but rather the result of unspecific interactions during sample processing. But it is possible that these proteins are at the IPOD, but not enough protein accumulates to generate a visible focus. In the case of Eno2, which showed some at least partial overlap with the IPOD after oxidative stress but no clear IPOD-like focus, it may also be that only a small subpopulation of the enzyme is heavily modified and accumulates. In this case, the signal might not be strong enough to allow for a visible focus that would stand out over the diffuse background fluorescence.

Furthermore, the treatment with H₂O₂ may have been too harsh, so that even if the candidate proteins were carbonylated and IPOD targets, they might not be recognized and transported there efficiently if the cell was already too damaged by the experimental treatment. Spotting

assays with a range of concentrations was performed and indicated that the used concentration was not lethal to the cells but did induce a growth arrest (data not shown).

On the other hand, carbonylated proteins are known to be degraded by the proteasome in different organisms^{318,319}, for which the oxidative stress-induced activation of the 20S proteasome is important³¹⁹. Furthermore, a role for the autophagic degradation of carbonylated biomolecules has been suggested in different models^{320–323}. Therefore, the proteolytic capacity of the cells may not be exceeded by excessive protein carbonylation under these experimental conditions and the steady state balance for these proteins may be more on the side of degradation without sufficient detectable accumulation. Interestingly, it has been inferred that the role of carbonylation may change over the age of an organism. Originally a part of the PQS and a degradation label for aberrant, damaged or idle proteins, it can become a problem in older age by negatively influencing cellular functions like proteasomal degradation and promoting aggregation^{240,269}.

In conclusion, while I was therefore unable to generate a robust visibly tractable marker for oxidatively damaged proteins that would lend itself to further experimentation (including a screen using the yeast deletion library to identify proteins that are involved in targeting of oxidatively damaged proteins to the IPOD or a pull-down of IPODs containing a fluorescently tagged marker protein like Pdc1-mCh), it is possible that only small, heavily modified subpopulations of candidate proteins are resident at the IPOD, which could not be visually identified.

4.1.2. Stress granules transiently colocalize with the IPOD

Stress granules (SGs) have been described as transient membrane-less organelles, which mainly consist of ribonucleoprotein assemblies which appear as part of an adaptive strategy to conserve energy and protect macromolecules in response to stress^{136–140}. Upon the end of stress and return to normal growth conditions, normal SGs dissolve^{141,144,324,325}. SG-inducing stress conditions also lead to the accumulation of misfolded proteins, including defective ribosome products (DRiPs), making it likely that SGs could co-aggregate with misfolded proteins. When DRiPs and other misfolded proteins accumulate inside SGs, the biochemical and dynamic properties of SGs are affected^{178,326}. These aberrant SGs containing misfolded proteins are less dynamic and RNase-resistant, perhaps due to aggregate-like core structures

containing high amounts of chaperones because of the contained misfolded proteins^{166,178,326}. Other chaperones are recruited as second line of defense at later time points, especially when SGs become enriched for additional misfolded proteins, to prevent conversion of aberrant SGs into irreversible aggregates^{178,326}. It has been shown that ZFAND1/Cuz1 and p97/Cdc48 are required for the efficient clearance of arsenite-induced SGs in mammalian and yeast cells, respectively¹⁸⁹. Absence of ZFAND1/Cuz1 causes formation of aberrant SGs containing DRiPs, which are targeted for autophagic degradation^{189,327}. Indeed, autophagy-deficient cells seem to accumulate SGs¹⁹¹. In this study the accumulation and persistence of arsenite-induced SGs in the absence of Cuz1, which leads to impaired targeting proper proteasomal degradation and accumulation¹⁸⁹ (refer to Fig. R19, section 4.4) could be reproduced. Furthermore, it is known that in mammalian cells, the formation of aggresomes, large inclusions harbouring misfolded and aggregated proteins, similar to the yeast IPOD, plays an important role in linking SG clearance to autophagy¹⁷⁸. Since SGs transiently localize to the aggresome before their autophagic clearance in mammalian cells, it was proposed that the IPOD may play a similar role in yeast. Its close perivacuolar localization as well as its involvement in the Hsp42- and Cue5-dependent maturation of proteasome storage granules^{133,134,287} hinted at a function of the IPOD as more than a deposition, perhaps also that of a sorting center on the way to autophagic degradation in cases like proteaphagy. In such a case, aberrant SGs may transiently interact with the IPOD. Indeed, in a Cuz1-deficient background, a sub population of aberrant arsenite-induced SGs marked by Pab1-mCh, colocalized with the IPOD after 30min of arsenite stress (refer to Fig. R20, section 4.4). The effect could be seen even more than 1h after stress removal. The number of cells displaying aberrant stress granules was reduced to almost basal, unstressed levels 5h after stress removal (refer to Fig. R19, section 4.4), indicating that aberrant SGs can indeed be degraded by autophagy. However, the dynamics of this interaction remain to be investigated. Since SGs may only transiently interact with the IPOD, only a smaller proportion of them may be associated with it at a time. If aberrant SGs containing accumulated DRiPs indeed interact with the IPOD, this may in part the abundant presence of ribosomal proteins at the IPOD in mass spectrometry analyses (see section 4.1 and 4.2). In this case, they may not have been part of an unspecific background brought on by post-lysis interactions but targeted there as part of the protein content of aberrant SGs.

4.1.3. Possibility of other substrate classes

The results of this study give a hint that the IPOD may indeed not only harbor amyloid aggregates, as previously supposed, but also other substrate classes, like aggregates of oxidatively damaged proteins as well as possibly aberrant SGs. Aberrant SGs have been found at the aggresome in mammalian cells¹⁷⁸ and transient deposition at the IPOD is involved in the maturation of proteasome storage granules, whereby damaged proteasomes are degraded by a process termed proteaphagy^{133,134,287}. Therefore, it becomes an interesting hypothesis that perhaps the IPOD represents a kind of sorting center for damaged, terminally misfolded, and aggregated proteins, resulting in either permanent storage or eventual degradation via selective autophagy (overview in Fig. D2). As the IPOD is located next to the phagophore assembly site (PAS)¹³¹, close to the vacuole^{59,130}, it may be an interesting possibility that in types of microautophagy other than proteaphagy or the degradation of aberrant stress granules, a maturation/sorting step associated with the IPOD may exist, like ribophagy and/or mitophagy. This could be hinted at by the finding of many ribosomal and mitochondrial proteins at the IPOD even after unstressed conditions (see chapter 3.1 and 3.2).

This is supported by previous findings from this research group, indicating that although no hint for autophagic turnover of the IPOD was observed thus far, IPOD depositions decayed progressively, but very slowly, over time, which may mean that IPOD contents are not processed in bulk but rather gradually. In a set of experiments using proteasome inhibitors and inhibitors of the known prion processing molecular chaperone Hsp104¹⁹⁵, it was revealed that PrD-GFP can be liberated from the IPOD by the action of Hsp104 and that only after this liberation, PrD-GFP could be turned over by autophagy³²⁸ or the proteasome³²⁹. It has been widely described that pathological amyloid aggregates hinder the autophagic degradation (e.g.^{330,331}) and can interfere with cellular physiology, for example, by disrupting transport of proteins and RNA³³² and by sequestering chaperones and proteasomes^{333,334}. The accumulation of PrD-GFP at the IPOD could therefore represent a temporary cytoprotective storage function to limit harmful effects of the aggregates³³⁵ until processing factors such as Hsp104 and possible downstream machineries are available. Furthermore, amyloid aggregates can sequester numerous other proteins³³⁶, leading to the disruption of cellular processes, which can also explain co-accumulation of non-amyloid proteins if there were no sorting hub function of the IPOD.

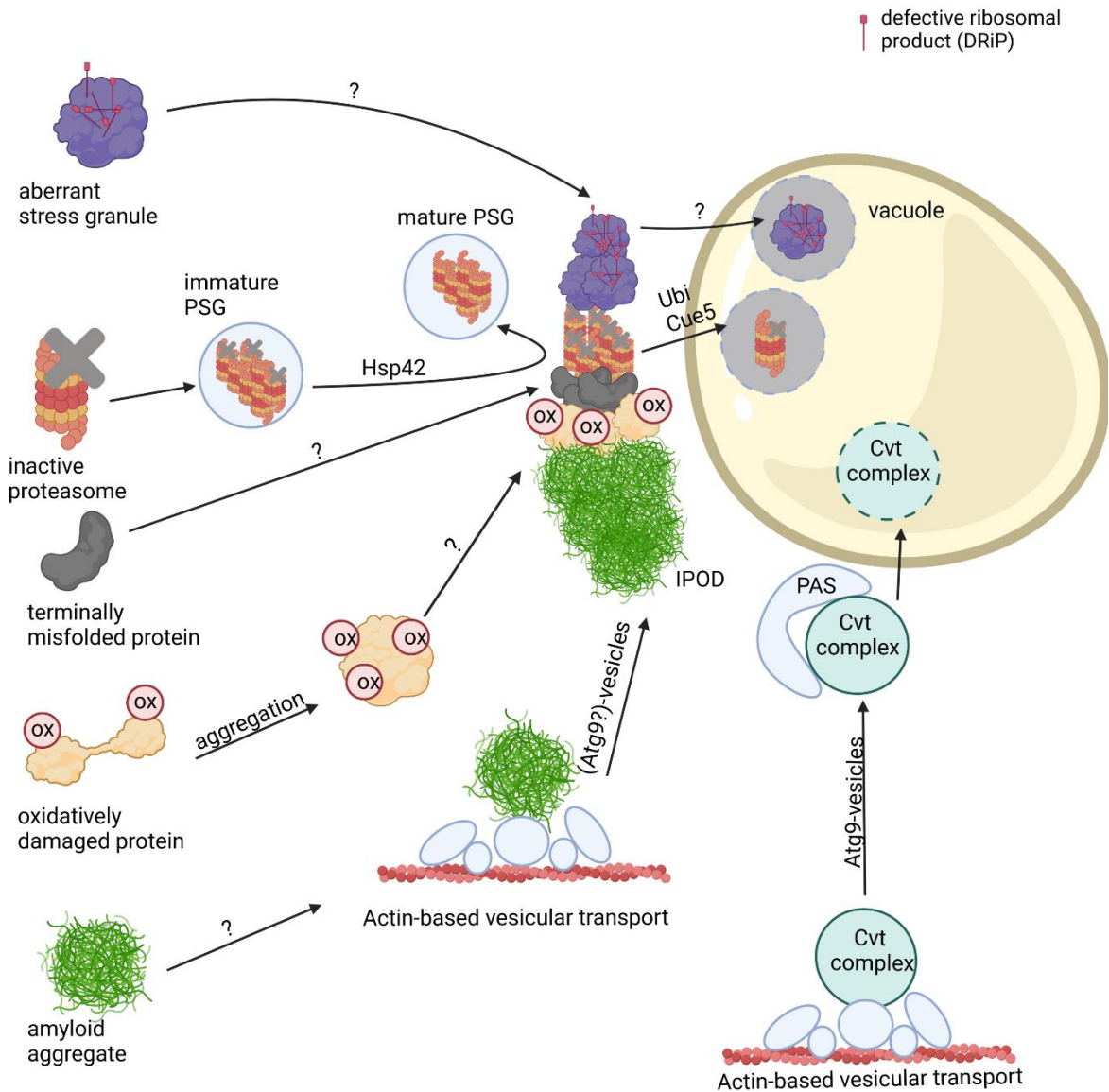


Figure D5. Updated overview of deposition of damaged or inactive proteins, amyloids or protein complexes at the IPOD. It is hypothesized that aberrant stress granules interact with IPOD on the way to autophagic degradation in the vacuole. Inactive proteasomes associated with Proteasome Storage Granules (PSGs) are known to accumulate at the IPOD in a Hsp42-dependent manner. Amyloid aggregates are targeted there by an actin-based transport machinery which overlaps with the recruitment machinery for vacuolar hydrolase precursors and their specific receptor (Cvt complex) to the pre-autophagosomal structure (PAS) via Atg9 vesicles, where these precursors are packaged into cytoplasm-to-vacuole vesicles for delivery to the lumen of the vacuole. It is hypothesized that large terminally misfolded proteins and oxidatively damaged proteins also accumulate at the IPOD in an as yet unknown manner. Created using BioRender.com.

4.2. Outlook

While the results of this study show some interesting hints of substrates like carbonylated proteins and aberrant stress granules at the IPOD and the potential physiological role of this co-accumulation, they should be seen as a starting point for more thorough investigation that was not possible under the temporal constraints of this study. Such experiments would include the following:

While there are hints for the colocalization of some potential IPOD substrates like Pdc1, it would be interesting to verify the colocalization of this and future substrate candidates observed in widefield fluorescent microscopy by other means, such as confocal or even electron microscopy.

Furthermore, the utilization of time lapse- or videomicroscopy enables the assessment of dynamic interactions. The colocalization of candidate protein foci or stress granules with the IPOD and its duration would clear up whether it is a transient interaction or permanent storage. This would also potentially shed light on the hypothesis that some substrates may be degraded via autophagy or other pathways over time.

If a better, robustly visually tractable marker protein for oxidatively damaged proteins (or other potential substrate classes) is found, it would be possible to conduct screens using the yeast deletion library to identify proteins that are involved in targeting of oxidatively damaged proteins to the IPOD. Another possibility would be the in situ detection of protein carbonyls by an oxyblot-like method, in which cells are fixed, treated with DNPH to derivatize carbonyl groups, and the carbonyl-DNP adducts are detected with a DNP-specific antibody. Furthermore, enrichment of IPODs containing oxidatively damaged proteins by pulling down fluorescently tagged candidate proteins or protein carbonyls would become possible, which would open the way for more targeted approaches to identify IPOD components under different conditions by mass spectrometry.

This laboratory has previously identified several components of the machinery required to recruit amyloid aggregates to the IPOD³³⁷. It would be interesting to address the question of whether different substrates, e.g. GFP-labeled inactive proteasomes, oxidatively damaged proteins, stress granules and possible new substrates identified, use the same recruitment machinery as compared to amyloid aggregates. To do so, promising candidates whose

deletion or depletion affected recruitment of amyloids to the IPOD, like Sec18 or Myo2, would be depleted/deleted in strains harbouring a fluorescently labeled candidate, to ask whether it can still be targeted successfully to the IPOD. In this way, one can deduce whether factors needed for deposition of amyloids are amyloid-specific or also required for the deposition of other substrates.

Furthermore, the disruption of mechanisms related to the degradation of some IPOD substrates (like Cue5 is for the macroautophagic degradation of proteasome storage granules) could bring about changes in dynamics also for other candidate proteins, which would be interesting to assess. As well, disruption of autophagy or the proteasomal pathway may affect the residency of particular substrates at the IPOD, which may be associated with changes in mean IPOD size and composition that could be assessed using microscopy and mass spectrometry methods, respectively. Previous findings indicate that although no hint for autophagic turnover of the IPOD was observed thus far, IPOD depositions decayed slowly over time. For example, PrD-GFP can be liberated from the IPOD by the action of Hsp104 and turned over by a pathway that can be inhibited by proteasomal inhibitors²⁹⁵. It would be interesting to see whether this is similar for other aggregated substrate types.

To study the fate of novel substrates deposited at the IPOD, it would be useful to perform pulse-chase type of experiments in which the substrate of interest is under control of inducible promoters to test whether a substrate is turned over or stored, as previously performed with PrD-GFP²⁹⁵.

The approach to the mass spectrometry-based assessment of carbonyl proteomics was an interesting start, but would need to be further refined to be surer that the results are indicative of real-world states in the cell. One could employ a more targeted approach with specific interesting candidates, which has been done before to identify modification sites of specific proteins (e.g. ³⁰³). Proteomics approaches, like fluorescent based 2D-gel electrophoresis and mass spectrometry methods, represent powerful tools for monitoring the extent of protein oxidative and related modifications at the proteome level and for identifying the targeted proteins.

Further down the line, it would be interesting to study the physiological impact of deposition of proteins at the IPOD and the consequences for a cell when this deposition fails.

6. References

1. Dobson, C. M. Protein folding and misfolding. **426**, (2003).
2. Chiti, F. & Dobson, C. M. Protein Misfolding , Functional Amyloid , and Human Disease. (2006). doi:10.1146/annurev.biochem.75.101304.123901
3. Breydo, L. & Uversky, V. N. Structural, morphological, and functional diversity of amyloid oligomers. *FEBS Lett.* **589**, 2640–2648 (2015).
4. Wolynes, P. G., Onuchic, J. N. & Thirumalai, D. Navigating the folding routes. *Science* **267**, 1619–1620 (1995).
5. Dill, K. A. & Chan, H. S. From Levinthal to pathways to funnels. *Nat. Struct. Biol.* **4**, 10–19 (1997).
6. Dobson, C. M. & Ellis, R. J. Protein folding and misfolding inside and outside the cell. *The EMBO journal* **17**, 5251–5254 (1998).
7. Dinner, A. R., Sali, A., Smith, L. J., Dobson, C. M. & Karplus, M. Understanding protein folding via free-energy surfaces from theory and experiment. *Trends Biochem. Sci.* **25**, 331–339 (2000).
8. Ellis, R. J. Macromolecular crowding: an important but neglected aspect of the intracellular environment. *Curr. Opin. Struct. Biol.* **11**, 114–119 (2001).
9. Bukau, B., Weissman, J. & Horwich, A. Molecular Chaperones and Protein Quality Control. *Cell* **125**, 443–451 (2006).
10. Hartl, F. U. & Hayer-Hartl, M. Converging concepts of protein folding in vitro and in vivo. *Nat. Struct. & Mol. Biol.* **16**, 574 (2009).
11. Olzscha, H. *et al.* Amyloid-like aggregates sequester numerous metastable proteins with essential cellular functions. *Cell* **144**, 67–78 (2011).
12. Arrasate, M., Mitra, S., Schweitzer, E. S., Segal, M. R. & Finkbeiner, S. Inclusion body formation reduces levels of mutant huntingtin and the risk of neuronal death. *Nature* **431**, 805–810 (2004).
13. Tanaka, M. *et al.* Aggresomes Formed by α -Synuclein and Synphilin-1 Are Cytoprotective. *J. Biol. Chem.* **279**, 4625–4631 (2004).
14. Wolfe, K. J., Ren, H. Y., Trepte, P. & Cyr, D. M. The Hsp70/90 cochaperone, Sti1, suppresses proteotoxicity by regulating spatial quality control of amyloid-like proteins. *Mol. Biol. Cell* **24**, 3588–3602 (2013).
15. Douglas, P. M. *et al.* Chaperone-dependent amyloid assembly protects cells from prion toxicity. *Proc. Natl. Acad. Sci. U. S. A.* **105**, 7206–7211 (2008).
16. Tyedmers, J., Mogk, A. & Bukau, B. Cellular strategies for controlling protein aggregation. *Nat. Rev. Mol. Cell Biol.* **11**, 777–788 (2010).
17. Tyedmers, J., Mogk, A. & Bukau, B. Cellular strategies for controlling protein aggregation. **11**, 22–24 (2010).
18. Kopito, R. R. Aggresomes, inclusion bodies and protein aggregation. *Trends Cell Biol.* **10**, 524–530 (2000).

19. Sunde, M. & Blake, C. The structure of amyloid fibrils by electron microscopy and X-ray diffraction. *Adv. Protein Chem.* **50**, 123–159 (1997).
20. Fitzpatrick, A. W. P. *et al.* Atomic structure and hierarchical assembly of a cross- β amyloid fibril. *Proc. Natl. Acad. Sci. U. S. A.* **110**, 5468–5473 (2013).
21. Fitzpatrick, A. W. P., Park, S. T. & Zewail, A. H. Exceptional rigidity and biomechanics of amyloid revealed by 4D electron microscopy. *Proc. Natl. Acad. Sci. U. S. A.* **110**, 10976–10981 (2013).
22. Chiti, F., Stefani, M., Taddei, N., Ramponi, G. & Dobson, C. M. Rationalization of the effects of mutations on peptide and protein aggregation rates. *Nature* **424**, 805–808 (2003).
23. Beerten, J. *et al.* Aggregation gatekeepers modulate protein homeostasis of aggregating sequences and affect bacterial fitness. *Protein Eng. Des. Sel.* **25**, 357–366 (2012).
24. Fiori, M. G. Intranuclear inclusions in Schwann cells of aged fowl ciliary ganglia. *J. Anat.* **154**, 201–214 (1987).
25. Peters, A., Josephson, K. & Vincent, S. L. Effects of aging on the neuroglial cells and pericytes within area 17 of the rhesus monkey cerebral cortex. *Anat. Rec.* **229**, 384–398 (1991).
26. Cuervo, A. M. & Dice, J. F. Age-related decline in chaperone-mediated autophagy. *J. Biol. Chem.* **275**, 31505–31513 (2000).
27. Koga, H. *et al.* Constitutive upregulation of chaperone-mediated autophagy in Huntington's disease. *J. Neurosci. Off. J. Soc. Neurosci.* **31**, 18492–18505 (2011).
28. Kruegel, U. *et al.* Elevated proteasome capacity extends replicative lifespan in *Saccharomyces cerevisiae*. *PLoS Genet.* **7**, e1002253 (2011).
29. Anderson, R. A., Qin, B., Canini, F., Poulet, L. & Roussel, A. M. Cinnamon counteracts the negative effects of a high fat/high fructose diet on behavior, brain insulin signaling and Alzheimer-associated changes. *PLoS One* **8**, e83243 (2013).
30. Öling, D., Eisele, F., Kvint, K. & Nyström, T. Opposing roles of Ubp3-dependent deubiquitination regulate replicative life span and heat resistance. *EMBO J.* **33**, 747–761 (2014).
31. Saez, I. & Vilchez, D. The Mechanistic Links Between Proteasome Activity, Aging and Age-related Diseases. *Curr. Genomics* **15**, 38–51 (2014).
32. Schneider, K. L., Nyström, T. & Widlund, P. O. Studying Spatial Protein Quality Control, Proteopathies, and Aging Using Different Model Misfolding Proteins in *S. Cerevisiae*. *Front. Mol. Neurosci.* **11**, 1–13 (2018).
33. Tanase, M. *et al.* Role of Carbonyl Modifications on Aging-Associated Protein Aggregation. *Sci. Rep.* **6**, 19311 (2016).
34. Frydman, J. & Hartl, F. U. Principles of chaperone-assisted protein folding: differences between in vitro and in vivo mechanisms. *Science* **272**, 1497–1502 (1996).
35. Mogk, A. & Bukau, B. Role of sHsps in organizing cytosolic protein aggregation and disaggregation. *Cell Stress Chaperones* **22**, 493–502 (2017).
36. Hipp, M. S., Kasturi, P. & Hartl, F. U. The proteostasis network and its decline in ageing. *Nat. Rev. Mol. Cell Biol.* **20**, 421–435 (2019).
37. Hartl, F. U. Molecular chaperones in cellular protein folding. *Nature* **381**, 571–579 (1996).

38. Hill, S. M., Hanzén, S. & Nyström, T. Restricted access: spatial sequestration of damaged proteins during stress and aging. *EMBO Rep.* **18**, 377–391 (2017).
39. Josefson, R., Andersson, R. & Nyström, T. How and why do toxic conformers of aberrant proteins accumulate during ageing? *Essays Biochem.* **61**, 317–324 (2017).
40. Sontag, E. M., Samant, R. S. & Frydman, J. Mechanisms and Functions of Spatial Protein Quality Control. *Annu. Rev. Biochem.* **86**, 97–122 (2017).
41. Xia, X., Longo, L. M., Sutherland, M. A. & Blaber, M. Evolution of a protein folding nucleus. *Protein Sci.* **25**, 1227–1240 (2016).
42. Kim, H. & Strange, K. Changes in translation rate modulate stress-induced damage of diverse proteins. *Am. J. Physiol. Cell Physiol.* **305**, C1257-64 (2013).
43. Kim, Y. E., Hipp, M. S., Bracher, A., Hayer-Hartl, M. & Hartl, F. U. Molecular chaperone functions in protein folding and proteostasis. *Annu. Rev. Biochem.* **82**, 323–355 (2013).
44. Balchin, D., Hayer-Hartl, M. & Hartl, F. U. In vivo aspects of protein folding and quality control. *Science* **353**, aac4354 (2016).
45. Liberek, K., Lewandowska, A. & Zietkiewicz, S. Chaperones in control of protein disaggregation. *EMBO J.* **27**, 328–335 (2008).
46. Haslbeck, M., Miess, A., Stromer, T., Walter, S. & Buchner, J. Disassembling protein aggregates in the yeast cytosol. The cooperation of Hsp26 with Ssa1 and Hsp104. *J. Biol. Chem.* **280**, 23861–23868 (2005).
47. Glover, J. R. & Lindquist, S. Hsp104, Hsp70, and Hsp40: a novel chaperone system that rescues previously aggregated proteins. *Cell* **94**, 73–82 (1998).
48. Mogk, A. *et al.* Identification of thermolabile Escherichia coli proteins: prevention and reversion of aggregation by DnaK and ClpB. *EMBO J.* **18**, 6934–6949 (1999).
49. Winkler, J., Tyedmers, J., Bukau, B. & Mogk, A. Chaperone networks in protein disaggregation and prion propagation. *J. Struct. Biol.* **179**, 152–160 (2012).
50. Tessarz, P., Mogk, A. & Bukau, B. Substrate threading through the central pore of the Hsp104 chaperone as a common mechanism for protein disaggregation and prion propagation. *Mol. Microbiol.* **68**, 87–97 (2008).
51. Tyedmers, J., Mogk, A. & Bukau, B. Cellular strategies for controlling protein aggregation. *Nat. Rev. Mol. Cell Biol.* **11**, 777–788 (2010).
52. Hanzén, S. *et al.* Lifespan Control by Redox-Dependent Recruitment of Chaperones to Misfolded Proteins. *Cell* **166**, 140–151 (2016).
53. MacDiarmid, C. W. *et al.* Peroxiredoxin chaperone activity is critical for protein homeostasis in zinc-deficient yeast. *J. Biol. Chem.* **288**, 31313–31327 (2013).
54. Trotter, E. W., Rand, J. D., Vickerstaff, J. & Grant, C. M. The yeast Tsa1 peroxiredoxin is a ribosome-associated antioxidant. *Biochem. J.* **412**, 73–80 (2008).
55. Lander, G. C. *et al.* Complete subunit architecture of the proteasome regulatory particle. *Nature* **482**, 186–191 (2012).
56. Smith, D. M. *et al.* Docking of the proteasomal ATPases' carboxyl termini in the 20S proteasome's alpha ring opens the gate for substrate entry. *Mol. Cell* **27**, 731–744 (2007).

57. Nillegoda, N. B. *et al.* Ubr1 and Ubr2 function in a quality control pathway for degradation of unfolded cytosolic proteins. *Mol. Biol. Cell* **21**, 2102–2116 (2010).
58. Heck, J. W., Cheung, S. K. & Hampton, R. Y. Cytoplasmic protein quality control degradation mediated by parallel actions of the E3 ubiquitin ligases Ubr1 and San1. *Proc. Natl. Acad. Sci. U. S. A.* **107**, 1106–1111 (2010).
59. Kaganovich, D., Kopito, R. & Frydman, J. Misfolded proteins partition between two distinct quality control compartments. *Nature* **454**, 1088–1095 (2008).
60. Bedford, L. *et al.* Depletion of 26S proteasomes in mouse brain neurons causes neurodegeneration and Lewy-like inclusions resembling human pale bodies. *J. Neurosci. Off. J. Soc. Neurosci.* **28**, 8189–8198 (2008).
61. Bedford, L. *et al.* Is malfunction of the ubiquitin proteasome system the primary cause of alpha-synucleinopathies and other chronic human neurodegenerative disease? *Biochim. Biophys. Acta* **1782**, 683–690 (2008).
62. Martín-Aparicio, E. *et al.* Proteasomal-dependent aggregate reversal and absence of cell death in a conditional mouse model of Huntington's disease. *J. Neurosci. Off. J. Soc. Neurosci.* **21**, 8772–8781 (2001).
63. Goldberg, A. L. Protein degradation and protection against misfolded or damaged proteins. *Nature* **426**, 895–899 (2003).
64. Baraibar, M. A. & Friguet, B. Changes of the proteasomal system during the aging process. *Prog. Mol. Biol. Transl. Sci.* **109**, 249–275 (2012).
65. Schmidt, M. & Finley, D. Regulation of proteasome activity in health and disease. *Biochim. Biophys. Acta* **1843**, 13–25 (2014).
66. Tseng, A., Inuzuka, H., Gao, D., Singh, A. & Wei, W. Experimental approaches to investigate the proteasomal degradation pathways involved in regulation of apoptosis. *Methods Enzymol.* **446**, 205–223 (2008).
67. Tseng, B. P., Green, K. N., Chan, J. L., Blurton-Jones, M. & LaFerla, F. M. Abeta inhibits the proteasome and enhances amyloid and tau accumulation. *Neurobiol. Aging* **29**, 1607–1618 (2008).
68. Bence, N. F., Sampat, R. M. & Kopito, R. R. Impairment of the ubiquitin-proteasome system by protein aggregation. *Science* **292**, 1552–1555 (2001).
69. Hyttinen, J. M. T. *et al.* Clearance of misfolded and aggregated proteins by aggrephagy and implications for aggregation diseases. *Ageing Res. Rev.* **18**, 16–28 (2014).
70. Venkatraman, P., Wetzel, R., Tanaka, M., Nukina, N. & Goldberg, A. L. Eukaryotic proteasomes cannot digest polyglutamine sequences and release them during degradation of polyglutamine-containing proteins. *Mol. Cell* **14**, 95–104 (2004).
71. Schipper-Krom, S., Juenemann, K. & Reits, E. A. J. The Ubiquitin-Proteasome System in Huntington's Disease: Are Proteasomes Impaired, Initiators of Disease, or Coming to the Rescue? *Biochem. Res. Int.* **2012**, 837015 (2012).
72. Dikic, I. Proteasomal and Autophagic Degradation Systems. *Annu. Rev. Biochem.* **86**, 193–224 (2017).
73. Lamb, C. A., Dooley, H. C. & Tooze, S. A. Endocytosis and autophagy: Shared machinery for degradation. *Bioessays* **35**, 34–45 (2013).

74. Lamb, C. A., Yoshimori, T. & Tooze, S. A. The autophagosome: origins unknown, biogenesis complex. *Nat. Rev. Mol. Cell Biol.* **14**, 759–774 (2013).
75. Mizushima, N., Yoshimori, T. & Ohsumi, Y. The role of Atg proteins in autophagosome formation. *Annu. Rev. Cell Dev. Biol.* **27**, 107–132 (2011).
76. Wen, X. & Klionsky, D. J. An overview of macroautophagy in yeast. *J. Mol. Biol.* **428**, 1681–1699 (2016).
77. Glick, D., Barth, S. & Macleod, K. F. Autophagy: cellular and molecular mechanisms. *J. Pathol.* **221**, 3–12 (2010).
78. Lamark, T. & Johansen, T. Mechanisms of Selective Autophagy. *Annu. Rev. Cell Dev. Biol.* **37**, 143–169 (2021).
79. Yang, Z. & Klionsky, D. J. Mammalian autophagy: core molecular machinery and signaling regulation. *Curr. Opin. Cell Biol.* **22**, 124–131 (2010).
80. Yorimitsu, T. & Klionsky, D. J. Autophagy: molecular machinery for self-eating. *Cell Death Differ.* **12 Suppl 2**, 1542–1552 (2005).
81. Nakatogawa, H., Suzuki, K., Kamada, Y. & Ohsumi, Y. Dynamics and diversity in autophagy mechanisms: lessons from yeast. *Nat. Rev. Mol. Cell Biol.* **10**, 458–467 (2009).
82. Galluzzi, L., Pietrocola, F., Levine, B. & Kroemer, G. Metabolic control of autophagy. *Cell* **159**, 1263–1276 (2014).
83. Tuttle, D. L., Lewin, A. S. & Dunn, W. A. J. Selective autophagy of peroxisomes in methylotrophic yeasts. *Eur. J. Cell Biol.* **60**, 283–290 (1993).
84. Sakai, Y., Koller, A., Rangell, L. K., Keller, G. A. & Subramani, S. Peroxisome degradation by microautophagy in *Pichia pastoris*: identification of specific steps and morphological intermediates. *J. Cell Biol.* **141**, 625–636 (1998).
85. Chiang, H. L., Schekman, R. & Hamamoto, S. Selective uptake of cytosolic, peroxisomal, and plasma membrane proteins into the yeast lysosome for degradation. *J. Biol. Chem.* **271**, 9934–9941 (1996).
86. Müller, O. *et al.* Autophagic tubes: vacuolar invaginations involved in lateral membrane sorting and inverse vesicle budding. *J. Cell Biol.* **151**, 519–528 (2000).
87. Campbell, C. L. & Thorsness, P. E. Escape of mitochondrial DNA to the nucleus in *yme1* yeast is mediated by vacuolar-dependent turnover of abnormal mitochondrial compartments. *J. Cell Sci.* **111** (Pt 1, 2455–2464 (1998).
88. Roberts, P. *et al.* Piecemeal microautophagy of nucleus in *Saccharomyces cerevisiae*. *Mol. Biol. Cell* **14**, 129–141 (2003).
89. van Zutphen, T. *et al.* Lipid droplet autophagy in the yeast *Saccharomyces cerevisiae*. *Mol. Biol. Cell* **25**, 290–301 (2014).
90. Schuck, S., Gallagher, C. M. & Walter, P. ER-phagy mediates selective degradation of endoplasmic reticulum independently of the core autophagy machinery. *J. Cell Sci.* **127**, 4078–4088 (2014).
91. Liu, X.-M. & Du, L.-L. A selective autophagy pathway takes an unconventional route. *Autophagy* **11**, 2381–2382 (2015).
92. Yang, X. *et al.* TORC1 regulates vacuole membrane composition through ubiquitin- and

- ESCRT-dependent microautophagy. *J. Cell Biol.* **219**, (2020).
93. Oku, M. *et al.* Evidence for ESC RT- and clathrin-dependent microautophagy. *J. Cell Biol.* **216**, 3263–3274 (2017).
 94. Iwama, R. & Ohsumi, Y. Analysis of autophagy activated during changes in carbon source availability in yeast cells. *J. Biol. Chem.* **294**, 5590–5603 (2019).
 95. Hatakeyama, R. *et al.* Spatially Distinct Pools of TORC1 Balance Protein Homeostasis. *Mol. Cell* **73**, 325–338.e8 (2019).
 96. Morshed, S., Sharmin, T. & Ushimaru, T. TORC1 regulates ESCRT-0 complex formation on the vacuolar membrane and microautophagy induction in yeast. *Biochem. Biophys. Res. Commun.* **522**, 88–94 (2020).
 97. Hatakeyama, R. & De Virgilio, C. TORC1 specifically inhibits microautophagy through ESCRT-0. *Curr. Genet.* **65**, 1243–1249 (2019).
 98. Schuck, S. Microautophagy - distinct molecular mechanisms handle cargoes of many sizes. *J. Cell Sci.* **133**, (2020).
 99. Nair, U. & Klionsky, D. J. Molecular mechanisms and regulation of specific and nonspecific autophagy pathways in yeast. *J. Biol. Chem.* **280**, 41785–41788 (2005).
 100. Schäfer, J. A. & Schuck, S. ESCRTing endoplasmic reticulum to microautophagic degradation. *Autophagy* **16**, 763–764 (2020).
 101. Schäfer, J. A. *et al.* ESCRT machinery mediates selective microautophagy of endoplasmic reticulum in yeast. *EMBO J.* **39**, e102586 (2020).
 102. Moeller, C. H. & Thomson, W. W. Uptake of lipid bodies by the yeast vacuole involving areas of the tonoplast depleted of intramembranous particles. *J. Ultrastruct. Res.* **68**, 38–45 (1979).
 103. Wang, C.-W. Stationary phase lipophagy as a cellular mechanism to recycle sterols during quiescence. *Autophagy* **10**, 2075–2076 (2014).
 104. Stromhaug, P. E. & Klionsky, D. J. Approaching the molecular mechanism of autophagy. *Traffic* **2**, 524–531 (2001).
 105. Mukaiyama, H. *et al.* Paz2 and 13 other PAZ gene products regulate vacuolar engulfment of peroxisomes during micropexophagy. *Genes Cells* **7**, 75–90 (2002).
 106. Mukaiyama, H. *et al.* Modification of a ubiquitin-like protein Paz2 conducted micropexophagy through formation of a novel membrane structure. *Mol. Biol. Cell* **15**, 58–70 (2004).
 107. Pan, X. *et al.* Nucleus-vacuole junctions in *Saccharomyces cerevisiae* are formed through the direct interaction of Vac8p with Nvj1p. *Mol. Biol. Cell* **11**, 2445–2457 (2000).
 108. Krick, R. *et al.* Piecemeal microautophagy of the nucleus requires the core macroautophagy genes. *Mol. Biol. Cell* **19**, 4492–4505 (2008).
 109. Mostofa, M. G. *et al.* rDNA Condensation Promotes rDNA Separation from Nucleolar Proteins Degraded for Nucleophagy after TORC1 Inactivation. *Cell Rep.* **28**, 3423–3434.e2 (2019).
 110. Otto, F. B. & Thumm, M. Mechanistic dissection of macro- and micronucleophagy. *Autophagy* **17**, 626–639 (2021).
 111. Kissová, I. *et al.* Selective and non-selective autophagic degradation of mitochondria in yeast. *Autophagy* **3**, 329–336 (2007).

112. Fukuda, T. & Kanki, T. Mechanisms and Physiological Roles of Mitophagy in Yeast. *Mol. Cells* **41**, 35–44 (2018).
113. Vigié, P. *et al.* The mitochondrial phosphatidylserine decarboxylase Psd1 is involved in nitrogen starvation-induced mitophagy in yeast. *J. Cell Sci.* **132**, (2019).
114. Lilienbaum, A. Relationship between the proteasomal system and autophagy. *Int. J. Biochem. Mol. Biol.* **4**, 1–26 (2013).
115. Lamark, T. & Johansen, T. Aggrephagy: selective disposal of protein aggregates by macroautophagy. *Int. J. Cell Biol.* **2012**, 736905 (2012).
116. Pankiv, S. *et al.* p62/SQSTM1 binds directly to Atg8/LC3 to facilitate degradation of ubiquitinated protein aggregates by autophagy. *J. Biol. Chem.* **282**, 24131–24145 (2007).
117. Kirkin, V., Lamark, T., Johansen, T. & Dikic, I. NBR1 cooperates with p62 in selective autophagy of ubiquitinated targets. *Autophagy* **5**, 732–733 (2009).
118. Lu, K., Psakhye, I. & Jentsch, S. A new class of ubiquitin-Atg8 receptors involved in selective autophagy and polyQ protein clearance. *Autophagy* **10**, 2381–2382 (2014).
119. Lu, K., Psakhye, I. & Jentsch, S. Autophagic clearance of PolyQ proteins mediated by ubiquitin-Atg8 adaptors of the conserved CUET protein family. *Cell* **158**, 549–563 (2014).
120. Bruderek, M. *et al.* IMiQ: a novel protein quality control compartment protecting mitochondrial functional integrity. *Mol. Biol. Cell* **29**, 256–269 (2018).
121. Gallina, I. *et al.* Cmr1/WDR76 defines a nuclear genotoxic stress body linking genome integrity and protein quality control. *Nat. Commun.* **6**, 6533 (2015).
122. Miller, S. B. M., Mogk, A. & Bukau, B. Spatially Organized Aggregation of Misfolded Proteins as Cellular Stress Defense Strategy. *J. Mol. Biol.* **427**, 1564–1574 (2015).
123. Miller, S. B. M. *et al.* Compartment-specific aggregases direct distinct nuclear and cytoplasmic aggregate deposition. *EMBO J.* **34**, 778–797 (2015).
124. Ahmadpour, D., Babazadeh, R. & Nystrom, T. Hitchhiking on vesicles: a way to harness age-related proteopathies? *FEBS J.* **287**, 5068–5079 (2020).
125. Specht, S., Miller, S. B. M., Mogk, A. & Bukau, B. Hsp42 is required for sequestration of protein aggregates into deposition sites in. **195**, (2011).
126. Miller, S. B. M. *et al.* Compartment-specific aggregases direct distinct nuclear and cytoplasmic aggregate deposition. **34**, (2015).
127. Spokoini, R. *et al.* Confinement to Organelle-Associated Inclusion Structures Mediates Asymmetric Inheritance of Aggregated Protein in Budding Yeast. *Cell Rep.* **2**, 738–747 (2012).
128. Escusa-Toret, S., Vonk, W. I. M. & Frydman, J. Spatial sequestration of misfolded proteins by a dynamic chaperone pathway enhances cellular fitness during stress. *Nat. Cell Biol.* **15**, 1231–1243 (2013).
129. Kaganovich, D., Kopito, R. & Frydman, J. Misfolded proteins partition between two distinct quality control compartments. *Nature* **454**, 1088–1095 (2008).
130. Tyedmers, J. *et al.* Prion induction involves an ancient system for the sequestration of aggregated proteins and heritable changes in prion fragmentation. *Proc. Natl. Acad. Sci. U. S. A.* **107**, 8633–8638 (2010).

131. Suzuki, K. & Ohsumi, Y. Current knowledge of the pre-autophagosomal structure (PAS). *FEBS Lett.* **584**, 1280–1286 (2010).
132. Sontag, E. M., Vonk, W. I. M. & Frydman, J. Sorting out the trash: The spatial nature of eukaryotic protein quality control. *Curr. Opin. Cell Biol.* **26**, 139–146 (2014).
133. Peters, L. Z., Karmon, O., Miodownik, S. & Ben-Aroya, S. Proteasome storage granules are transiently associated with the insoluble protein deposit in *Saccharomyces cerevisiae*. *J. Cell Sci.* **129**, 1190–1197 (2016).
134. Peters, L. Z. *et al.* The Protein Quality Control Machinery Regulates Its Misassembled Proteasome Subunits. *PLoS Genet.* **11**, 1–17 (2015).
135. Marshall, R. S., McLoughlin, F. & Vierstra, R. D. Autophagic Turnover of Inactive 26S Proteasomes in Yeast Is Directed by the Ubiquitin Receptor Cue5 and the Hsp42 Chaperone. *Cell Rep.* **16**, 1717–1732 (2016).
136. Deniz, A. A. Networking and Dynamic Switches in Biological Condensates. *Cell* **181**, 228–230 (2020).
137. Guillén-Boixet, J. *et al.* RNA-Induced Conformational Switching and Clustering of G3BP Drive Stress Granule Assembly by Condensation. *Cell* **181**, 346–361.e17 (2020).
138. Sanders, D. W. *et al.* Competing Protein-RNA Interaction Networks Control Multiphase Intracellular Organization. *Cell* **181**, 306–324.e28 (2020).
139. Yang, P. *et al.* G3BP1 Is a Tunable Switch that Triggers Phase Separation to Assemble Stress Granules. *Cell* **181**, 325–345.e28 (2020).
140. Riggs, C. L., Kedersha, N., Ivanov, P. & Anderson, P. Mammalian stress granules and P bodies at a glance. *J. Cell Sci.* **133**, (2020).
141. Anderson, P. & Kedersha, N. Stress granules: the Tao of RNA triage. *Trends Biochem. Sci.* **33**, 141–150 (2008).
142. Buchan, J. R. & Parker, R. Eukaryotic stress granules: the ins and outs of translation. *Mol. Cell* **36**, 932–941 (2009).
143. Decker, C. J. & Parker, R. P-bodies and stress granules: possible roles in the control of translation and mRNA degradation. *Cold Spring Harb. Perspect. Biol.* **4**, a012286 (2012).
144. Boncella, A. E. *et al.* Composition-based prediction and rational manipulation of prion-like domain recruitment to stress granules. *Proc. Natl. Acad. Sci. U. S. A.* **117**, 5826–5835 (2020).
145. Kedersha, N. & Anderson, P. Stress granules: sites of mRNA triage that regulate mRNA stability and translatability. *Biochem. Soc. Trans.* **30**, 963–969 (2002).
146. Panas, M. D., Ivanov, P. & Anderson, P. Mechanistic insights into mammalian stress granule dynamics. *J. Cell Biol.* **215**, 313–323 (2016).
147. Marnik, E. A. & Updike, D. L. Membraneless organelles: P granules in *Caenorhabditis elegans*. *Traffic* **20**, 373–379 (2019).
148. Cao, X., Jin, X. & Liu, B. The involvement of stress granules in aging and aging-associated diseases. *Aging Cell* **19**, e13136 (2020).
149. Wang, T. *et al.* Intracellular energy controls dynamics of stress-induced ribonucleoprotein granules. *Nat. Commun.* **13**, 5584 (2022).

150. Chew, J. *et al.* Aberrant deposition of stress granule-resident proteins linked to C9orf72-associated TDP-43 proteinopathy. *Mol. Neurodegener.* **14**, 9 (2019).
151. Cook, C. & Petrucelli, L. Genetic Convergence Brings Clarity to the Enigmatic Red Line in ALS. *Neuron* **101**, 1057–1069 (2019).
152. Todd, T. W. *et al.* Hexanucleotide Repeat Expansions in c9FTD/ALS and SCA36 Confer Selective Patterns of Neurodegeneration In Vivo. *Cell Rep.* **31**, 107616 (2020).
153. Alberti, S. & Dormann, D. Liquid-Liquid Phase Separation in Disease. *Annu. Rev. Genet.* **53**, 171–194 (2019).
154. Shorter, J. Phase separation of RNA-binding proteins in physiology and disease: An introduction to the JBC Reviews thematic series. *J. Biol. Chem.* **294**, 7113–7114 (2019).
155. Taylor, J. P., Brown, R. H. J. & Cleveland, D. W. Decoding ALS: from genes to mechanism. *Nature* **539**, 197–206 (2016).
156. Wolozin, B. & Ivanov, P. Stress granules and neurodegeneration. *Nat. Rev. Neurosci.* **20**, 649–666 (2019).
157. Li, Y. R., King, O. D., Shorter, J. & Gitler, A. D. Stress granules as crucibles of ALS pathogenesis. *J. Cell Biol.* **201**, 361–372 (2013).
158. Molliex, A. *et al.* Phase Separation by Low Complexity Domains Promotes Stress Granule Assembly and Drives Pathological Fibrillization. *Cell* **163**, 123–133 (2015).
159. Boeynaems, S. *et al.* Phase Separation of C9orf72 Dipeptide Repeats Perturbs Stress Granule Dynamics. *Mol. Cell* **65**, 1044-1055.e5 (2017).
160. Freibaum, B. D. & Taylor, J. P. The Role of Dipeptide Repeats in C9ORF72-Related ALS-FTD. *Front. Mol. Neurosci.* **10**, 35 (2017).
161. Hofmann, S., Kedersha, N., Anderson, P. & Ivanov, P. Molecular mechanisms of stress granule assembly and disassembly. *Biochim. Biophys. Acta. Mol. Cell Res.* **1868**, 118876 (2021).
162. Guzikowski, A. R., Chen, Y. S. & Zid, B. M. Stress-induced mRNP granules: Form and function of processing bodies and stress granules. *Wiley Interdiscip. Rev. RNA* **10**, e1524 (2019).
163. Cushman, M., Johnson, B. S., King, O. D., Gitler, A. D. & Shorter, J. Prion-like disorders: blurring the divide between transmissibility and infectivity. *J. Cell Sci.* **123**, 1191–1201 (2010).
164. Gilks, N. *et al.* Stress granule assembly is mediated by prion-like aggregation of TIA-1. *Mol. Biol. Cell* **15**, 5383–5398 (2004).
165. Patel, A. *et al.* A Liquid-to-Solid Phase Transition of the ALS Protein FUS Accelerated by Disease Mutation. *Cell* **162**, 1066–1077 (2015).
166. Jain, S. *et al.* ATPase-Modulated Stress Granules Contain a Diverse Proteome and Substructure. *Cell* **164**, 487–498 (2016).
167. Wheeler, J. R., Matheny, T., Jain, S., Abrisch, R. & Parker, R. Distinct stages in stress granule assembly and disassembly. *Elife* **5**, (2016).
168. Alberti, S., Mateju, D., Mediani, L. & Carra, S. Granulostasis: Protein Quality Control of RNP Granules. *Front. Mol. Neurosci.* **10**, 84 (2017).
169. Grousl, T., Vojtova, J., Hasek, J. & Vomastek, T. Yeast stress granules at a glance. *Yeast* **39**, 247–261 (2022).

170. Cherkasov, V. *et al.* Coordination of translational control and protein homeostasis during severe heat stress. *Curr. Biol.* **23**, 2452–2462 (2013).
171. Anderson, P. & Kedersha, N. RNA granules. *J. Cell Biol.* **172**, 803–808 (2006).
172. Tian, S., Curnutte, H. A. & Trcek, T. RNA Granules: A View from the RNA Perspective. *Molecules* **25**, (2020).
173. Kedersha, N. *et al.* Evidence that ternary complex (eIF2-GTP-tRNA(i)(Met))-deficient preinitiation complexes are core constituents of mammalian stress granules. *Mol. Biol. Cell* **13**, 195–210 (2002).
174. Mateju, D. *et al.* An aberrant phase transition of stress granules triggered by misfolded protein and prevented by chaperone function. *EMBO J.* **36**, 1669–1687 (2017).
175. Bolhuis, S. & Richter-Landsberg, C. Effect of proteasome inhibition by MG-132 on HSP27 oligomerization, phosphorylation, and aggresome formation in the OLN-93 oligodendroglia cell line. *J. Neurochem.* **114**, 960–971 (2010).
176. Ganassi, M. *et al.* A Surveillance Function of the HSPB8-BAG3-HSP70 Chaperone Complex Ensures Stress Granule Integrity and Dynamism. *Mol. Cell* **63**, 796–810 (2016).
177. Ju, J.-S., Miller, S. E., Hanson, P. I. & Weihl, C. C. Impaired protein aggregate handling and clearance underlie the pathogenesis of p97/VCP-associated disease. *J. Biol. Chem.* **283**, 30289–30299 (2008).
178. Mateju, D. *et al.* An aberrant phase transition of stress granules triggered by misfolded protein and prevented by chaperone function. *EMBO J.* **36**, 1669–1687 (2017).
179. Hughes, M. F. Arsenic toxicity and potential mechanisms of action. *Toxicol. Lett.* **133**, 1–16 (2002).
180. Khairul, I., Wang, Q. Q., Jiang, Y. H., Wang, C. & Naranmandura, H. Metabolism, toxicity and anticancer activities of arsenic compounds. *Oncotarget* **8**, 23905–23926 (2017).
181. Jacobson, T. *et al.* Arsenite interferes with protein folding and triggers formation of protein aggregates in yeast. *J. Cell Sci.* **125**, 5073–5083 (2012).
182. Kedersha, N. L., Gupta, M., Li, W., Miller, I. & Anderson, P. RNA-binding proteins TIA-1 and TIAR link the phosphorylation of eIF-2 alpha to the assembly of mammalian stress granules. *J. Cell Biol.* **147**, 1431–1442 (1999).
183. Kirkpatrick, D. S., Dale, K. V., Catania, J. M. & Gandolfi, A. J. Low-level arsenite causes accumulation of ubiquitinated proteins in rabbit renal cortical slices and HEK293 cells. *Toxicol. Appl. Pharmacol.* **186**, 101–109 (2003).
184. Tamás, M. J., Sharma, S. K., Ibstedt, S., Jacobson, T. & Christen, P. Heavy metals and metalloids as a cause for protein misfolding and aggregation. *Biomolecules* **4**, 252–267 (2014).
185. Stanhill, A. *et al.* An arsenite-inducible 19S regulatory particle-associated protein adapts proteasomes to proteotoxicity. *Mol. Cell* **23**, 875–885 (2006).
186. Tillotson, J. *et al.* Arsenic Compromises Both p97 and Proteasome Functions. *Chem. Res. Toxicol.* **30**, 1508–1514 (2017).
187. Isakov, E. & Stanhill, A. Stalled proteasomes are directly relieved by P97 recruitment. *J. Biol. Chem.* **286**, 30274–30283 (2011).

188. Yun, C. *et al.* Proteasomal adaptation to environmental stress links resistance to proteotoxicity with longevity in *Caenorhabditis elegans*. *Proc. Natl. Acad. Sci. U. S. A.* **105**, 7094–7099 (2008).
189. Turakhiya, A. *et al.* ZFAND1 Recruits p97 and the 26S Proteasome to Promote the Clearance of Arsenite-Induced Stress Granules. *Mol. Cell* **70**, 906–919.e7 (2018).
190. Buchan, J. R., Kolaitis, R. M., Taylor, J. P. & Parker, R. XEukaryotic stress granules are cleared by autophagy and Cdc48/VCP function. *Cell* **153**, 1461–1474 (2013).
191. Ryu, H.-H. *et al.* Autophagy regulates amyotrophic lateral sclerosis-linked fused in sarcoma-positive stress granules in neurons. *Neurobiol. Aging* **35**, 2822–2831 (2014).
192. Hunter, N. Scrapie. *Mol. Biotechnol.* **9**, 225–234 (1998).
193. Prusiner, S. B. Prions. *Proc. Natl. Acad. Sci. U. S. A.* **95**, 13363–13383 (1998).
194. Harrison, P. M., Bamorough, P., Daggett, V., Prusiner, S. B. & Cohen, F. E. The prion folding problem. *Curr. Opin. Struct. Biol.* **7**, 53–59 (1997).
195. Shorter, J. & Lindquist, S. Prions as adaptive conduits of memory and inheritance. *Nat. Rev. Genet.* **6**, 435–450 (2005).
196. Chernoff, Y. O. Prions and related phenomena. *Prion* **1**, 81–82 (2007).
197. Chernoff, Y. O. Stress and prions: lessons from the yeast model. *FEBS Lett.* **581**, 3695–3701 (2007).
198. Halfmann, R., Alberti, S. & Lindquist, S. Prions, protein homeostasis, and phenotypic diversity. *Trends Cell Biol.* **20**, 125–133 (2010).
199. Halfmann, R. & Lindquist, S. Epigenetics in the extreme: prions and the inheritance of environmentally acquired traits. *Science* **330**, 629–632 (2010).
200. Alberti, S., Halfmann, R., King, O., Kapila, A. & Lindquist, S. A Systematic Survey Identifies Prions and Illuminates Sequence Features of Prionogenic Proteins. *Cell* **137**, 146–158 (2009).
201. Cox, B., Ness, F. & Tuite, M. Analysis of the generation and segregation of propagons: entities that propagate the [PSI⁺] prion in yeast. *Genetics* **165**, 23–33 (2003).
202. Chernoff, Y. O., Lindquist, S. L., Ono, B., Inge-Vechtomov, S. G. & Liebman, S. W. Role of the chaperone protein Hsp104 in propagation of the yeast prion-like factor [psi⁺]. *Science* **268**, 880–884 (1995).
203. Wickner, R. B. [URE3] as an altered URE2 protein: evidence for a prion analog in *Saccharomyces cerevisiae*. *Science* **264**, 566–569 (1994).
204. Saupe, S. J. The [Het-s] prion of *Podospora anserina* and its role in heterokaryon incompatibility. *Semin. Cell Dev. Biol.* **22**, 460–468 (2011).
205. Wickner, R. B., Edskes, H. K., Son, M., Wu, S. & Niznikiewicz, M. How Do Yeast Cells Contend with Prions? *Int. J. Mol. Sci.* **21**, (2020).
206. Tuite, M. F., Staniforth, G. L. & Cox, B. S. [PSI⁺] turns 50. *Prion* **9**, 318–332 (2015).
207. Glover, J. R. *et al.* Self-seeded fibers formed by Sup35, the protein determinant of [PSI⁺], a heritable prion-like factor of *S. cerevisiae*. *Cell* **89**, 811–819 (1997).
208. Paushkin, S. V., Kushnirov, V. V., Smirnov, V. N. & Ter-Avanesyan, M. D. In vitro propagation of the prion-like state of yeast Sup35 protein. *Science* **277**, 381–383 (1997).

209. King, C.-Y. & Diaz-Avalos, R. Protein-only transmission of three yeast prion strains. *Nature* **428**, 319–323 (2004).
210. Tanaka, M., Chien, P., Naber, N., Cooke, R. & Weissman, J. S. Conformational variations in an infectious protein determine prion strain differences. *Nature* **428**, 323–328 (2004).
211. True, H. L. & Lindquist, S. L. A yeast prion provides a mechanism for genetic variation and phenotypic diversity. *Nature* **407**, 477–483 (2000).
212. Chernoff, Y. O., Derkach, I. L. & Inge-Vechtomov, S. G. Multicopy SUP35 gene induces de-novo appearance of psi-like factors in the yeast *Saccharomyces cerevisiae*. *Curr. Genet.* **24**, 268–270 (1993).
213. Reidy, M. & Masison, D. C. Modulation and elimination of yeast prions by protein chaperones and co-chaperones. *Prion* **5**, 245–249 (2011).
214. Zhou, Z. & Xiao, G. Conformational conversion of prion protein in prion diseases. *Acta Biochim. Biophys. Sin. (Shanghai)*. **45**, 465–476 (2013).
215. Alberti, S. Molecular mechanisms of spatial protein quality control. 437–442 (2012).
216. Sondheimer, N. & Lindquist, S. Rnq1: an epigenetic modifier of protein function in yeast. *Mol. Cell* **5**, 163–172 (2000).
217. Derkach, I. L. *et al.* Dependence and independence of [PSI(+)] and [PIN(+)] : a two-prion system in yeast? *EMBO J.* **19**, 1942–1952 (2000).
218. Helsen, C. W. & Glover, J. R. A new perspective on Hsp104-mediated propagation and curing of the yeast prion [PSI (+)]. *Prion* **6**, 234–239 (2012).
219. Liu, J.-J., Sondheimer, N. & Lindquist, S. L. Changes in the middle region of Sup35 profoundly alter the nature of epigenetic inheritance for the yeast prion [PSI+]. *Proc. Natl. Acad. Sci. U. S. A.* **99 Suppl 4**, 16446–16453 (2002).
220. Li, L. & Lindquist, S. Creating a protein-based element of inheritance. *Science* **287**, 661–664 (2000).
221. Tyedmers, J. *et al.* Prion induction involves an ancient system for the sequestration of aggregated proteins and heritable changes in prion fragmentation. *Proc. Natl. Acad. Sci.* **107**, 8633–8638 (2010).
222. Sies, H., Berndt, C. & Jones, D. P. Oxidative Stress. *Annu. Rev. Biochem.* **86**, 715–748 (2017).
223. Sies, H. Hydrogen peroxide as a central redox signaling molecule in physiological oxidative stress: Oxidative eustress. *Redox Biol.* **11**, 613–619 (2017).
224. Sies, H. Oxidative eustress: On constant alert for redox homeostasis. *Redox Biol.* **41**, 101867 (2021).
225. Sies, H. & Ursini, F. Homeostatic control of redox status and health. *IUBMB Life* **74**, 24–28 (2022).
226. Facchinetti, F., Dawson, V. L. & Dawson, T. M. Free radicals as mediators of neuronal injury. *Cell. Mol. Neurobiol.* **18**, 667–682 (1998).
227. Toulorge, D., Schapira, A. H. V & Hajj, R. Molecular changes in the postmortem parkinsonian brain. *J. Neurochem.* **139 Suppl**, 27–58 (2016).
228. Ansari, M. A. & Scheff, S. W. Oxidative stress in the progression of Alzheimer disease in the

- frontal cortex. *J. Neuropathol. Exp. Neurol.* **69**, 155–167 (2010).
229. Tabner, B. J., El-Agnaf, O. M. A., German, M. J., Fullwood, N. J. & Allsop, D. Protein aggregation, metals and oxidative stress in neurodegenerative diseases. *Biochem. Soc. Trans.* **33**, 1082–1086 (2005).
 230. Halliwell, B. Biochemistry of oxidative stress. *Biochem. Soc. Trans.* **35**, 1147–1150 (2007).
 231. Kohen, R. & Nyska, A. Oxidation of biological systems: oxidative stress phenomena, antioxidants, redox reactions, and methods for their quantification. *Toxicol. Pathol.* **30**, 620–650 (2002).
 232. Ji, L. L., Dillon, D. & Wu, E. Alteration of antioxidant enzymes with aging in rat skeletal muscle and liver. *Am. J. Physiol.* **258**, R918-23 (1990).
 233. Sohal, R. S., Sohal, B. H. & Orr, W. C. Mitochondrial superoxide and hydrogen peroxide generation, protein oxidative damage, and longevity in different species of flies. *Free Radic. Biol. Med.* **19**, 499–504 (1995).
 234. Butterfield, D. A. & Sultana, R. Redox proteomics: understanding oxidative stress in the progression of age-related neurodegenerative disorders. *Expert review of proteomics* **5**, 157–160 (2008).
 235. Levine, R. L. & Stadtman, E. R. Oxidative modification of proteins during aging. *Exp. Gerontol.* **36**, 1495–1502 (2001).
 236. Levine, R. L., Wehr, N., Williams, J. A., Stadtman, E. R. & Shacter, E. Determination of carbonyl groups in oxidized proteins. *Methods Mol. Biol.* **99**, 15–24 (2000).
 237. Bollineni, R. C., Hoffmann, R. & Fedorova, M. Free Radical Biology and Medicine Proteome-wide profiling of carbonylated proteins and carbonylation sites in HeLa cells under mild oxidative stress conditions. *Free Radic. Biol. Med.* **68**, 186–195 (2014).
 238. Nyström, T. Role of oxidative carbonylation in protein quality control and senescence. *EMBO J.* **24**, 1311–1317 (2005).
 239. Berlett, B. S. & Stadtman, E. R. Protein oxidation in aging, disease, and oxidative stress. *J. Biol. Chem.* **272**, 20313–20316 (1997).
 240. Nyström, T. Role of oxidative carbonylation in protein quality control and senescence. *EMBO J.* **24**, 1311–1317 (2005).
 241. Tamarit, J., Cabisco, E. & Ros, J. Identification of the major oxidatively damaged proteins in Escherichia coli cells exposed to oxidative stress. *J. Biol. Chem.* **273**, 3027–3032 (1998).
 242. Requena, J. R., Levine, R. L. & Stadtman, E. R. Recent advances in the analysis of oxidized proteins. *Amino Acids* **25**, 221–226 (2003).
 243. Dalle-donne, I., Rossi, R., Giustarini, D., Milzani, A. & Colombo, R. Protein carbonyl groups as biomarkers of oxidative stress. **329**, 23–38 (2003).
 244. Maisonneuve, E., Fraysse, L., Lignon, S., Capron, L. & Dukan, S. Carbonylated proteins are detectable only in a degradation-resistant aggregate state in Escherichia coli. *J. Bacteriol.* **190**, 6609–6614 (2008).
 245. Beal, M. F. Oxidatively modified proteins in aging and disease. *Free Radic. Biol. Med.* **32**, 797–803 (2002).
 246. Dalle-Donne, I., Rossi, R., Giustarini, D., Milzani, A. & Colombo, R. Protein carbonyl groups as

- biomarkers of oxidative stress. *Clin. Chim. Acta.* **329**, 23–38 (2003).
247. Sohal, R. S. & Weindruch, R. Oxidative stress, caloric restriction, and aging. *Science* **273**, 59–63 (1996).
 248. Dukan, S. & Nyström, T. Bacterial senescence: stasis results in increased and differential oxidation of cytoplasmic proteins leading to developmental induction of the heat shock regulon. *Genes Dev.* **12**, 3431–3441 (1998).
 249. Dukan, S. & Nyström, T. Oxidative stress defense and deterioration of growth-arrested *Escherichia coli* cells. *J. Biol. Chem.* **274**, 26027–26032 (1999).
 250. Dukan, S. *et al.* Protein oxidation in response to increased transcriptional or translational errors. *Proc. Natl. Acad. Sci. U. S. A.* **97**, 5746–5749 (2000).
 251. Nyström, T. Translational fidelity, protein oxidation, and senescence: lessons from bacteria. *Ageing Res. Rev.* **1**, 693–703 (2002).
 252. Sohal, R. S. Role of oxidative stress and protein oxidation in the aging process. *Free Radic. Biol. Med.* **33**, 37–44 (2002).
 253. Sohal, R. S., Agarwal, S. & Sohal, B. H. Oxidative stress and aging in the Mongolian gerbil (*Meriones unguiculatus*). *Mech. Ageing Dev.* **81**, 15–25 (1995).
 254. Stadtman, E. R. Protein oxidation and aging. *Science* **257**, 1220–1224 (1992).
 255. Stadtman, E. R. & Levine, R. L. Protein oxidation. *Ann. N. Y. Acad. Sci.* **899**, 191–208 (2000).
 256. Desmyter, L. *et al.* Expression of the human ferritin light chain in a frataxin mutant yeast affects ageing and cell death. *Exp. Gerontol.* **39**, 707–715 (2004).
 257. Aguilaniu, H., Gustafsson, L., Rigoulet, M. & Nyström, T. Protein oxidation in G0 cells of *Saccharomyces cerevisiae* depends on the state rather than rate of respiration and is enhanced in *pos9* but not *yap1* mutants. *J. Biol. Chem.* **276**, 35396–35404 (2001).
 258. Jazwinski, S. M. Yeast replicative life span--the mitochondrial connection. *FEMS Yeast Res.* **5**, 119–125 (2004).
 259. Grune, T., Jung, T., Merker, K. & Davies, K. J. A. Decreased proteolysis caused by protein aggregates, inclusion bodies, plaques, lipofuscin, ceroid, and 'aggresomes' during oxidative stress, aging, and disease. *Int. J. Biochem. Cell Biol.* **36**, 2519–2530 (2004).
 260. Ballesteros, M., Fredriksson, A., Henriksson, J. & Nyström, T. Bacterial senescence: protein oxidation in non-proliferating cells is dictated by the accuracy of the ribosomes. *EMBO J.* **20**, 5280–5289 (2001).
 261. Levine, R. L. Carbonyl modified proteins in cellular regulation, aging, and disease. *Free Radic. Biol. Med.* **32**, 790–796 (2002).
 262. Lass, A., Sohal, B. H., Weindruch, R., Forster, M. J. & Sohal, R. S. Caloric restriction prevents age-associated accrual of oxidative damage to mouse skeletal muscle mitochondria. *Free Radic. Biol. Med.* **25**, 1089–1097 (1998).
 263. Sohal, R. S., Agarwal, S., Dubey, A. & Orr, W. C. Protein oxidative damage is associated with life expectancy of houseflies. *Proc. Natl. Acad. Sci. U. S. A.* **90**, 7255–7259 (1993).
 264. Cabisco, E., Piulats, E., Echave, P., Herrero, E. & Ros, J. Oxidative stress promotes specific protein damage in *Saccharomyces cerevisiae*. *J. Biol. Chem.* **275**, 27393–27398 (2000).

265. Yan, L. J., Levine, R. L. & Sohal, R. S. Oxidative damage during aging targets mitochondrial aconitase. *Proc. Natl. Acad. Sci. U. S. A.* **94**, 11168–11172 (1997).
266. Johansson, E., Olsson, O. & Nyström, T. Progression and specificity of protein oxidation in the life cycle of *Arabidopsis thaliana*. *J. Biol. Chem.* **279**, 22204–22208 (2004).
267. Kristensen, B. K., Askerlund, P., Bykova, N. V., Egsgaard, H. & Møller, I. M. Identification of oxidised proteins in the matrix of rice leaf mitochondria by immunoprecipitation and two-dimensional liquid chromatography-tandem mass spectrometry. *Phytochemistry* **65**, 1839–1851 (2004).
268. Castegna, A. *et al.* Proteomic identification of oxidatively modified proteins in Alzheimer's disease brain. Part I: creatine kinase BB, glutamine synthase, and ubiquitin carboxy-terminal hydrolase L-1. *Free Radic. Biol. Med.* **33**, 562–571 (2002).
269. Höhn, A. *et al.* Lipofuscin inhibits the proteasome by binding to surface motifs. *Free Radic. Biol. Med.* **50**, 585–591 (2011).
270. Höhn, A., Sittig, A., Jung, T., Grimm, S. & Grune, T. Lipofuscin is formed independently of macroautophagy and lysosomal activity in stress-induced prematurely senescent human fibroblasts. *Free Radic. Biol. Med.* **53**, 1760–1769 (2012).
271. Grune, T., Reinheckel, T., Li, R., North, J. A. & Davies, K. J. A. Proteasome-dependent turnover of protein disulfide isomerase in oxidatively stressed cells. *Arch. Biochem. Biophys.* **397**, 407–413 (2002).
272. Kueper, T. *et al.* Vimentin is the specific target in skin glycation. Structural prerequisites, functional consequences, and role in skin aging. *J. Biol. Chem.* **282**, 23427–23436 (2007).
273. Kueper, T. *et al.* Modification of vimentin: a general mechanism of nonenzymatic glycation in human skin. *Ann. N. Y. Acad. Sci.* **1126**, 328–332 (2008).
274. Höhn, A., Jung, T., Grimm, S. & Grune, T. Lipofuscin-bound iron is a major intracellular source of oxidants: role in senescent cells. *Free Radic. Biol. Med.* **48**, 1100–1108 (2010).
275. Carboni, E. & Lingor, P. Insights on the interaction of alpha-synuclein and metals in the pathophysiology of Parkinson's disease. *Metallomics* **7**, 395–404 (2015).
276. Bota, D. A. & Davies, K. J. A. Lon protease preferentially degrades oxidized mitochondrial aconitase by an ATP-stimulated mechanism. *Nat. Cell Biol.* **4**, 674–680 (2002).
277. Grune, T., Merker, K., Sandig, G. & Davies, K. J. A. Selective degradation of oxidatively modified protein substrates by the proteasome. *Biochem. Biophys. Res. Commun.* **305**, 709–718 (2003).
278. Miller, N. E. & Halpert, J. R. Mechanism-based inactivation of the major beta-naphthoflavone-inducible isozyme of rat liver cytochrome P-450 by the chloramphenicol analog N-(2-p-nitrophenethyl)dichloroacetamide. *Drug Metab. Dispos.* **15**, 846–851 (1987).
279. Aguilaniu, H., Gustafsson, L., Rigoulet, M. & Nyström, T. Asymmetric inheritance of oxidatively damaged proteins during cytokinesis. *Science* **299**, 1751–1753 (2003).
280. Erjavec, N., Larsson, L., Grantham, J. & Nyström, T. Accelerated aging and failure to segregate damaged proteins in Sir2 mutants can be suppressed by overproducing the protein aggregation-remodeling factor Hsp104p. *Genes Dev.* **21**, 2410–2421 (2007).
281. Desnues, B. *et al.* Differential oxidative damage and expression of stress defence regulons in culturable and non-culturable *Escherichia coli* cells. *EMBO Rep.* **4**, 400–404 (2003).

282. Tong, A. H. Y. & Boone, C. 16 High-Throughput Strain Construction and Systematic Synthetic Lethal Screening in *Saccharomyces cerevisiae*. *Methods Microbiol.* **36**, (2007).
283. Brachmann, C. B. *et al.* Designer deletion strains derived from *Saccharomyces cerevisiae* S288C: A useful set of strains and plasmids for PCR-mediated gene disruption and other applications. *Yeast* **14**, 115–132 (1998).
284. Meurer, M. *et al.* Genome-wide C-SWAT library for high-throughput yeast genome tagging. *Nat. Methods* **15**, 598–600 (2018).
285. Bärenz, F. *et al.* The centriolar satellite protein SSX2IP promotes centrosome maturation. *J. Cell Biol.* **202**, 81–95 (2013).
286. Spokoini, R. *et al.* Confinement to organelle-associated inclusion structures mediates asymmetric inheritance of aggregated protein in budding yeast. *Cell Rep.* **2**, 738–747 (2012).
287. Marshall, R. S., Mcloughlin, F. & Vierstra, R. D. Autophagic Turnover of Inactive 26S Proteasomes in Yeast Is Directed by the Ubiquitin Receptor Cue5 and the Hsp42 Chaperone Article Autophagic Turnover of Inactive 26S Proteasomes in Yeast Is Directed by the Ubiquitin Receptor Cue5 and the Hsp42 Chaperone. *CellReports* **16**, 1717–1732 (2016).
288. Kim, J., Scott, S. V., Oda, M. N. & Klionsky, D. J. Transport of a large oligomeric protein by the cytoplasm to vacuole protein targeting pathway. *J. Cell Biol.* **137**, 609–618 (1997).
289. Lynch-Day, M. A. & Klionsky, D. J. The Cvt pathway as a model for selective autophagy. *FEBS Lett.* **584**, 1359–1366 (2010).
290. Suzuki, K. Selective autophagy in budding yeast. *Cell Death Differ.* **20**, 43–48 (2013).
291. Shiber, A., Breuer, W. & Ravid, T. Flow cytometric quantification and characterization of intracellular protein aggregates in yeast. *Prion* **8**, 276–284 (2014).
292. Ramdzan, Y. M. *et al.* Tracking protein aggregation and mislocalization in cells with flow cytometry. *Nat. Methods* **9**, 467–470 (2012).
293. Hidalgo, I. H. *et al.* Characterization of aggregate load and pattern in living yeast cells by flow cytometry. *Biotechniques* **61**, 137–148 (2016).
294. Munder, M. C. *et al.* A pH-driven transition of the cytoplasm from a fluid- to a solid-like state promotes entry into dormancy. *Elife* **5**, 1–30 (2016).
295. Kumar, R., Nawroth, P. P. & Tyedmers, J. Prion Aggregates Are Recruited to the Insoluble Protein Deposit (IPOD) via Myosin 2-Based Vesicular Transport. 1–31 (2016). doi:10.1371/journal.pgen.1006324
296. Bagriantsev, S. N., Gracheva, E. O., Richmond, J. E. & Liebman, S. W. Variant-specific [PSI⁺] infection is transmitted by Sup35 polymers within [PSI⁺] aggregates with heterogeneous protein composition. *Mol. Biol. Cell* **19**, 2433–2443 (2008).
297. Saibil, H. R. *et al.* Heritable yeast prions have a highly organized three-dimensional architecture with interfiber structures. *Proc. Natl. Acad. Sci. U. S. A.* **109**, 14906–14911 (2012).
298. Dennis, G. J. *et al.* DAVID: Database for Annotation, Visualization, and Integrated Discovery. *Genome Biol.* **4**, P3 (2003).
299. Mellacheruvu, D. *et al.* The CRAPome: a contaminant repository for affinity purification-mass spectrometry data. *Nat. Methods* **10**, 730–736 (2013).

300. Kryndushkin, D., Ihrke, G., Piermartiri, T. C. & Shewmaker, F. A yeast model of optineurin proteinopathy reveals a unique aggregation pattern associated with cellular toxicity. *Mol. Microbiol.* **86**, 1531–1547 (2012).
301. Timón-Gómez, A., Sanfeliu-Redondo, D., Pascual-Ahuir, A. & Proft, M. Regulation of the stress-activated degradation of mitochondrial respiratory complexes in yeast. *Front. Microbiol.* **9**, 1–16 (2018).
302. Maisonneuve, E. *et al.* Rules governing selective protein carbonylation. *PLoS One* **4**, e7269 (2009).
303. Sultan, C. S. *et al.* Impact of carbonylation on glutathione peroxidase-1 activity in human hyperglycemic endothelial cells. *Redox Biol.* **16**, 113–122 (2018).
304. Cabiscol, E., Tamarit, J. & Ros, J. Protein carbonylation: Proteomics, specificity and relevance to aging. *Mass Spectrom. Rev.* **33**, 21–48 (2014).
305. Butterfield, D. A. & Lange, M. L. B. Multifunctional roles of enolase in Alzheimer's disease brain: beyond altered glucose metabolism. *J. Neurochem.* **111**, 915–933 (2009).
306. Mizukami, Y. *et al.* ERK1/2 regulates intracellular ATP levels through alpha-enolase expression in cardiomyocytes exposed to ischemic hypoxia and reoxygenation. *J. Biol. Chem.* **279**, 50120–50131 (2004).
307. Alberti, S., Mateju, D., Mediani, L. & Carra, S. Granulostasis: Protein quality control of RNP granules. *Front. Mol. Neurosci.* **10**, 1–14 (2017).
308. Nyström, T. Aging in bacteria. *Curr. Opin. Microbiol.* **5**, 596–601 (2002).
309. Sohal, R. S. Oxidative stress hypothesis of aging. *Free Radic. Biol. Med.* **33**, 573–574 (2002).
310. Chernova, T. A. *et al.* Prion induction by the short-lived, stress-induced protein Lsb2 is regulated by ubiquitination and association with the actin cytoskeleton. *Mol. Cell* **43**, 242–252 (2011).
311. Andréasson, C., Fiaux, J., Rampelt, H., Mayer, M. P. & Bukau, B. Hsp110 is a nucleotide-activated exchange factor for Hsp70. *J. Biol. Chem.* **283**, 8877–8884 (2008).
312. Song, J. *et al.* Essential Genetic Interactors of SIR2 Required for Spatial Sequestration and Asymmetrical Inheritance of Protein Aggregates. *PLoS Genet.* **10**, 17–19 (2014).
313. Liu, B. *et al.* The polarisome is required for segregation and retrograde transport of protein aggregates. *Cell* **140**, 257–267 (2010).
314. Tamarit, J. *et al.* Analysis of oxidative stress-induced protein carbonylation using fluorescent hydrazides. *J. Proteomics* **75**, 3778–3788 (2012).
315. Reverter-Branchat, G., Cabiscol, E., Tamarit, J. & Ros, J. Oxidative damage to specific proteins in replicative and chronological-aged *Saccharomyces cerevisiae*: common targets and prevention by calorie restriction. *J. Biol. Chem.* **279**, 31983–31989 (2004).
316. Mannarino, S. C. *et al.* Glutathione is necessary to ensure benefits of calorie restriction during ageing in *Saccharomyces cerevisiae*. *Mech. Ageing Dev.* **129**, 700–705 (2008).
317. Cabiscol, E., Tamarit, J. & Ros, J. Protein carbonylation: proteomics, specificity and relevance to aging. *Mass Spectrom. Rev.* **33**, 21–48 (2014).
318. Coliva, G., Duarte, S., Pérez-Sala, D. & Fedorova, M. Impact of inhibition of the autophagy-lysosomal pathway on biomolecules carbonylation and proteome regulation in rat cardiac

- cells. *Redox Biol.* **23**, 101123 (2019).
319. Ben-Nissan, G. & Sharon, M. Regulating the 20S proteasome ubiquitin-independent degradation pathway. *Biomolecules* **4**, 862–884 (2014).
 320. Xiong, Y., Contento, A. L., Nguyen, P. Q. & Bassham, D. C. Degradation of oxidized proteins by autophagy during oxidative stress in *Arabidopsis*. *Plant Physiol.* **143**, 291–299 (2007).
 321. Zhao, Y. *et al.* Autophagy is induced by UVA and promotes removal of oxidized phospholipids and protein aggregates in epidermal keratinocytes. *J. Invest. Dermatol.* **133**, 1629–1637 (2013).
 322. Pajares, M. *et al.* Redox control of protein degradation. *Redox Biol.* **6**, 409–420 (2015).
 323. Zhang, Y. *et al.* Autophagy protects against oxidized low density lipoprotein-mediated inflammation associated with preeclampsia. *Placenta* **48**, 136–143 (2016).
 324. Buchan, J. R. & Parker, R. Eukaryotic Stress Granules: The Ins and Outs of Translation. *Mol. Cell* **36**, 932–941 (2009).
 325. Decker, C. J. & Parker, R. P-bodies and stress granules: Possible roles in the control of translation and mRNA degradation. *Cold Spring Harb. Perspect. Biol.* **4**, (2012).
 326. Ganassi, M. *et al.* A Surveillance Function of the HSPB8-BAG3-HSP70 Chaperone Complex Ensures Stress Granule Integrity and Dynamism. *Mol. Cell* **63**, 796–810 (2016).
 327. Buchan, J. R., Kolaitis, R.-M., Taylor, J. P. & Parker, R. Eukaryotic stress granules are cleared by autophagy and Cdc48/VCP function. *Cell* **153**, 1461–1474 (2013).
 328. Speldewinde, S. H., Doronina, V. A. & Grant, C. M. Autophagy protects against de novo formation of the [PSI⁺] prion in yeast. *Mol. Biol. Cell* **26**, 4541–4551 (2015).
 329. Chernova, T. A., Wilkinson, K. D. & Chernoff, Y. O. Physiological and environmental control of yeast prions. *FEMS Microbiol. Rev.* **38**, 326–344 (2014).
 330. Winslow, A. R. *et al.* α -Synuclein impairs macroautophagy: Implications for Parkinson's disease. *J. Cell Biol.* **190**, 1023–1037 (2010).
 331. Cuervo, A. M., Stefanis, L., Fredenburg, R., Lansbury, P. T. & Sulzer, D. Impaired degradation of mutant alpha-synuclein by chaperone-mediated autophagy. *Science* **305**, 1292–1295 (2004).
 332. Ruan, L. *et al.* Cytosolic proteostasis through importing of misfolded proteins into mitochondria. *Nature* **543**, 443–446 (2017).
 333. Guo, Q. *et al.* In Situ Structure of Neuronal C9orf72 Poly-GA Aggregates Reveals Proteasome Recruitment. *Cell* **172**, 696-705.e12 (2018).
 334. Park, S. H. *et al.* PolyQ proteins interfere with nuclear degradation of cytosolic proteins by sequestering the Sis1p chaperone. *Cell* **154**, 134–145 (2013).
 335. Miller, S. B. M., Mogk, A. & Bukau, B. Spatially organized aggregation of misfolded proteins as cellular stress defense strategy. *J. Mol. Biol.* **427**, 1564–1574 (2015).
 336. Olzscha, H. *et al.* Amyloid-like aggregates sequester numerous metastable proteins with essential cellular functions. *Cell* **144**, 67–78 (2011).
 337. Kumar, R., Neuser, N. & Tyedmers, J. Hitchhiking vesicular transport routes to the vacuole: Amyloid recruitment to the Insoluble Protein Deposit (IPOD). *Prion* **11**, 71–81 (2017).

7. Acknowledgements

Firstly, I would like to thank my supervisor Dr. Jens Tyedmers for giving me the opportunity to work on such an interesting topic. Your insight, feedback, motivation and support were invaluable to me during the course of research and writing of this dissertation.

My thanks go also to the members of my thesis advisory committee, PD Dr. Axel Mogk and Dr. Sebastian Schuck for their support, fruitful discussions, and help. Your advice and expertise have been instrumental to me in this journey. Thank you also to Prof. Dr. Tobias Dick and Prof. Dr. Matthias Mayer for agreeing to join my examination committee.

I thank members of Prof. Bernd Bukau's research group at the Center for Molecular Biology Heidelberg (ZMBH) for allowing me to take part in their lab meetings as well as research field-specific sub-meetings, which have always been helpful and interesting.

I am happy to thank Dr. Holger Lorenz and Christian Hörth of the ZMBH imaging facility as well as Dr. Christian Ackermann of the Nikon Imaging Center for access to the facilities as well as very helpful advice.

My gratitude goes to Monika Langlotz of the ZMBH Flow Cytometry Facility for our great collaboration on FACS-based enrichment of protein aggregate species.

I would also like to thank Dr. Thomas Ruppert and Sabine Merker of the ZMBH Core Facility for Mass Spectrometry and Proteomics, as well as Dr. Dominic Helm and Martin Schneider of the DKFZ Genomics and Proteomics Facility for our fruitful collaboration and helpful advice. Additionally, I would like to thank Dr. Thomas Fleming for his continuous support, advice and help.

I sincerely thank my colleagues in the department, Abaya, Claus, Johanna, Bilgen, Gretchen, Minako, Sevgican, Annika, Ruben, and Elisabeth for the fun times we spent together, the nice lab atmosphere and the stimulating and helpful scientific and casual discussions.

On top of current lab members, I also want to thank my previous scientific advisors and mentors, Dr. Ana Oliveira, Dr. Anna Hagenston Hertle, Dr. Rosanna Parlato, and Prof. Dr. Karl-

Peter Giese for their roles in my scientific education, their encouragement and advice. You made me realize how much I enjoy science and research and I learned so much from you.

I am immensely grateful to my friends Sara, Inma, Banafsheh, Gwen, Harsha, Jasmin, Manuel, Florian, Bahar, Alison, Aynur, Kira, and Sonja. You always supported me, cheered me up when things went wrong and on when things went right, and gave me a great balance to academic life.

Many thanks go to my husband Benny. You always lift me up all while anchoring me in reality. Thank you for your love, patience, encouragement, the laughs and hugs and making everything brighter and more colourful.

Without my family, I would not be where I am today and I am so grateful for their continuous support, love, advice, and encouragement.

I thank my godmother Bettina, my aunt Marianne and my great aunt Sophie with Renate, Michael and Nadina and my mother-in-law Ursula for their patience and encouragement.

Especially, I want to thank my parents, Peter and Inge Rothe, for always being there for me with their love, advice, and encouragement, while all the while giving me the freedom to explore my interests. You always inspire me even in the hardest of times with your resilience, your ability to see the good things in any situation, and your support of each other and me. I am grateful for my late canine "siblings," Airon and Isa, for their companionship as well as the many smiles and exercise.